THE MEASUREMENT AND MODELLING OF ELECTROLUMINESCENCE IN HIGH VOLTAGE POLYMERIC CABLE INSULATION MATERIALS

by

Azrul Mohd Ariffin

A thesis submitted for the degree of Doctor of Philosophy

School of Electronics and Computer Science,

University of Southampton,

United Kingdom.

July, 2008

UNIVERSITY OF SOUTHAMPTON

ABSTRACT

FACULTY OF ENGINEERING, SCIENCE AND MATHEMATICS

SCHOOL OF ELECTRONICS AND COMPUTER SCIENCE

Doctor of Philosophy

THE MEASUREMENT AND MODELLING OF ELECTROLUMINESCENCE IN HIGH VOLTAGE POLYMERIC CABLE INSULATION MATERIALS

by Azrul Mohd Ariffin

Since space charge plays a significant role in long-term electrical degradation of polymeric insulation in high voltage cables, there is growing interest in the measurement of the energy dissipation of mobile and trapped charges in the dielectric molecules. The dissipation process is associated with the emission of visible photons, a process known as electroluminescence (EL) and can be used, potentially, as an indicator for the initiation of electrical ageing of insulation. This thesis is based on an investigation into the occurrence of EL in dielectric materials as a result of applying high ac stresses. The phenomenon has been observed and analyzed for different types of thin polymeric films using a charge coupled device (CCD) detection system. This unique experimental setup enables a range of measurements to be performed including the imaging of EL, its temporal behaviour, spectral analysis and phase-resolved measurements using the same detector. The effects of several factors such as the types of material under study and local gas environment have been assessed based on the results obtained. Previously, different research groups have monitored the occurrence of EL under ac conditions by applying a sinusoidal electric field across the polymer but in this project, the emission is also examined under the influence of triangular and square voltage waveforms, together with their asymmetrical counterparts. In addition to this, a dynamic bipolar charge recombination model has been developed in order to simulate studies of EL under an alternating field. By comparing experimental results with the simulation, the theories relating to the processes responsible for the occurrence of EL have been evaluated and a good agreement was found between the simulation and experimental results.

ACKNOWLEDGEMENTS

This project would not have been possible without the help from the following people: Dr. Paul Lewin and Dr. Steve Dodd for their valuable supervision and guidance in conducting the research; the brilliant technical staff of the Tony Davies High Voltage Laboratory for their patience and time in providing the necessary assistance; numerous academics who lent me their kind words and ears; work colleagues Mr. Nam Trung Tran, Mr. Chris Green, Dr. Ian Hosier, Ms. Zhiqiang Xu, Dr. Liwei Hao and Mr. Wilson Choo for throwing fruitful thoughts and advices on this project; my close friends especially Mr. Mukhzeer Mohamad Shahimin and Mr. Che Rozid Mamat for their ongoing words of encouragement; Mr. David Mills for his help in carrying out some of the experimental work; the university for supporting my studies; my parents and family for the many sacrifices they have made throughout my life; and God for giving me the strength to persevere whenever I need it the most.

I am forever grateful.

TABLE OF CONTENTS

LIST OF FIGURES

LIST OF TABLES

SYMBOLS AND ABBREVIATIONS

A	Richardson-Dushman constant ($1.20 \times 10^{6} Am^{-2}K^{-2}$)
e^{-}	Electron
E, E_0, E_s	Relevant electric field strength
E_f	Fermi energy
E_g	Energy gap / Band gap
h	Plank constant ($4.14 \times 10^{-15} eVs$)
j	Current density
k_B	Boltzmann constant ($8.62 \times 10^{-5} eVK^{-1}$)
m	Mass of electron ($9.11 \times 10^{-31} kg$)
n_i	Intrinsic carrier concentration
q_e	Charge on an electron ($-1.60 \times 10^{-19} C$)
q_h	Charge on a hole ($1.60 \times 10^{-19} C$)
S_0	Ground state (singlet state)
S_1	Excited state with same electron spin (singlet state)
T	Absolute temperature
T_1	Excited state with reversed electron spin (triplet state)
V, V_0	Relevant applied voltage
ε_0	Permittivity of vacuum ($8.85 \times 10^{-12} Fm^{-1}$)
ε_r	Relative permittivity
ρ	Charge carrier density
φ	Work function
φ_m	Work function of metal
φ_0	Effective potential barrier

χ	Electron affinity
χ_p	Electron affinity of polymer
ω	Angular frequency
ac	Alternating current
A/D	Analogue to digital
CCD	Charge-coupled device
dc	Direct current
eV	Electronvolt, a unit of energy ($1eV=1.6x10^{-19}J$)
EL	Electroluminescence
GUI	Graphic user interface
HDPE	High-density polyethylene
LDPE	Low-density polyethylene
N_2	Nitrogen
O_2	Oxygen
ODE	Ordinary differential equation
PD	Partial discharge
PEA	Pulsed electro-acoustic
PEI	Polyetherimide
PEN	Polyethylene naphthalate
PES	Polyethersulfone
PET	Polyethylene terephthalate
PI	Polyimide
PMT	Photomultiplier tube
PP	Polypropylene
PTFE	Polytetrafluoroethylene
PVC	Polyvinylchloride
PWP	Pressure wave propagation
rms	Root mean square
SF_6	Sulphur hexafluoride
TPM	Thermal pulse method
TSM	Thermal step method
XLPE	Cross-linked polyethylene

Chapter One

INTRODUCTION

1.1 High Voltage Underground Cable

There has been a constant debate nowadays in deciding which form of electrical energy transmission; overhead lines or underground cables, offer greater benefits to consumers as well as to the power companies. As far as the economy is concerned, the cost to manufacture overhead lines is ten times lower than underground cables with equal energy transfer [1]. In addition to this, the installation and maintenance cost for overhead lines are much lower than its rival since the system faults can be detected and repaired relatively faster and at a reasonable cost. The performance of an underground cable is also partly dictated by its thermal capacity as it is buried in the ground whereas overhead lines have their own natural source for coolant due to the convection of the ambient air. Nevertheless, there are clear indications that progress in underground

electric power transmission has been escalating as fast as overhead lines since 1930 [2] and this is for a number of reasons.

These days, there has been a growing public awareness in preserving the environment and underground system has reduced impact on this matter compared to overhead lines. Moreover buried cables are preferred when it comes to areas that have restricted access for power transmission lines; for instance airports and congested urban regions. Additionally, densely populated urban areas will have comparatively high costs for land and the installation costs for transmission of electric energy via lines will be greatly increased and the costs of obtaining planning permission may escalate. It can also be argued that since underground cables are a closed system, they are less affected by environment conditions. Lightning strikes, dust and air-borne pollutants can cause overhead line components to be damage-prone and thus recurring maintenance procedures may become increasingly expensive. For these reasons, underground transmission cables, both ac and dc are seeing increased use within high voltage networks.

1.1.1 Historical Evolution

The first underground power cable was constructed in the late 19^{th} century and was pioneered by Sebastian de Ferranti [3]. At that time, most power cables were insulated with vulcanized rubber. Ferranti later realized that his rubber insulated underground cable was not suitable for 10kV, 50Hz transmission so he began to search for an alternative insulator. Paper had already been used as insulation in telephone cables, and this had encouraged Ferranti to investigate the possibility of using the material as a replacement for rubber in transmission cables. He later discovered that by impregnating paper with a by-product of wax known as ozokerite, it could withstand very high voltage [2]. This tape-wound paper insulated cable design, also known as Ferranti Tubular Main (Figure 1.1), was quickly patented and its general structure has remained in the forefront of underground power transmission cable design ever since.

By the 1920s, the development of underground power cables came to a crisis when the number of cable insulation failures across the globe reached significant proportions. As a result of this, research work was undertaken in order to improve the ability of paper for cable insulation. It was discovered that by impregnating paper with low viscosity

oil, the existence of gas or air-filled cavities inside the insulator could be prevented and this could result in slowing the deterioration of the paper insulation by gas discharges [4]. Another approach to solve this problem was by pressurizing chemically inert gas into the insulation. It was found that filling paper insulated cable with this type of gas, typically nitrogen, could raise the corona inception voltage stress [5]. The presence of such gaseous molecules would reduce the mean free path of electrons, causing higher kinetic energy required for collision ionization. Therefore the process for cable insulation degradation could be prolonged.

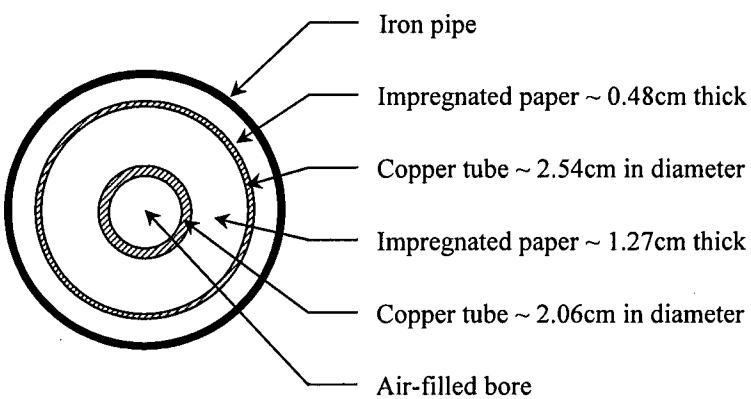

Figure 1.1: The original design of Ferranti 10kV ac Tubular Main [2].

Oil-paper and gas-pressure insulated cables shared a fair degree of success but the high cost of production for both had instigated power companies to find a relatively cheaper material without compromising the operating stresses that it can withstand. The development of polyethylene as a low loss dielectric for communication cables in 1940s raised hopes of reducing the cost of underground power transmission. Polyethylene is widely known for its excellent electrical, chemical and mechanical properties [6, 7]. It has a very high breakdown strength (~900kVmm^{-1}), low dielectric loss (tanδ less than 10^{-3}) and high dc resistivity (ρ greater than $10^{16}\Omega$m). The material also exhibits good mechanical stiffness, high corrosion resistance and ease of formation, in addition to having a reasonably low cost for manufacturing and maintenance. This has encouraged the extensive use of polyethylene in high voltage cable insulation systems.

In 1965, the first short-length polyethylene insulated transmission cable was installed in Puerto Rico, operating at 138kV [8]. The cable, which was only 123m long, had copper as its conductor and was insulated with voltage stabilized high-molecular-

weight polyethylene. Although this type of cable had been a success in the low voltage distribution field, its use for higher voltages was relatively slow as potential customers were influenced by test failures in Waltz Mill cable test site [9]. Subsequently, it was shown that the test failures were due to thermal expansion of the insulation which had caused permanent damage. Even so, high voltage cables with extruded polyethylene insulation were installed successfully as part of the French 225kV transmission network in 1969 [10]. The cables were never subjected to full load over extended periods of time so they were unlikely to operate above its temperature rating of 65°C. This ensured that the differential thermal expansion between the conductor and insulation was always within 1% [11], preventing the deformation of the dielectric during load cycling. Similar operational success was also accomplished in Sweden when a 200km of 123-145kV cross-linked polyethylene cable was put into service in 1976 [12]. These two landmark achievements firmly established the possibilities of using polyethylene as underground cable insulation, and since then it has become the main competitor for the long established oil-impregnated paper cable insulation technology.

1.1.2 Polymer Insulated Cable Structure

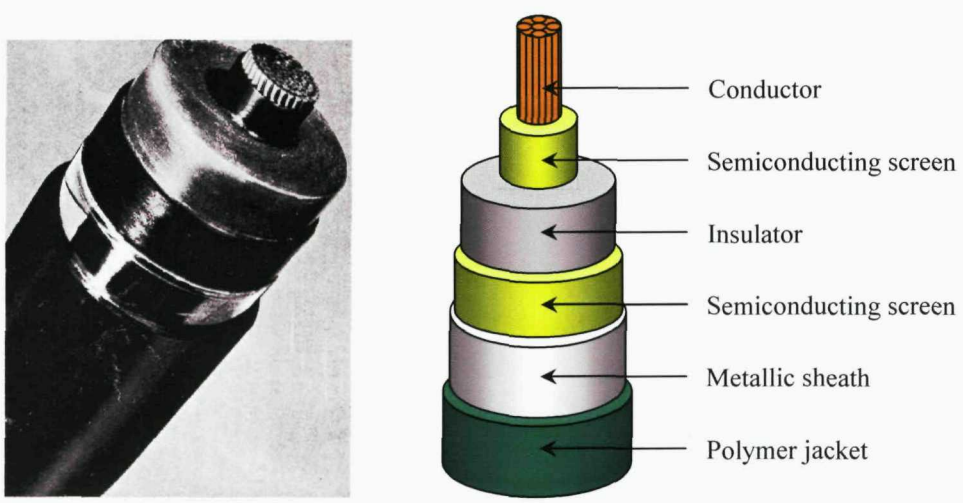

Figure 1.2: The assembly of high voltage polymeric underground cable.

Generally, high voltage polymeric cables are designed in such a way that they can operate at a certain voltage level and current rating. The typical construction of the cable is shown in Figure 1.2. Depending on the load current it carries, the central conductor is usually made from aluminium or copper and it is covered by a semiconducting screen to ensure a smooth electrical interface between the conductor

and the polymeric insulation. The choice of polymer to be used as an insulator depends on several criteria, including the operating temperature of the cable. Typical polyethylene insulated cables are limited to service temperatures of 70°C [13] due to its softening point whereas cables with crosslinked polyethylene have a rated maximum conductor temperature of 90°C [13]. Surrounding this insulation is another semiconducting screen and then a metallic sheath, used to prevent penetration of moisture into the cable. In order to protect the sheath from corrosion, the cable is enclosed in a polymer jacket.

Failure of underground polymeric high voltage cable has always been a major concern for the electrical power distribution industries. Fault location and repair of faulty cables are expensive and time-consuming; causing disruption for customers. Underground cables are generally exposed to a wide variety of stresses, which lead to ageing and ultimately failure. Among ageing processes are thermal stresses due to load cycling or seasonal temperature fluctuations, and mechanical stresses due to bending of cable or vibrations from external sources such as excavation activities [14]. The cable may also be subjected to environmental stresses due to the presence of gases and water in the soil. Nonetheless, it is ageing caused by electrical stress that has received significant research attention. Under the continuous application of a strong electric field, the insulating material of a high voltage cable may experience some form of degradation, such as electrical treeing, that can inevitably cause catastrophic breakdown. Thus a lot of research has been undertaken in investigating the nature of the changes to a polymeric dielectric that high electrical stress can cause.

1.2 Electrical Degradation of Cable Insulation

It is accepted that the main cause for electrical breakdown in high voltage cable insulation is usually due to the microscopic impurities and defects located in the bulk, or even at the interfaces of the material, as illustrated in Figure 1.3. When a polymeric material is subjected to an electrical stress, imperfections such as protrusions, contaminants and microvoids, will all act as points where the electric field is enhanced, increasing the likelihood that degradation processes will be initiated [14, 15]. As manufacturing technology improves however, insulation systems are becoming cleaner and their interfaces smoother. The reduction in concentration and size of impurities has

led to more research at the atomic scale where space charge can play a fundamental role in triggering ageing phenomena [16].

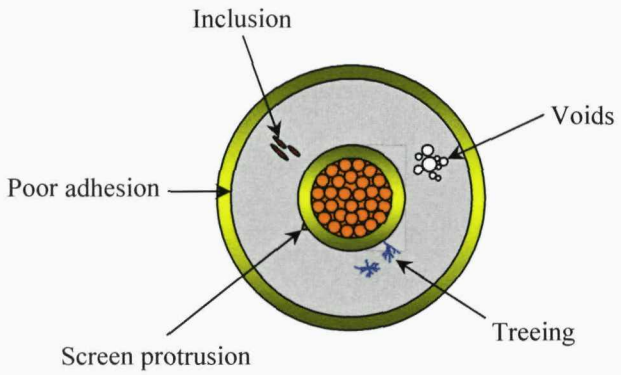

Figure 1.3: Possible defects within cable insulation.

1.2.1 Space Charge Formation

In principle, 'space charge' can be defined as all charge carriers; electrons, holes, charged particles and ions, that can exist within the dielectric material and can be trapped by the material or transported through the material on application of an external electric field. The existence of space charge has been linked to the degradation and ageing processes of insulating polymeric materials. Sanche [17] argued that in the absence of electrical field, these low-energy charges can produce molecule dissociations and the released fragments (of about 2eV) will quickly react to the surrounding molecules and form new products; implying that the effect of these charges is mainly chemical, rather than electrical. Several other reports [18, 19] on the other hand, have suggested that there is a possible correlation between space charges and electrical degradation of polymers. It was suggested that these charges store electro-mechanical energy that is able to promote cracks and plastic deformations in the polymer structure. Their presence could constitute the equivalent of the aforementioned impurities on an electronic scale, in terms of their capability to weaken insulation.

Charge carriers may be injected across the contact between a conducting electrode and the insulating material by application of an applied electric field. The mechanisms by which charge is injected will be discussed later. The accumulation of injected charge in the insulating material adjacent to the injecting electrode is called homocharge as the

sign of this charge is the same as the polarity of the injecting electrode. Therefore, in the case of homocharge, when a dc voltage is applied to the contacts of a sample, space charge of negative sign will accumulate adjacent to the negative electrode and positive charge will accumulate adjacent to the positive electrode. Homocharge is usually formed due to the trapping of the injected charge in the polymer adjacent to the metal-polymer interface and would lead to a reduction in the electric field at the interface. Alternatively, space charge may accumulate if the applied electric field is sufficiently high such that ionization of impurities within the polymer may occur. Positive ions will migrate towards the negative contact and negative ions will migrate towards the positive contact under the influence of the applied field. As the ions cannot penetrate into the metal contact, a space charge is formed adjacent to each contact which has a sign which is opposite that of the polarity of the contact. In this case, the accumulated space charge is called heterocharge and its formation would lead to an increase in the electric field at the interface. Figure 1.4 depicts the formation of homocharge and heterocharge at the electrode and polymer interface.

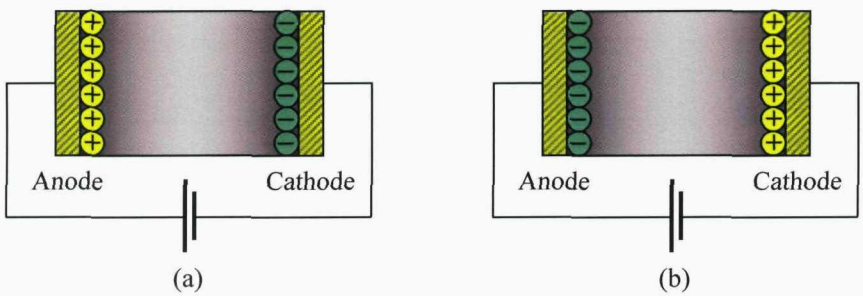

Figure 1.4: The formation of (a) homocharge and (b) heterocharge layer near the interface region.

1.2.2 Measurements of Space Charge

When a polymer is subjected to high electric stresses, it will become charged and the charges may remain inside the dielectric for a period of time. As explained earlier, these charges are due to the injection and extraction of charge carriers and ionization of impurities within the material itself. The accumulation of space charge at the interface of an electrically stressed polymer can lead to unnecessary electric field modifications; causing further deterioration in the insulator. The interfaces between the dielectric and the electrode in high voltage power cables are generally considered as the weakest point where the probability of failure is much higher than that of the bulk [20, 21].

This crucial problem has prompted numerous studies to develop techniques for the measurement of space charge distributions within polymeric materials under the influence of an applied electric field and studies using these techniques have been undertaken to consider the effect of space charge on the electrical characteristics of insulation materials. Currently, space charge distributions within insulating materials can be measured using a range of complementary techniques and these are listed in Table 1.1. They differ in the way in which the internal space charge is perturbed in such a way that they will produce a time dependent signal that can be detected externally and allowing the internal space charge distribution within the material to be determined.

Table 1.1: Various devices for the measurement of space charge.

Method	Literature Reference
Thermal Pulse Method (TPM)	22
Thermal Step Method (TSM)	23, 24
Laser Intensity Modulation Method (LIMM)	25
Laser Induced Pressure Pulse (LIPP)	26, 27
Piezoelectrically Induced Pressure Step (PIPS)	28, 29
Pulsed Electro Acoustic (PEA)	30-32

1.3 Space Charge and Electroluminescence

Another technique that can potentially be used to investigate the onset of electrical degradation in polymeric materials subjected to high field is by monitoring the occurrence of light emission known as electroluminescence (EL). This phenomenon may arise due to the interaction of mobile and trapped charges within the dielectric under the influence of an applied electric field [33]. The mechanism of EL is therefore associated with the accumulation of space charge within the dielectric and the subsequent recombination of this charge with mobile injected carriers. The causes and nature of this process will be fully explained in the next chapter. Since the existence of space charge has been widely regarded as one of the major causes for failure of solid dielectrics, it can be said that EL measurements may provide an alternative way to investigate the electrical ageing and degradation of polymer besides space charge probing.

There is a growing interest to measure both space charge and EL to see how one correlates to the other. It was observed by Cao *et al.* [34] that under ac conditions, the onset voltage for EL was found to be the same as the onset voltage for space charge accumulation within the material. Therefore, it was concluded that the formation of EL is associated with the formation of space charge and hence the two processes are linked. A good agreement was also achieved by Laurent *et al.* [35] for their time-resolved space charge and EL measurements whereby the phase angles in which the space charge is a maximum coincides with the phase angles at which the measured EL was also significantly high. These two examples are among numerous ongoing experimental projects that have been established in order to examine the extent that space charge behaviour affects EL. The relationship with space charge also demonstrates the possibility that EL measurements can be used as a tool to observe the degradation process of polymeric insulation, in particular during the incubation phase of a more severe feature such as electrical treeing, a known electrical degradation mechanism which can lead to insulator failure. However, before techniques based on the characteristics of EL can be used to study ageing processes in insulating materials it is necessary to first develop an understanding the underlying physical processes that give rise to EL and to be able to identify possible influencing factors that would need to be taken into account before techniques based on EL characteristics could be used reliably characterize material ageing.

1.4 Research Aims and Objectives

This research project has been undertaken to achieve the following aims:

1. To simulate EL phenomenon in insulating materials subjected to a uniform alternating electric field based on simple theories of charge injection and bipolar charge recombination processes.
2. To monitor the occurrence of EL in polymers at room temperature and to distinguish its behaviour in relation to the imaging analysis, temporal behaviour and spectral measurement.
3. To compare EL characteristics from different types of dielectric, which comprise of low-density polyethylene (LDPE), polyethylene terephthalate (PET) and polyethylene naphthalate (PEN) and to determine if material factors such as the chemical constituents play an important role in the formation of EL.

4. To study the effect of different gas environments on the observed EL, to determine if absorbed gas within the polymeric material plays an important role in the mechanisms giving rise to EL and to conclude whether the effect correlates to EL observations undertaken by other researchers using gas-impregnated polymeric samples.
5. To determine the occurrence of EL with respect to the typical sinusoidal applied voltages using a charge coupled device (CCD) detection system as opposed to the conventional photomultiplier tube (PMT) technique and to compare the experimental results with simulations based on a charge injection model.
6. To compare the effect of different waveforms of applied voltages on EL in order to further understand the mechanism responsible for the detected light emission.

1.5 Outline of Report

The report is divided into seven separate chapters. The background theories on the key processes leading to EL are described in Chapter 2. Its main focus is to explain how light can be emitted from an insulating material when it is subjected to high electric fields. Some of the previous EL investigations conducted by different researchers are also compared and discussed critically. Chapter 3 focuses on the development of a model to simulate the phenomenon under a uniform ac electric field condition. The model was developed based on the mechanisms that give rise to light emission and the computation results can be used to verify the theories that have been proposed by the EL research community.

In addition to modelling the phenomenon, the report also includes experimental work to measure EL from polymeric materials and this is described thoroughly in Chapters 4 and 5. Chapter 4 describes the overall detection system that was designed and built to conduct EL experiments, and the necessary procedures to perform the different types of measurement. The results of the measurements are detailed and discussed in Chapter 5. A thorough discussion on the measured EL including a comparison between the experimental data and simulation results is presented in Chapter 6. Finally the conclusion of this research project on EL is outlined in Chapter 7, together with several proposals for the future directions of this research.

Chapter Two

ELECTROLUMINESCENCE IN INSULATING POLYMERS

2.1 Introduction

The fact that the average service field of most insulating polymers used in high voltage systems is only a fraction (typically ~10%) of their breakdown strength has led to the belief that the existence of space charges within the insulation may well be the key factor for its long-term electrical degradation. As the applied voltage is raised, the presence of these charges may lead to a rapid increase of current and can cause catastrophic breakdown in the insulation. As a result of this, a lot of research has placed great emphasis in understanding the behaviour and distribution of space charge in polymeric materials, together with charge injection mechanisms [36, 37] and the role in which impurities can be ionized within the material and contribute to the formation of space charge.

As space charge plays a significant role in long-term electrical degradation of polymeric insulation in high voltage cables, there has been a growing interest to investigate further the energy dissipation of mobile and trapped charges in the molecules of the dielectric medium. This dissipation process is associated with the emission of visible photons, a process known as electroluminescence (EL), which has been observed in various materials. Optical emission has been generally regarded as a direct proof of excited and chemically reactive states [38] so the study of the phenomenon could give a better understanding of the processes leading to dielectric material degradation. In order to understand the nature of this phenomenon, a brief overview of the characteristics of a typical polymer used in high voltage cable insulation, namely polyethylene, is presented in this chapter before discussing the processes that lead to photon emission.

2.2 Polyethylene

Polyethylene was first produced by polymerizing ethylene gas at high temperatures (80-300°C) and pressures (1000-3000 atmosphere); a process which started in the 1930s and is still being used today [39]. Its hydrophobic nature, high corrosion resistance and most importantly, excellent dielectric properties facilitate polyethylene's widespread use for high voltage insulation systems. In the polymerization process, the monomer molecules (ethylene) are repeatedly linked together to produce one long polymer chain (polyethylene) and these repeat units are covalently bonded together to form giant macromolecules. The chemical structure for polyethylene and its monomer can be represented as in Figure 2.1.

The molecule that has a near perfect linear sequence of repeat units is known as high-density polyethylene (HDPE). Some molecules on the other hand, may contain side branches and vary in terms of their length, separation and number of branches; such polymer is called low-density polyethylene (LDPE). Typically LDPE has around 30 side branches per 1000 carbon atoms [39], and these branches can be short (up to several monomer units long) or as long as the main chain [6]. Branching reduces the potential for regular molecular packing crystallization and ostensibly lowers the density of the material. Therefore LDPE is mechanically inferior as compared to HDPE.

The typical melting temperature for polyethylene in general is 100-125°C [13]. To some extent, cable core conductors can become sufficiently hot enough to melt the insulation. Crosslinking is a process by which the polyethylene molecules are reacted together in order to retain its dimensional stability under such conditions. Crosslinked polyethylene (XLPE) in principle is one gigantic molecule and it becomes rubber-like rather than liquid when heated, preventing the individual molecules from flowing past one another. The most common way to achieve crosslinking is by the incorporation of a catalyst, such as dicumyl peroxide or silane into the polymer [6, 40]. This process however can promote the formation of residual by-products such as acetophenone, cumyl alcohol, methanol and methyl styrene [41, 42]. Thus the accumulation of these residues, together with the low molecular weight additives within the material may become a possible source of impurity in XLPE. Crosslinking can also be achieved by radiation but the process can cause some physical degradation to the polymer such as the reduction in chain length of the polyethylene molecules [6].

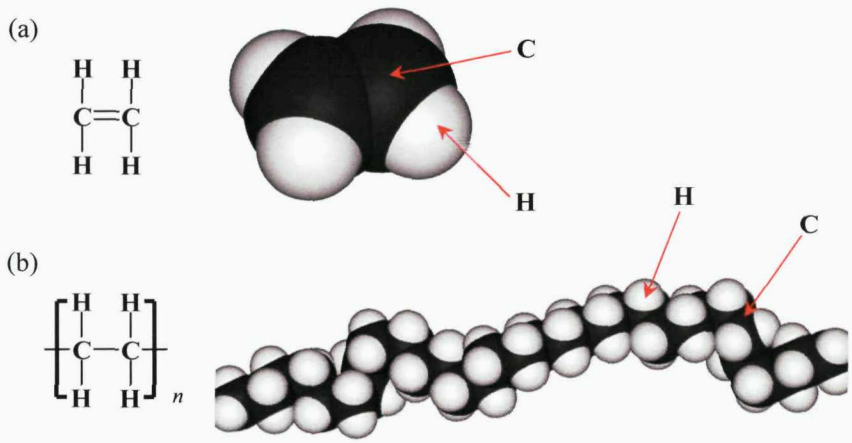

Figure 2.1: Chemical structure for (a) ethylene (b) polyethylene.

2.2.1 Generic Microstructure

The long chains of polyethylene can fold back and forth on themselves or onto other chains and they are bonded together by Van der Waals forces. These parallel regions form the crystalline part whereby the molecules are arranged into a well-ordered regular structure [43], as shown in Figure 2.2 (a). The crystalline part, known as lamellar, has the dimension of 10-20nm in thickness, and around 1-10μm in width and length. During crystallization from molten polyethylene, lamellae grow from a single

nucleus and are arranged radially to form spherulites. Figure 2.2 (b) and (c) illustrates the formation of spherulites and lamellae respectively.

A spherulite behaves more as a collection of lamellar crystallites rather than a single crystal, and can be up to 100μm in diameter. Nonetheless, some of the polyethylene, particularly the branched chains follow a disordered path and hence create amorphous regions between the lamellae. As a result, a polyethylene solid will have a complicated physical microstructure that contains both crystalline and amorphous domains. Due to its semi-crystalline morphology, polyethylene's electrical properties are not as well interpreted as those for semiconductor materials using the simple energy band model.

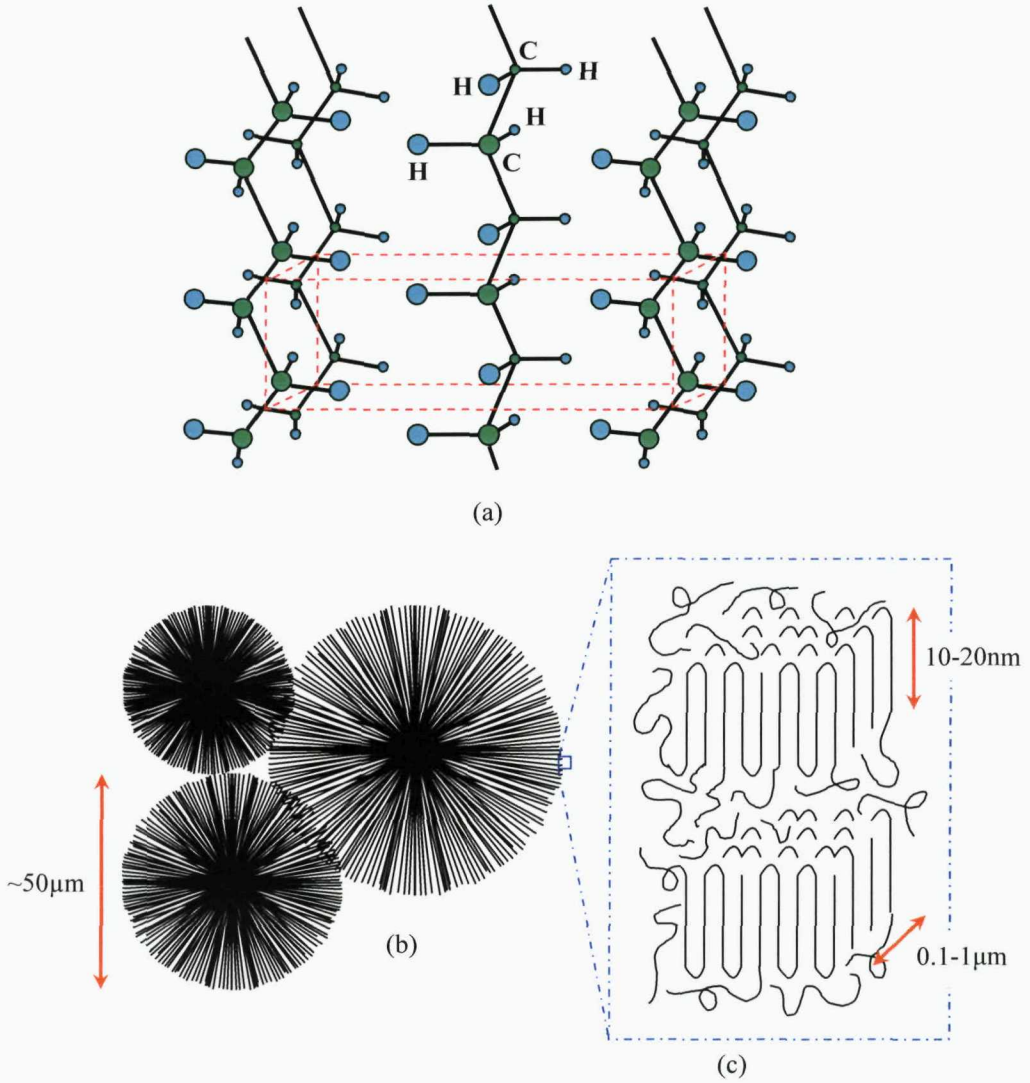

Figure 2.2: (a) The basic crystal unit cell for orthombic polyethylene and the morphology of a polyethylene's (b) spherulite (c) lamellae.

2.2.2 The Energy Band Model

In an isolated atom, each electron is uniquely defined by its energy level, which corresponds to the orbital of the electron itself in the conventional Bohr model. When these atoms are brought closer together, the electrons of the same orbitals will interact, causing them to have slightly different energies from their original orbital energies. As more and more atoms are combined, a band of allowed energies will be produced. Since polyethylene has crystalline properties, it is necessary to develop its energy band model with reference to the already-established, covalently-bonded crystal energy scheme.

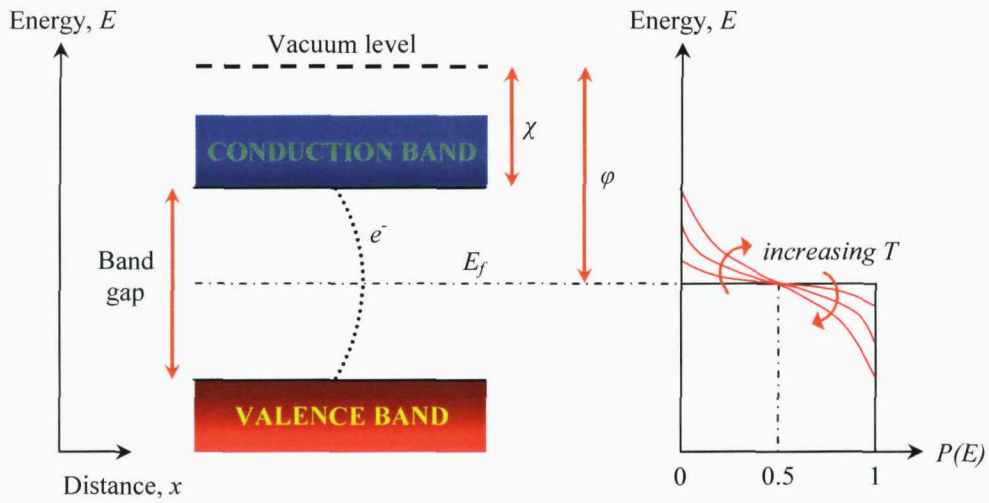

Figure 2.3: Simple energy band diagram for covalently-bond crystal.

According to the simple electronic band theory for a covalent bond crystal, there are two electron energy bands separated by a band gap that determine the electrical properties of the material. The highest energy band that is completely filled with electrons at absolute zero temperature is known as the valence band as the electrons within this band are the valence electrons which form the covalent bonds between adjacent atoms of the crystal. In the case of an insulator, the energy band having allowed electron energies above that of the valence band and separated from the valence band by a band gap, is called the conduction band as electrons having such energies are able to move freely through the lattice. The number of electrons at absolute zero temperature in the conduction band is zero.

The band gap theory assumes that the conductivity of the material is due to the thermal promotion of valence electrons into the conduction band leaving a positively charged hole in the valence band. The conductivity of the material is therefore determined by a drift of electrons in the conduction band and a drift of positive holes in the valence band. The number of electrons in the conduction band and holes in the valence band is dependent on the width of the forbidden gap and the temperature of the material. The average thermal energy of electrons at a temperature T is equal to the product of Boltzmann constant ($8.62\text{x}10^{-5}\text{eVK}^{-1}$) times the absolute temperature in Kelvin; thus at room temperature of 293K, the average thermal energy of electrons is approximately 0.025eV. The probability, P that an electron attains an energy E at temperature T is given by the Fermi-Dirac distribution function:

$$P(E,T) = \left[1 + \exp\left\{\frac{E - E_f}{k_B T}\right\}\right]^{-1} \qquad \{2.1\}$$

where k_B is the Boltzmann constant and E_f is the Fermi energy level and is defined as the level of energy that has a 50% probability of being occupied. The work function, indicated by φ in Figure 2.3, is the energy required to free an electron from the material to the vacuum level whereas the electron affinity, χ represents the energy released when an electron is placed at the bottom of the conduction band. Both work function and electron affinity are specific characteristics for a particular material.

In the case of polyethylene, the nature of its energy scheme is rather complex since it consists of both crystalline and amorphous regions. Since polymers like polyethylene are characterized by very long molecule chains formed by strong covalently-bonded monomers, it can be said that the molecule orbitals are in fact linear combinations of the different constituent atoms' orbitals [6]. These molecule chains will then produce different bonding and anti-bonding orbital, which leads to the formation of valence and conduction bands. The gap between these two bands is wide due to the less significant overlapping in electron orbitals of adjacent molecular chains of the polymer. Since the energy gap E_g is quite big (~7.6 to 9eV [44]), the probability of an electron occupying the lowest level in the conduction band due to thermal excitation, which is ~0.026eV at 300K, will be very small. Therefore the conduction process in this type of material is far more complicated than the simple creation of carriers by thermal excitation across the band gap.

When polyethylene crystallizes to form spherulites, a considerable amount of structural disorder is produced. Instead of forming a band-like energy states, the defects will cause localized states to appear and this will lead to the formation of trapping sites [45]. In such materials an extended conduction band may not exist. All charge carriers that enter these localized states are therefore not available for conduction since they will become 'trapped'. The traps may take the form of donors (hole traps) with energy levels above the top of the valence band, or acceptors (electron traps) at the bottom of the conduction band. The time which the carriers will spend in the traps depends on the depth of the traps, ranging from 0.1eV (shallow traps) to a few eVs (deep traps) [46]. Thus the energy band diagram for polyethylene may therefore be best represented as shown in Figure 2.4.

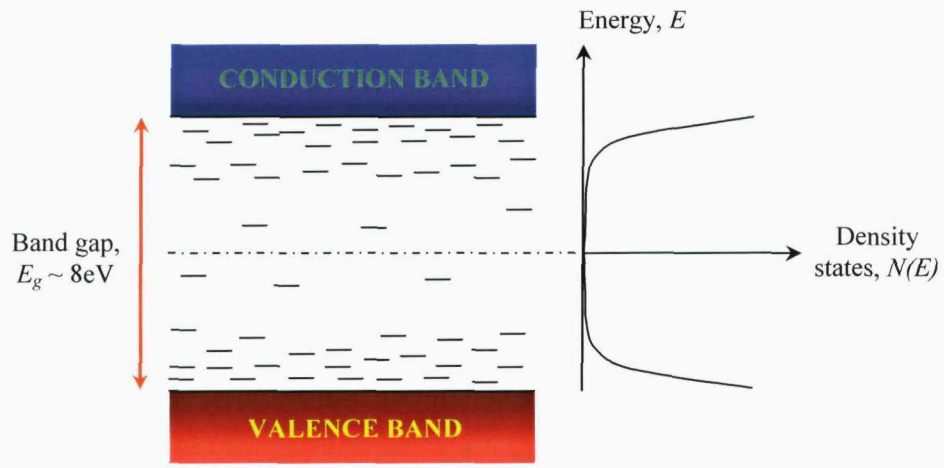

Figure 2.4: Schematic diagram representing energy scheme for polyethylene.

2.2.3 Charge Carrier Species

In an ideal perfect crystal and assuming that the Fermi energy E_f is situated half way between the bottom of the conduction band and top of valence band, the intrinsic carrier concentration, n_i is related to the energy band gap, E_g such that:

$$n_i \propto \exp\left(-E_g / 2k_B T\right) \qquad \{2.2\}$$

Assuming all other parameters remain the same, a small increase in E_g will cause a significant reduction of n_i due the exponential term; therefore the electrical conductivity will also decrease. By using this simple rule of thumb, a material with a wide band gap such as polyethylene will have a very small n_i and this rules out the intrinsic contribution towards its minute conductivity. It can be concluded that the conduction process within this material is mainly due to other mechanisms.

The low relative permittivity for polyethylene implies that this material is non-dipolar but ions can be produced by the dissociation of neutral molecules due to the application of electric field. In addition to this, foreign impurities such as oxygen and moisture may be introduced within the polymer during fabrication processes and they can be polarized and also ionized. The presence of such molecules can affect electrical properties as they could contribute to the material's total conductivity. Nevertheless, the accommodation and transport of massive ions through polyethylene structure means that a continuing change in morphology has to take place [47]. It may also be argued that there may not be a large number of impurities to cause significant conduction, especially as technological advancements in polymer manufacturing have minimized this problem substantially; hence the increased emphasis on investigating the conduction process electronically. This involves the movement of electrons and holes within the material. A 'hole' can be defined as the condition where an electron is absent; therefore it may be regarded as a 'conceptual' positive counterpart to the negatively charged species in the simplest sense.

Works by Serra *et al.* [48] and Meunier *et al.* [49] have indicated that the electron affinity for polyethylene has a negative value and is of the order of 1eV. The negativity of the affinity suggests electrons will be confined to 'tunnel'-like paths in the low density intermolecular regions where energy is lower [50]. Such paths exist between the ordered parallel chains in the crystalline lamellae but they are likely to be much more accessible in the amorphous phases [50]. Moreover, Serra *et al.* [48] has also reported that electrons that are being injected into the system will travel within the free volume and sub-microvoid spaces within the polymer structure. On the contrary, holes only exist via electron vacancies in the valence band of the polyethylene molecules and therefore it can be said that they are confined to polymer chains. Due to tight chain folds in the crystalline lamellae, hole transport is likely to be most extensive in the amorphous phases near chain ends. Figure 2.5 illustrates the conduction paths for electrons and holes in a polyethylene structure.

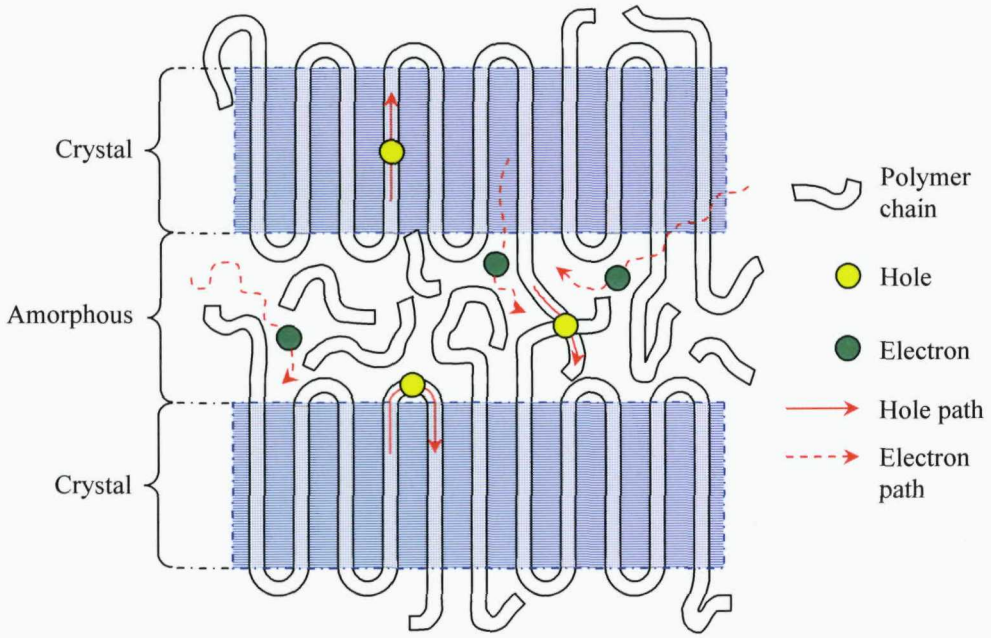

Figure 2.5: Charge transport in semi-crystalline polyethylene.

2.3 Metal-Polymer Interface

In order to understand electrical ageing and degradation of an insulating material, it is necessary to consider the interfacial nature of the contacts between the metallic electrode and the polymer. These contacts are important since they control the amount and distribution of charge in the dielectric material. When a contact between a metal and a polymer exists, a state of equilibrium across the interfaces has to be reached so that the Fermi energy levels for both become continuous. Electrons will flow from one side to another until the Fermi levels coincide. When this is achieved, all possible mechanisms that relate to charge injection from the electrode into the polymer and degradation processes may be considered, taking into account the parameters that describe both types of material.

By studying the behaviour of photocurrent transient in polyethylene, Murata [51] concluded that there is a significant degree of localization of energy states that exist in the forbidden band at the surface region of a polymer. In addition to disorders created during crystallization such as bond adjustment, molecular folding and protrusions, these 'surface states' originate from external factors like additives, impurities and absorbed molecules. The depth of the surface region has been reported to range from several hundreds of molecules length [52] to several micrometers [53]. Figure 2.6 illustrates the extended band diagram at the metal-polymer interface.

The level of energy that an electron needs to gain in order for it to be injected from the electrode into the dielectric depends on the characteristics of the metal and polymer being considered. In the case of zero applied electric field shown by Figure 2.6, polyethylene has electron affinity χ_p of -1eV so the vacuum level will be below its conduction band. Exchange of charge between the metal electrode and the polymer establishes an equilibrium when the Fermi energies of the metal and the polymer become equal. This phenomena is known as contact charging as the exchange of charge due to electron tunnelling results in a net transfer of electrons from valence band of the metal to the surface states in the polymer and giving rise to a contact potential. As a state of equilibrium has been reached, the total energy barrier that the electron must overcome for it to be excited into the conduction band is the sum of the metal's work function φ_m and the polymer's affinity χ_p. However it is important to remember that the determination of barrier height is not as simple as outlined since the presence of physical, electrical and chemical defects at the interface (such as imperfect contact and surface roughness) has not being taken into consideration. The role of this energy barrier will be discussed further when the charge injection process is examined in the following section.

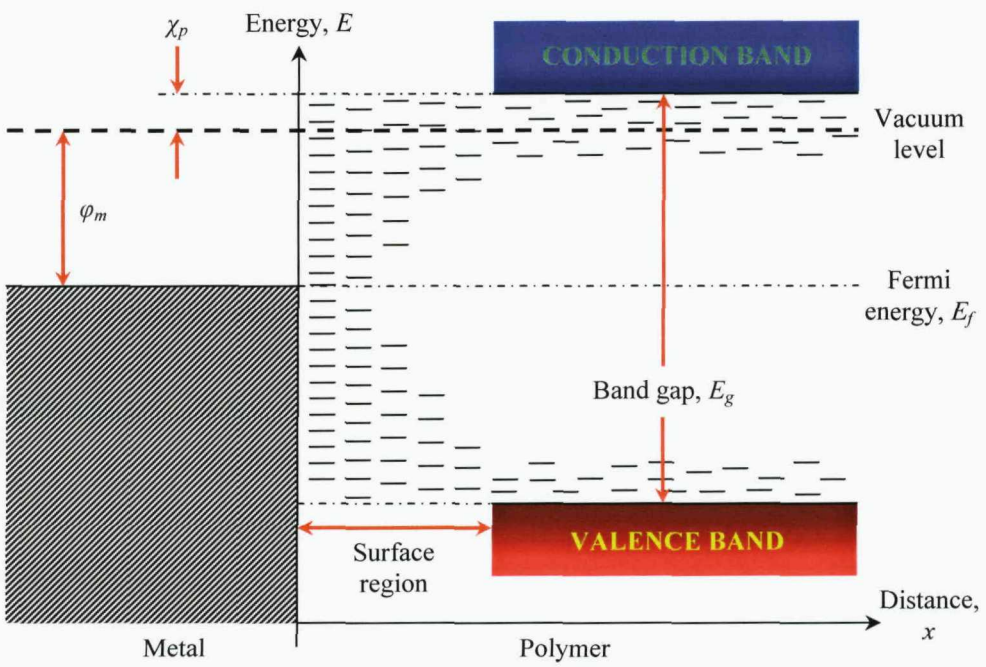

Figure 2.6: Energy scheme of the metal-polymer interface with the existence of surface states under zero applied electric field.

2.3.1 Charge Injection Process

The two most common theories related to charge injection from a metal electrode into a dielectric material are known as the Richardson-Schottky and the Fowler-Nordheim mechanisms. These processes can be explained with reference to Figure 2.7. As mentioned earlier, the energy for electrons must have in order to free themselves from a particular metal and move into a polymer is dictated by the metal's work function φ_m and the electron affinity of the dielectric χ_p. For analysis purposes, the total potential barrier for an electron to leave the metal and enter the insulator is simply denoted by φ_0, where φ_0 is essentially:

$$\varphi_0 = \varphi_m - \chi_p \qquad \{2.3\}$$

In reaching Fermi equilibrium, the electrons that leave the metal will cause the electrode to become positively charged after some time. Electrons in the polymer will then experience an electrostatic force of attraction by the positively charged metal and therefore work has to be done in pulling them apart. If the electron is at a distance x from the interface, then the distance between the electron and its corresponding image charge will be $2x$. According to the Coulomb's law, the force of attraction between these two charges, F_{image} can be written as:

$$F_{image} = \frac{e^2}{4\pi\varepsilon_0\varepsilon_r(2x)^2} = \frac{e^2}{16\pi\varepsilon_0\varepsilon_r x^2} \qquad \{2.4\}$$

where e is electronic charge (-1.60×10^{-19}C), ε_0 is vacuum permittivity (8.85×10^{-12}Fm^{-1}) and ε_r is the relative permittivity of the material. Integrating {2.4} with respect to x will give the energy required to bring the electron from position x to infinity, V_{image}:

$$V_{image} = \int_x^\infty F_{image}\,dx = -\frac{e^2}{16\pi\varepsilon_0\varepsilon_r x} \qquad \{2.5\}$$

When a constant electric field across the interface, E is applied on the other hand, the electron will experience a force proportional to its charge, $F_{field}=-eE$ and the potential energy of this electron, due to this effect, is given by $V_{field}=-eEx$. Therefore the reduced potential barrier, V may be expressed as:

$$V = V_{image} + V_{field} = -\frac{e^2}{16\pi\varepsilon_0\varepsilon_r x} - eEx \qquad \{2.6\}$$

Since the curve now has a maximum value, differentiating {2.6} with respect to x and equating it to zero yields the value of x where the stationary point occurs:

$$\frac{dV}{dx} = \frac{e^2}{16\pi\varepsilon_0\varepsilon_r x^2} - eE = 0 \qquad \{2.7\}$$

$$\Rightarrow x = \left(\frac{e}{16\pi\varepsilon_0\varepsilon_r E} \right)^{1/2} \qquad \{2.8\}$$

Substituting {2.8} into {2.6} gives the reduction of the potential energy, given as $\Delta\varphi$ in Figure 2.8, under the effect of both Coulombic image force and applied electric field. The resultant energy barrier height, φ_{res} for electrons to move from the metal into the polymer is now $\varphi_0 + \Delta\varphi$, where $\Delta\varphi$ is given as:

$$\Delta\varphi = -\left(\frac{e^3 E}{4\pi\varepsilon_0\varepsilon_r} \right)^{1/2} \qquad \{2.9\}$$

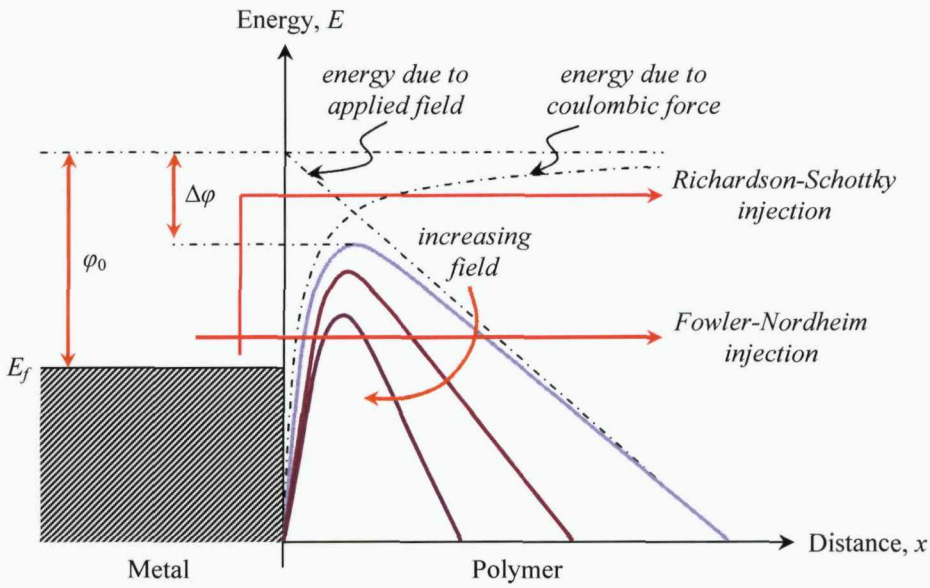

Figure 2.7: Schematic diagram for Richarson-Schottky and Fowler-Nordheim charge injection.

It has to be pointed out that not only the charge injection depends on the electric field, this mechanism is also affected by temperature since electrons can be thermally activated over the barrier and enter the polymeric material with some kinetic energy. This process is known as Richardson-Schottky thermionic emission, and expression for current density, j of a metal-polymer interface can be written as [6]:

$$j = AT^2 \exp\left(-\frac{\varphi_{res}}{k_B T} \right) \qquad \{2.10\}$$

where A is the Richardson-Dushman constant ($1.20 \times 10^6 Am^{-2}K^{-2}$), T is the absolute temperature and k_B is the Boltzmann constant ($8.62 \times 10^{-5} eVK^{-1}$). If electric field is increased, there will come to a point when the potential barrier becomes very thin (as illustrated in Figure 2.8) and electrons may be able to tunnel through the interfacial barrier into the insulator despite having insufficient thermal energy to surmount them.

The potential barrier is therefore equal to φ_0 and this process, called the Fowler-Nordheim injection is characterized by the following expression [6]:

$$j = \frac{e^3 E^2}{8\pi h \varphi_0} \exp\left(-\frac{4}{3}\left(\frac{2m}{\hbar^2}\right)^{1/2} \frac{\varphi_0^{3/2}}{eE} \right) \quad \{2.11\}$$

where h is the Planck constant (4.14×10^{-15}eVs), $\hbar$ is $h/2\pi$ and m is the effective mass of electron (9.11×10^{-31}kg).

2.4 Mechanisms for Electroluminescence

Luminescence can be defined as the emission of light resulting from atomic excitations in a certain material by sources other than a hot, incandescent body. When the atoms of the material are being excited due to the application of an electrical field, it is called electroluminescence (EL) [33]. Basically the mechanisms behind luminescence are the same for all types of excitation and can be explained using quantum mechanics theories. Electrons surrounding an isolated atom reside within an array of orbitals that are defined by a unique set of quantum numbers (or energy levels). As the atom is excited, some electrons are able to jump into free orbitals, causing different excited states to be formed.

The energy levels of the filled and unfilled electron states are governed by quantum mechanics [54]. Transitions between the various energy states are determined by transition probabilities. In particular, the spin of an electron (a quantum of angular momentum of the electron spinning on its axis) can take one of two values, either +1/2 or -1/2, and the probability of two identical electrons in the atom occupying the same energy state is zero according to the Pauli Exclusion Principle [54]. Thus the spin of the electron can lead to two different schemes for the radiative transfer back to the ground state as described below.

The discrete energy levels of an atom provide the mechanism for excitation and de-excitation and the possible emission of light. Electrons would normally occupy the lowest energy levels in an atom and the atom is therefore said to be in its ground state (denoted as S_0). Not all electrons of an atom can occupy the lowest energy level, as according to Pauli Exclusion Principle, only two electrons can occupy a given energy level and these must have opposite spin such that the total spin is zero. Excitation of an electron from one energy state to a higher energy state requires the absorption of

energy either from colliding hot electrons or by absorption of a photon of light. During the excitation process, the electron may keep its spin or reverse it dependent on the nature of the transition. If the spin of the electron is maintained during excitation, the atom is said to be in a singlet excited state (denoted as S_1) or if the spin is reversed during promotion to a higher energy state, the excited atom is said to be in an excited triplet state (denoted by T_1). The excitation into a singlet or triplet state will lead to two very different lifetimes for the excited state before transition of the excited state back to the ground state can occur. In the case of the excited singlet state, the transition of the electron back to the ground state is an allowed transition according to the Pauli Exclusion Principle; the electron will again occupy its original electron orbit such that the total spin of the energy state is zero. A transition to the ground state can occur very quickly leading to short lifetimes for the excited state ($\sim 10^{-9}$s). During its transition to the ground state, the electron must lose energy by an amount that is equal to the energy difference between the excited state and the ground state. The electron may lose energy by emission of a photon of light (radiative transition to the ground state) or by interaction with the lattice phonons (non-radiative transition to the ground state). In the case of a radiative transition of the excited singlet state to the ground state, the light emitted is called fluorescence. However, in the case of the excited triplet state, a direct transfer of the excited electron to the ground state is not possible as the electron would have the same spin as the existing electron in the ground state energy level. The excited electron must take an indirect transfer to the ground state in which the spin of the excited electron is reversed. This generally involves an interaction with the lattice phonons in which the spin of the electron is reversed before a radiative transition to the ground state can occur. This leads to much longer lifetimes for the excited triplet state (~a few seconds) and the light emitted during this indirect transition is called phosphorescence. Figure 2.8 illustrates the various excitation and recombination schemes and in addition shows that it is possible for some of the excited singlet electrons to reverse their spin and to occupy a triplet excited state via intersystem crossing. Inter-system crossing involves the exchange of energy via a transition from an excited singlet state to a triplet state with the reversal of spin of the electron.

As EL is related to the successive excitation and de-excitation (relaxation) of the valence electrons of the polymer molecules due to the application of electric field, it is imperative to consider the behaviour of the charge being injected into the material and how they can cause the creation of the excitation states.

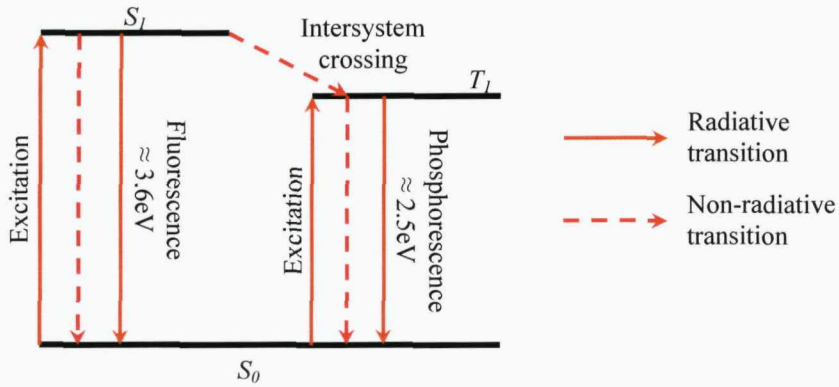

Figure 2.8: Diagram for fluorescence and phosphorescence emission.

2.4.1 Excitation Process

EL excitation processes are categorized according to their mode of excitation. The first one is known as direct high-field EL. In this process, it is assumed that an external field excites the electronic states directly. This involves the Zener effect, whereby electrons 'tunnel' from the valence to the conduction band. From a practical point of view however, this mechanism seems impossible for dielectrics such as polyethylene. The material has a large band gap (~8eV) and it is much greater than thermal energies of electrons at room temperature (~0.026eV). Thus the field required to induce this effect is much higher than the breakdown field for polyethylene.

Another mode of excitation is known as impact EL, or hot electron excitation. In this process, injected or de-trapped carriers are accelerated by obtaining sufficient kinetic energy from the applied electrical field. They collide inelastically with the molecules of the material causing them to be excited. Electrons are brought into excited states without being free to move in the conduction band due to the fact that they are still bound to the centre by electrostatic interaction. To some extent, the interaction could absorb a significant fraction of energy extracted from the field by the charge carriers; leading to ionization of molecules. An additional electron is released upon collision and it may be may be accelerated by the presence of electric field. This will cause further reactions and subsequently, electron avalanching. The molecular approach for these scenarios can be written as:

Impact excitation: $$AB + e^-_{hot} \rightarrow AB^* + e^-_{th} \quad \{2.12\}$$

Impact ionization: $$AB + e^-_{hot} \rightarrow AB^+ + 2e^-_{th} \quad \{2.13\}$$

where AB is the neutral molecule, e^-_{hot} is the hot electron, e^-_{th} is the thermalized electron, AB^* is the excited molecule and AB^+ is the ionized molecule.

It can be argued that hot electron mechanism is only relevant assuming that a significant free volume exists within the polymer and the injected electrons have a very high kinetic energy. A more realistic approach called the bipolar charge recombination model has been used by most researchers to explain the electroluminescence phenomenon [55]. This process can occur at a relatively low field as compared to that of hot electron processes since the injected carriers need not to be as energetic as the ones for impact EL. Although there is no kinetic energy involved, electronically excited states are created due to the recombination of charge carriers of opposite polarity at the trapping sites. Since it has been mentioned earlier that electrons and holes do not follow the same transport path; recombination however can still occur via internal interface states where polymer chains are exposed in free volume and sub-microvoid spaces [50].

Under dc conditions, electrons and holes are injected from anode and cathode into the polymer. These injected charge carriers slowly migrate across the material where they meet charge carriers of opposite polarity migrating in the opposite direction and hence recombination of these charge carriers can take place within the bulk of the material. On the other hand, most of the injected charge carriers are trapped in the interface region under an ac field, as they do not have sufficient time to move further into the bulk states. During the negative half cycle of the ac applied voltage for instance, some of the injected electrons will recombine with trapped holes and subsequently form an excited electron-hole pair. These trapped holes are actually those that did not manage to de-trap during the previous positive cycle when holes were being injected. This mechanism will be discussed in detail when the effect of ac fields on EL measurements is considered in Section 2.6.3.

2.4.3 Relaxation Process

After the formation of the excited states, de-excitation processes occur which are either chemical or physical in nature [38]. For a chemical process, the energy stored due to excitation can dissociate molecules into fragments and free radicals that can be very chemically reactive, leading to further degradation reactions. The excited molecular

states are transformed into excited, neutral and charged fragment molecule species, as shown below:

$$AB^* \rightarrow A + B^* \quad \{2.14\}$$

$$AB^* \rightarrow A + B \quad \{2.15\}$$

$$AB^* \rightarrow A^+ + B^- \quad \{2.16\}$$

where AB^* is the excited molecule, A,B are the neutral fragments of the excited molecules and A^+,B^- are the positive and negative charged species.

On the other hand, a physical process occurs when the excited centre returns to its ground state without any further chemical reaction. It is a purely reversible effect that can lead to fluorescence or phosphorescence emissions. In some cases, the relaxation may also be non-radiative in the sense that the energy is released thermally (in the form of phonons rather than photons). These reactions may be represented as:

Fluorescence emission: $${}^1A^* \rightarrow A_0 + {}^1hv \quad \{2.17\}$$

Phosphorescence emission: $${}^3A^* \rightarrow A_0 + {}^3hv \quad \{2.18\}$$

Energy conversion: $$A^* \rightarrow A_0 + nkT \quad \{2.19\}$$

where A_0 is the molecular ground states, ${}^1A^*$ is the first excited singlet state, ${}^3A^*$ is the first excited triplet state, ${}^1hv$ is photon energy radiated by fluorescence, ${}^3hv$ is the photon energy radiated by phosphorescence and nkT is thermal energy released as phonons.

2.5 Electroluminescence as a Pre-Breakdown Event

Radiative transitions from excited states of the order of 2-3eV above the ground state will yield photons of light having wavelengths in the visible and near infrared region of the electromagnetic spectrum. Although this level of energy is not high enough to break the covalent bond of the molecules, it is sufficient to cause serious damage to intermolecular bonds within a polymeric material [56, 57]. In addition to this, Teyssedre *et al.* [58] have observed the similarity in spectral characteristics for both EL and cathodoluminescence experiments undertaken on polyethylene; indicating that a degree of molecular deformation occurs when polymers are subjected to high electric fields. Crine [59] has further suggested that the increase in light emission in the 400-700nm wavelength corresponds to the presence of radicals within the dielectric's

vicinity and therefore indicates the build up of degradation region as these radicals could lead to more chemical reactions.

The issue of whether EL is an effect or cause of electrical degradation for insulating materials is still not clearly resolved. On one hand it can be said that EL occurs as a result of chemical reactions of injected charges with impurities that lead to low levels of energy interacting with the Van der Waals bonds of the polymer [59]. On the other hand, it can also be argued that injected charge carriers can cause molecular excitations and the relaxation mechanism will release energy in the form of photons. Whatever the answer, the discovery of faint light emission prior to dielectric breakdown [60, 61] may provide an indicator for the initiation of electrical ageing of insulation. Hence it is just safe to conclude that EL and degradation of polymers are closely related phenomena.

2.6 Measurements of Electroluminescence

Typically, the detection of degradation is achieved when ageing is already prominent; for instance when partial discharge (PD) activity already exists. As EL precedes the onset of detectable current pulses of PD, it could provide some insight about the early stages of polymer degradation. A lot of studies have been undertaken to examine the factors that influence the behaviour of this phenomenon [61-75]. The experiments to observe EL are varied based on several aspects, including the material under examination, the detection system implemented and the type of electric field being applied [61-75].

2.6.1 Detection Method and Sample Material

In observing EL, extra-sensitive optical detection methods have to be used as the light emitted is considerably faint. For this reason, researchers have opted to use photomultiplier tubes (PMT) technology [7, 61] or charge-coupled device (CCD) imaging sensor [62, 63] since they both have high sensitivity, operating over a very broad spectrum. The active area of the sample is focused onto the detector using lenses or ellipsoidal mirrors [64, 65]. The obvious advantage that a CCD setup has over a PMT system is that it can take the image of the emission as well as measure the intensity level of the light. This is the simplest way to ensure that the intensity measured is not due to other modes of discharge. There is a growing trend nowadays to

implement both devices for EL investigations [66, 67] with the intention of improving the reliability of measurement.

EL experiments have been undertaken on different types of insulating polymer, including those that are commonly used in electrical engineering. They are cross-linked polyethylene (XLPE) [67], low-density polyethylene (LDPE) [68], polyethylene naphthalate (PEN) [69], polyethylene terephthalate (PET) [69], polypropylene (PP) [70], polytetrafluoroethylene (PTFE) [70], polyvinylchloride (PVC) [70], polyetherimide (PEI) [71], polyimide (PI) [71], polyethersulfone (PES) [71], polybutadiene [72], polyolefin [73] and epoxy resins [74]. Various materials have been examined in order to understand the processes that lead to EL and see how this phenomenon can be used for pre-breakdown diagnostic purposes. Although the intensity level of the light produced is different from one material to another, it is found that all measurements exhibit a threshold-like behaviour. This could well be an indication of the onset for EL excitations; with different materials have different inception voltage. However, it is also possible to argue that this characteristic might be due to the limitation of the detection system's sensitivity, rather than giving a true physical meaning of the process itself.

2.6.2 Electric Field Configuration

Polymeric samples can be subjected to either divergent or uniform electric fields in order to generate EL. Both types of field are attained by careful sample preparation but the main disadvantage for the typical divergent configuration is that it is limited to samples that can be prepared with embedded electrodes. The uniform field, on the other hand, can be achieved easily in any kind of polymer film with metallic layers on both sides. Figure 2.9 shows the two commonly used sample configurations to investigate the behaviour of EL under divergent and uniform electric field.

In order to achieve divergent field configuration, also known as the pin-plane geometry, the sample is prepared with a needle electrode inserted into the bulk of the polymer. The insertion of the needle can be made in different ways: metallic electrodes can either be inserted into the polymer block at elevated temperature or compression-moulded into the sample, where the electrodes are sandwiched between two pre-moulded polymer plaques. Typical electrodes are made of steel or tungsten, but some

tests have been performed with embedded semi-conductor electrode tips made from partially cross-linked ribbons of carbon loaded polymer [75]. In a power cable, the insulation is not in contact with the metal but with semiconducting shields; therefore a more realistic analysis can be achieved using semicon protrusions. Prior to tests, the needle electrode is connected to high voltage whereas the ground electrode is usually a conducting plane located about 3mm from the tip of the electrode. A double-needle configuration has also been used in the past [76] and a work conducted by Griseri *et al.* [74] had a network of gold-plated tungsten wires moulded into the polymer block to achieve similar electrical field arrangement.

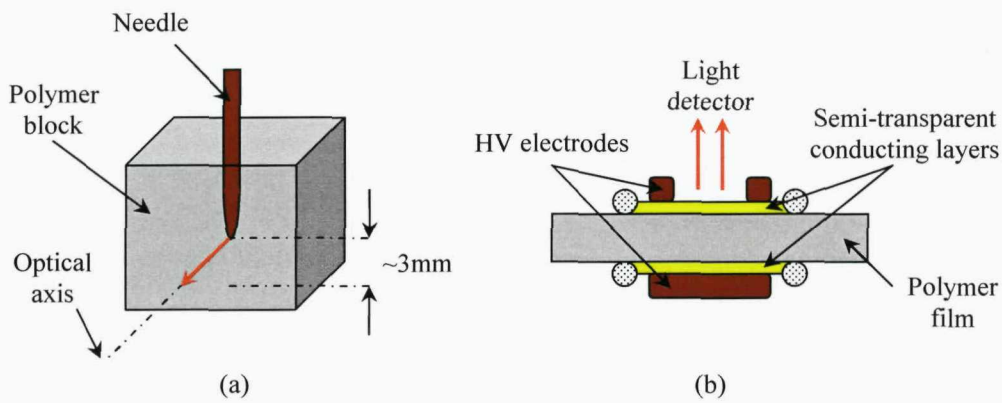

Figure 2.9: Typical (a) divergent and (b) uniform field sample configurations.

Uniform field configuration (or the plane-plane geometry) is accomplished by introducing a conducting layer on both sides of a polymer film. Previous work [77] had used a glass electrode covered with a thin, transparent metal layer where the light emitted can be detected. Nevertheless, semi-transparent metallized electrodes are usually preferred since the contact of the conducting layer with the polymer can be controlled more efficiently, resulting in better interface between the polymer and the electrode [78]. The layer is deposited by means of sputtering or thermal evaporation processes, and materials typically used as electrodes are either gold or aluminium. Since the metallic layer is semi-transparent, light can be directly detected using a ring electrode to provide electrical contact with the metallized surface of the sample.

An advantage of the pin-plane electrode geometry is that electric field enhancement at the pin tip ensures that injection of charge and therefore the generation of EL occurs at one electrode only. This allows EL to be studied as a function of the polarity of the applied voltage. This is not possible in plane-plane electrode geometry where charge

injection and EL will occur at both electrodes. The detected light in this case will be the summation of the intensities of EL that occur at both electrodes.

2.6.3 Effect of Voltage Form

Although the existence of faint light occurring prior to complete breakdown of polymeric insulations has been demonstrated extensively through experiments, the actual mechanism leading to this phenomenon is still inadequately understood. By observing EL under both dc and ac conditions however, researchers hope that it can give some insight as to how the light emission is related to the charge injection processes.

Work by Hozumi *et al.* [79] had shown a gradual increase in EL intensity when a polymer is subjected to a dc stress after a long period of time (more than 600s). It has been suggested that this effect could be due to the recombination of positive and negative charge carriers in the bulk of the material. The long period of time is required for the migration of charge carriers from the electrodes into the bulk of the material and recombination of the charge carriers occurs when the carriers meet in the bulk of the polymer. Evidence of correlation based on simultaneous EL and current measurements, demonstrating similar onset voltages also suggests that the onset voltage for EL is not limited by the sensitivity of the detection system but is related to the mechanisms occurring within the bulk of the material that give rise to EL [71]. Moreover, this threshold value decreases when temperature is increased; indicating greater numbers of charge carriers are being injected according to Richardson-Schottky equation [80].

Whilst it is probably safe to say that EL detected under dc stress occurs within the bulk of the material, the light emission observed under an ac field is more likely an interfacial phenomenon. In theory, if migration of charge carriers is small over a time period of one half cycle of the applied voltage, then injected charge will remain in the material close to the injecting electrode. In the opposite half cycle, some of this charge may be extracted while the remaining may recombine with injected charge carriers of opposite sign. Hence under these conditions, recombination and the production of EL can only occur close to the interface regions each half cycle. The fact that the threshold EL voltage for ac stress was found to be significantly lower than for dc applied voltages

[71, 80] would suggest that under alternating fields, the process is dictated by charge injection rather than a charge transport mechanism. As a consequence, various attempts have been made to determine the occurrence of EL with respect to alternating applied fields. Although these measurements were undertaken by different researchers under different field configurations, one identical observation was noted: EL is a maximum within the first and third quadrant of the applied sinusoidal voltage where the first quadrant is defined as the first positive quadrant of the applied voltage cycle. Figure 2.10 presents some of the different phase-resolved results that have appeared in literature and drawing the same conclusion.

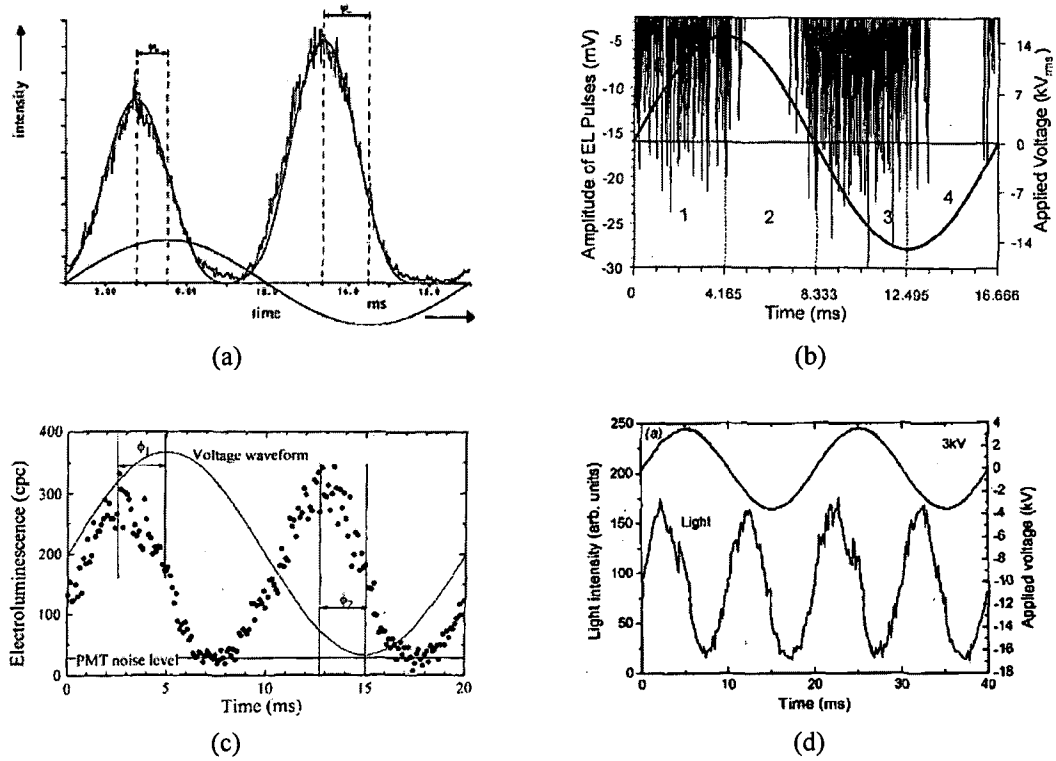

Figure 2.10: Phase-resolved EL measurements undertaken by (a) Krause *et al.* [81], (b) Bamji *et al.* [78], (c) Cisse *et al.* [82] and (d) Zhang *et al.* [83] showing intensity peaks occurring prior to the applied voltage maxima and minima.

In relation to this observation, a model has been proposed by Laurent *et al.* [84] and Bamji *et al.* [85, 86] for EL mechanism based on the bipolar recombination process. The underlying argument for this hypothesis is that it is almost impossible for electrons to gain sufficient energy from the electric field to produce ionized or excited molecules. Therefore EL emission is most likely due to recombination of charges at the trapping centres in the polymer. Figure 2.11 illustrates the proposed model.

During the negative half cycle, electrons are injected into the polymer due to the application of a high electric field. The electrons are then trapped in shallow and deep traps and some of them recombine with the trapped holes. These holes occupy deep traps (trapped during the previous half cycle) and could not de-trap and return to the electrode when the polarity was reversed. The recombination of the electrons and holes will then give rise to light emission. During the second negative quadrant of the applied voltage cycle, some of the trapped electrons will manage to de-trap but those in the deep traps will not. Therefore during the increasing positive quadrant of the applied voltage cycle, some of the injected holes will recombine with these electrons and light emission will again occur. This process is repeated every cycle of the ac voltage leading to light emission during quadrants 1 and 3 of the applied ac cycle.

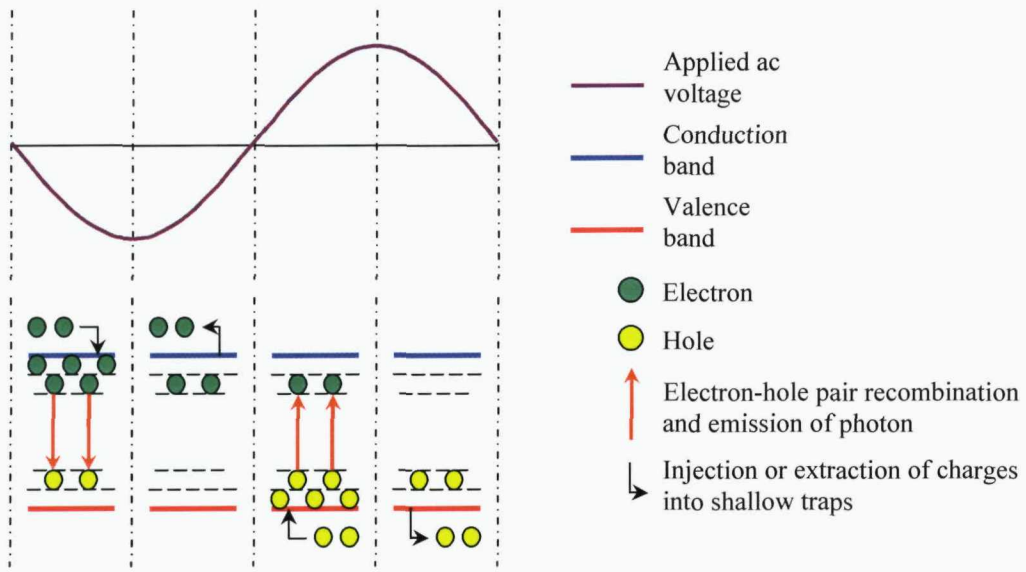

Figure 2.11: A model of charge injection mechanism under ac voltage.

2.6.4 Influence of Gases

It was found that presence of gases can, to some extent, affect the EL behaviour of polymer under the applied electrical stress. For semi-crystalline polymer, gases are dissolved and localized in the amorphous regions only, and have zero solubility in the crystalline domains [84]. Research with LDPE and XLPE materials [85, 87] have shown that absorbed gas molecules can affect the emission threshold and the amplitude of light emitted, depending on the chemical reactivity of the gas and its electron affinity. It was also found that the EL spectra from samples impregnated with various gases were identical, indicating that the recombination and therefore the light detected

was due to the recombination occurring within the host resin and not from the dissolved gases [84]. The fact that dissolved gas can affect the EL may suggest a more complex excitation scheme, than that described in Section 2.4.2, involving excitation of the dissolved gas molecules and the exchange of this energy to the polymer via interactions of the gas molecules with the polymer.

In recent years, research work has examined the role of absorbed nitrogen (N_2) on the EL behaviour [88, 89] and have come to the conclusion that the EL from degassed and N_2 impregnated samples of polyethylene are not significantly different. This is understandable since N_2 is chemically inert and therefore it will not react with radicals created by the breaking of the polymer. It also has zero electron affinity, making it unable to capture injected electrons. This would also indicate that the reduction in free volume of the polymer due to the absorption of N_2 plays little role in the formation of EL. Nevertheless, it has been observed by Shimizu *et al.* [90] that the voltage dependence measurement for samples under the influence of N_2 gas has a slightly higher EL voltage inception and lower intensity level, as shown by Figure 2.12. A possible reason for this finding is that the injected electrons have less room to acquire kinetic energy from the electric field and hence cause less ionization in the case of hot electron excitation.

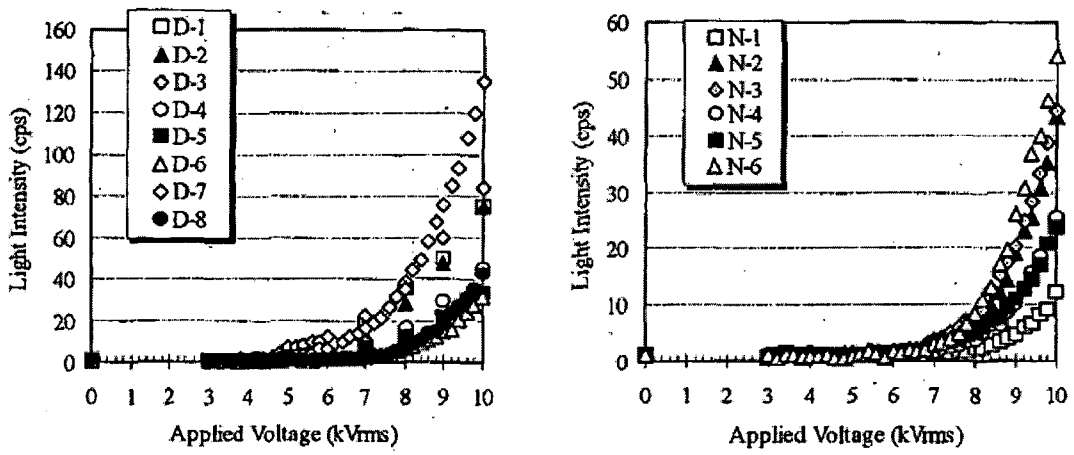

Figure 2.12: EL voltage dependence results obtained for (a) degassed and (b) N_2-impregnated LDPE samples [90]. Prefixes 'D' and 'N' in the legend refer to degassed and N_2-impregnated, whereas the numbers correspond to sample number. For example, 'D-1' represents the data obtained for degassed LDPE sample number 1.

The influence of electronegative gases such as oxygen (O_2) and sulphur hexafluoride (SF_6) on electrical tree inception has been investigated by Bamji *et al.* [88]. It was found that by lowering the concentration of these gases, the time taken to electrical tree inception will increase. This demonstrates that the presence both O_2 and SF_6 gases play an important role in the material degradation process. The strong reactivity characteristic of these gases suggests that the radical sites created on the polymer chains will react with the O_2 and SF_6 molecules, producing more breaks in the bonds [88]. In addition to this, Mizuno *et al.* [87] also suggest that the existence of oxygen can affect the metal-polymer interface by introducing new localized electronic states. The gaseous atoms or molecules absorbed at the polymer surface will be trapped at the metal-dielectric interface, leading to oxidation which then will give rise to the creation of surface states. Due to the band bending caused by such states, migration path length of injected charge carriers is reduced, which results in the enhancement of charge injection from the electrode into the surface states [87].

Although it has been found that the inception voltage reduces with the increase of electronegative gas concentration, the change in EL level is very different. As reported by Bamji *et al.* [88], the light intensity level is almost one order of magnitude higher in degassed and N_2-impregnated XLPE as compared to the SF_6-impregnated samples. Similar observation was also found by Laurent *et al.* [84] using O_2. EL emission is shown to be characterized by the presence of gas molecules that could interact with the polymer surface. Gases with high electronegativity will be able to capture the injected electrons and this will cause a reduction of light intensity since there are less charge carriers available for radiative recombination to occur.

2.7 Summary

This chapter has outlined the main features of polyethylene and how EL processes are related to its complex characteristics. Generally speaking, it can be deduced that the phenomenon occurs as a result of the interaction between the injected charge carriers from the metallic electrode with the space charge that exists within the vicinity of the dielectric material. Excited states can be generated via hot electron or bipolar charge recombination processes, and their subsequent relaxations will cause energy to be released in the form of light.

The characteristics of EL as a measure for electrical degradation in polymeric material are still unclear and a lot of research is still being undertaken to put a decisive conclusion to this statement. EL has been observed under both divergent and uniform field configurations for various types of insulating material. In understanding the relationship of the phenomenon with charge injection and transport processes, the effect of dc and ac voltages has also been investigated by different researchers. In addition, the influence of gases on EL has paved ways to examine closely what are the actual causes responsible for this light emission.

Chapter Three

MODELLING OF ELECTROLUMINESCENCE

3.1 Introduction

The occurrence of EL is related to the injection and recombination of charge carriers into the material and which may be responsible for the electrical ageing process of an insulating material and several models for the EL phenomenon have been proposed [34, 91-97]. The effects of voltage level and current density on EL for example, can be simulated and used to predict the onset of electrical degradation of polymers. This is usually achieved by examining the changes to the electric field at the injecting electrode due to the presence of the injected charge carriers [72, 98]. More importantly, the modelling of EL allows comparison to be made with the numerous experimental observations of the phenomenon. Several hypotheses have been proposed to explain the mechanisms responsible for light emission based on the results obtained

from various polymers; therefore by comparing model simulation results with experimental results, the theories relating to the existence of EL can be validated.

A lot of attention has been given to simulating EL emission in a dc field [94-97] as the mechanism describing the charge carrier transport within a dielectric material for this type of field has been well-established [99-101]. In an ac field on the other hand, the modelling of EL is different since it involves the injection and extraction of charge carriers each half cycle of the voltage applied. Nevertheless, the model described here attempts to gain a better understanding of the phenomenon occurring under ac stress. It is an extension to a previous model proposed by Alison *et al.* [92] that was based on EL observed in epoxy resin with a pin-plane geometry [102]. Modifications were made to this original model [103] in order to simulate EL in a uniform alternating field having plane-plane electrodes in which EL can occur at the two metal polymer interfaces. In addition to this, one of the key EL experiments undertaken was observing the occurrence of the light emission with respect to the applied electrical stresses (discussed thoroughly in Chapters 5 and 6). Thus it is hypothesized that by developing an EL model based on simple theories of charge injection and recombination processes, the computation results may be compared with experimental measurements in order to validate the assumption that EL is due to a bipolar recombination process.

3.2 Background Theory

It has been suggested that the existence of EL in a 50Hz ac field is more of an interfacial phenomenon rather than a bulk process [71]. This is understandable since charge injection and extraction will occur continuously each half cycle so charge carriers will not have sufficient time to migrate and recombine with those from the opposite electrode within the bulk of the insulating material. Nevertheless, some of these injected charges might not be able to de-trap themselves during extraction and thus they will form a region of 'trapped' space charge. As a result of this, the recombination of these space charges with the subsequent ones from the next half-cycle of the alternating voltage will lead to EL. In general, two primary equations describing time-dependent space charge flow for a single charge carrier in an ac field are:

$$\text{Continuity equation:} \quad \nabla \cdot j = -\frac{\partial \rho}{\partial t} \qquad \{3.1\}$$

$$\text{Poisson's equation:} \quad \nabla \cdot E = \frac{\rho}{\varepsilon_0 \varepsilon_r} \qquad \{3.2\}$$

where j is the current density (Am^{-2}), E is the electric field (Vm^{-1}), $\varepsilon_0\varepsilon_r$ is the permittivity value ($2.3\varepsilon_0$ for polyethylene), ρ is the space charge density (Cm^{-3}) and t is time (s). The transport of charge through the insulation material is not considered and charge is assumed to occupy a small region of the insulation adjacent to the injecting electrode. Using these two equations, the numerical solutions for the electric field and current density of charge carriers within a polymeric material may be obtained.

3.2.1 Formation of Space Charge Region

In order to analyze the field at the injecting electrode, E_0, only the space charge region at one side of the polymer is considered first. Figure 3.1 depicts this scenario at one electrode only and how it can affect the electric field distribution from that obtained in the absence of space charge (Laplacian field). Several assumptions were made in order to derive the field distribution. First, it is assumed that any charge injected into the material of thickness L, is uniformly distributed with a charge density of ρ within a thickness of X from the electrode surface. It is also assumed that no charge transport or diffusion occurs outside the space charge region and X remains constant over time; independent of the field applied.

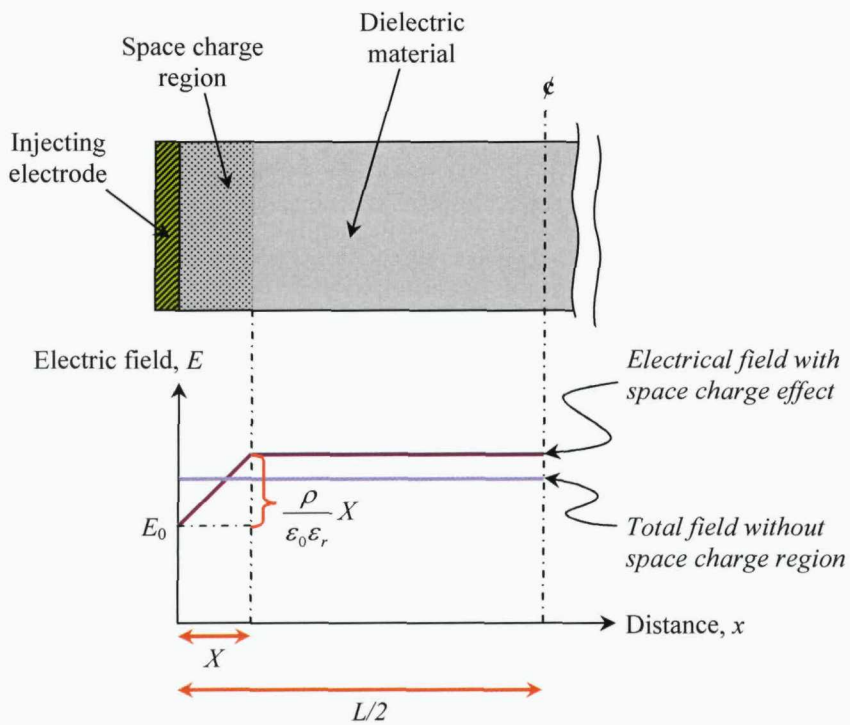

Figure 3.1: Electric field modification at the interface region of a polymer and a metallic electrode due to the presence of space charge.

The electric field as a function of distance between the electrodes is shown by the graph in Figure 3.1 for half of the parallel plate electrode configuration. Assuming that the net space charge created at any instant is homocharge in nature, the field at the injecting electrode is reduced from the Laplacian field and increases linearly with distance from the injecting electrode according to the Poisson's equation. Beyond the space charge region, the electric field is constant albeit slightly higher than the Laplacian value since the electric potential between the electrodes needs to be maintained. The potential across the material, V, is equal to the integral of the field E shown in Figure 3.1; hence the expression relating the electric field at the injecting electrode with the corresponding applied voltage and charge density as a function of time may be derived as follows:

$$V = \int_0^L E dx$$

$$= \left[\left(E_0 + \frac{\rho}{\varepsilon_0 \varepsilon_r}\right)(L - X)\right] + [E_0 X] + \left[\left(\frac{\rho}{\varepsilon_0 \varepsilon_r}\right)\frac{X^2}{2}\right] \qquad \{3.3\}$$

$$\Rightarrow E_0(t) = \frac{V(t)}{L} - \frac{\rho(t)}{\varepsilon_0 \varepsilon_r}\left(X - \frac{X^2}{2L}\right) \qquad \{3.4\}$$

Equation {3.4} corresponds to the modification of the Laplacian field due the existence of the space charge region adjacent to the injecting electrode. Differentiating this equation with respect to time gives:

$$\frac{\partial}{\partial t}\{E_0(t)\} = \frac{\partial}{\partial t}\left\{\frac{V(t)}{L}\right\} - \frac{\partial}{\partial t}\left\{\frac{\rho(t)}{\varepsilon_0 \varepsilon_r}\left(X - \frac{X^2}{2L}\right)\right\} \qquad \{3.5\}$$

$$\therefore \dot{E}_0(t) = \frac{\dot{V}(t)}{L} - \frac{\dot{\rho}(t)}{\varepsilon_0 \varepsilon_r}\left(X - \frac{X^2}{2L}\right) \qquad \{3.6\}$$

The continuity equation, indicated by {3.1}, implies that the charge density across the surface area of the injecting electrode into the space charge region is related to the rate of change of increase in charge density within the volume. Thus the continuity equation can be alternatively written as {3.7} and by incorporating this equation into {3.6} will result in Equation {3.8}.

$$\dot{\rho}(t) = \frac{j(t)}{X} \qquad \{3.7\}$$

$$\therefore \dot{E}_0(t) = \frac{\dot{V}(t)}{L} - \frac{j(t)}{\varepsilon_0 \varepsilon_r}\left(1 - \frac{X}{2L}\right) \qquad \{3.8\}$$

It is feasible to assume that the space charge region is very near to the injecting electrode (that X is much less than L). As reported in Section 2.3, the depth of surface states available in trapping charge carriers can be significantly smaller compared to the total thickness of several hundreds micrometers for a typical polymeric film. Therefore {3.8} can be further simplified to:

$$\dot{E}_0(t) = \frac{\dot{V}(t)}{L} - \frac{j(t)}{\varepsilon_0 \varepsilon_r} \qquad (\text{for } X \ll L) \qquad \{3.9\}$$

3.2.2 Charge Injection Law

To solve for electric field at the injecting electrode $E_0(t)$ as given by {3.9}, the governing equation for current density j needs to be determined. As the focus for the occurrence of EL is in an alternating electric field within a restricted region very close to the electrode, it can be said that the flow of charge carriers is predominantly dictated by the injection mechanism. In Section 2.4.1, it has been established that charge carriers from electrode can be injected into polymer via thermionic emission known as the Richardson-Schottky injection, or field dependent emission known as the Fowler-Nordheim injection. The expressions for j as a function of E for the Richardson-Schottky and Fowler-Nordheim charge injection may be written as:

$$j(E) \propto \exp\left(E^{1/2}\right) \qquad \{3.10\}$$

$$j(E) \propto E^2 \exp(-1/E) \qquad \{3.11\}$$

respectively, where both functions are the simplified versions of Equation {2.10} and {2.11}. In addition, previous EL experiments undertaken using epoxy resin samples [102] have shown that the Fowler-Nordheim equation gives a good representation for fields as high as ~1MVmm^{-1} range whereas the lower field region follows the Richardson-Schottky behaviour. Thus the behaviour of the current density can be distinguished according to the level of electric field applied.

Nevertheless, a thorough investigation conducted by Hare *et al.* [104, 105] has shown that in certain cases, the current density does not follow the thermionic nor the field emission characteristics. The numerical solution shown by Figure 3.2 indicates that there is a significant part of the field range that is not covered by either approximations, and this scenario shown for the case of charge injection overcoming potential barrier of 1eV into a dielectric with relative permittivity ε_r=2.3 at typical room temperature of

293K. Therefore a better approximation for the current density calculation has been established and it takes the form of:

$$j(E) = \alpha \exp(\beta E) \qquad \{3.12\}$$

where α and β are constants. It can be seen from the figure as well that this approximation has a very close resemblance to the Richardson-Schottky plot and has good reliability for fields up to 330kVmm^{-1}. As all experimental measurements for this work were conducted in the range of several tens of kVmm^{-1}, it is feasible to implement {3.12} into {3.9} in order to obtain the solution for the electric field at the injecting electrode and it may be simply written as:

$$\dot{E}_0(t) = \frac{\dot{V}(t)}{L} - \frac{\alpha}{\varepsilon_0 \varepsilon_r} \exp(\beta E_0(t)) \qquad \{3.13\}$$

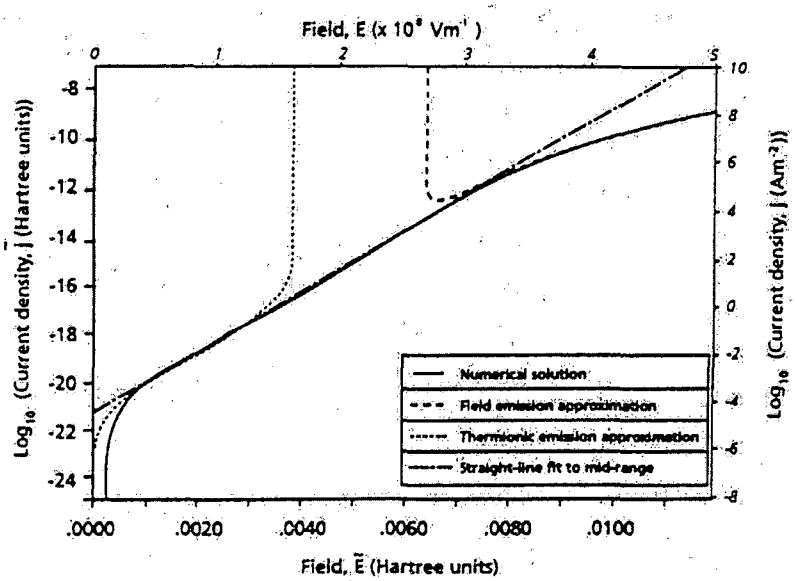

Figure 3.2: The numerical solution obtained by Hare [105] in investigating the charge injection law in a dielectric with permittivity ε_r=2.3 with potential barrier φ=1eV at room temperature T= 293K.

3.2.3 The Runge-Kutta Method

Equation {3.13} resembles an ordinary differential equation (ODE) and there are several numerical methods that can be used to formulate the solution. The Runge-Kutta analysis is one of the simplest and most common methods in solving first-order differential equations. In addition to fast computation, the method allows high degree of accuracy since it involves four evaluations per each step of iteration [106]. Figure 3.3 illustrates the schematic process in solving an ODE using the Runge-Kutta method. If the derivative of the function is written as $\dot{y}_n = f(t_n, y_n)$, then the solution for the equation per every increment h is obtained by using the following equations:

$$y_{n+1} = y_n + \frac{1}{6}(k_1 + 2k_2 + 2k_3 + k_4) \qquad \{3.14\}$$

where:

$$k_1 = hf(t_n, y_n) \qquad \{3.15\}$$

$$k_2 = hf\left(t_n + \frac{1}{2}h, y_n + \frac{1}{2}k_1\right) \qquad \{3.16\}$$

$$k_3 = hf\left(t_n + \frac{1}{2}h, y_n + \frac{1}{2}k_2\right) \qquad \{3.17\}$$

$$k_4 = hf(t_n + h, y_n + k_3) \qquad \{3.18\}$$

As indicated by the plot in Figure 3.3, the derivative is evaluated four times in each step increase; once at the initial point, twice at trial midpoints, and once at a trial endpoint. The 'trial' points, indicated by the blue dots, represent function values that are discarded once their derivatives have been calculated and used. From these derivatives, the final function value is determined (shown by a red dot) and the same iteration process is repeated in the next step increment. To solve for $E_0(t)$ using the Runge-Kutta method in the model, the time increment to calculate $\dot{V}(t)/L$ is set to 10μs whereas the value for h is fixed at 20μs.

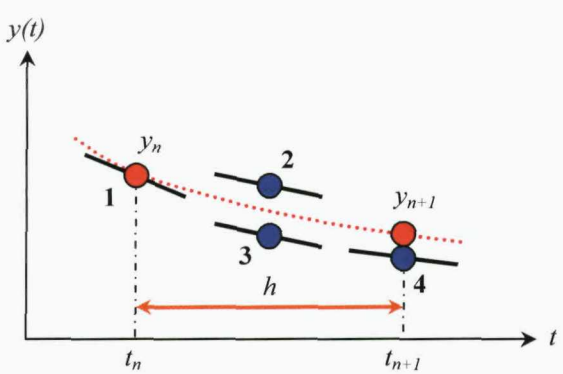

Figure 3.3: 4-point iteration process of Runge-Kutta method to solve first-order differential equation.

3.3 Modelling EL Emission

The central assumption here in modelling the occurrence of light emission is that the phenomenon occurs due to the recombination of the injected charge with the trapped charge of opposite polarity. This will subsequently lead to molecular excitation within the dielectric, which then gives rise to EL. Using the solutions obtained for the electric field at the electrode, $E_0(t)$ the corresponding current density at the electrode $j(t)$ can be determined and these will assist in the computation of the phase-resolved EL emission.

3.3.1 EL based on Bipolar Charge Recombination

It is important to develop the simulation of EL emission by considering the equations describing the current density of the injected charge carriers. Several researchers [44, 55, 107] have reported that the occurrence of EL in polymers is directly related to the injected current density; therefore the effect of charge injection over a small time interval Δt needs to be first determined. In this case, Δt is set to 20μs; which is significantly smaller than the 20ms period of the applied voltage.

Initially it is assumed that at time zero, there are no trapped electrons, $\rho_{e,t}$ or holes, $\rho_{h,t}$ in the dielectric. Charge carriers are then injected into the system and this process depends on the polarity of the electric field E_0. If the field at the injecting electrode is negative, electron injection occurs and the equations for the corresponding current and mobile charge densities over the interval time of Δt can be derived from Equation {3.12} and {3.7}. Thus the injected electron current density, j_e and the mobile electron charge density, $\rho_{e,m}$ are given as:

$$j_e = -\alpha_e \exp(-\beta_e E_0) \qquad \{3.19\}$$

$$\rho_{e,m} = j_e \frac{\Delta t}{X} \qquad \{3.20\}$$

respectively. If E_0 is positive on the other hand, injection of holes occur so its current density, j_h and the mobile charge density, $\rho_{h,m}$ can be written as:

$$j_h = \alpha_h \exp(\beta_h E_0) \qquad \{3.21\}$$

$$\rho_{h,m} = j_h \frac{\Delta t}{X} \qquad \{3.22\}$$

It is assumed that for every time interval, the charge carriers injected will either be trapped or recombine with the trapped charges of the opposite polarity, as illustrated by

Figure 3.4. The mobile-trapped charge recombination density over the time interval is proportional to the density of mobile and trapped charges in such a way that:

$$r_{e,m} = \left| M_{e,h} \rho_{e,m} \rho_{h,t} \right| \quad \{3.23\}$$

$$r_{h,m} = \left| M_{h,e} \rho_{h,m} \rho_{e,t} \right| \quad \{3.24\}$$

where $r_{e,m}$ is the recombination density for mobile electrons and trapped holes, $r_{h,m}$ is the recombination density of mobile holes and trapped electrons and $M_{e,h}$ and $M_{h,e}$ are the respective recombination coefficients. The resultant EL intensity, I in the time interval Δt is assumed to be proportional to the recombination rate [92] and therefore can be expressed as:

$$I = \frac{A\left(r_{e,m} + r_{h,m}\right)}{\Delta t} \quad \{3.25\}$$

where A is the photon detection coefficient. Bearing in mind that only the processes at one electrode are being considered so far, the total light intensity should include the emission taking place at the secondary electrode. In an alternating field, whenever there is electron injection from one electrode, there will be holes injected simultaneously from the other electrode. The light may be transmitted through the sample and therefore the total EL intensity, I_{total} may be extended from Equation {3.25} into the following expression:

$$I_{total} = I_1 + I_2 \quad \{3.26\}$$

$$= \frac{A\left(r_{e,m} + r_{h,m}\right)}{\Delta t} + \frac{AB\left(r_{e,m} + r_{h,m}\right)}{\Delta t} \quad \{3.27\}$$

where I_1 is the intensity from electrode near the CCD camera, I_2 is the intensity from the secondary electrode at the other side of the sample and B is the transmission coefficient for the light propagating through the dielectric. In the simulation, A is set to 1 whilst B is set to 0.8; assuming loss of emission by 20% travelling from one electrode to the other.

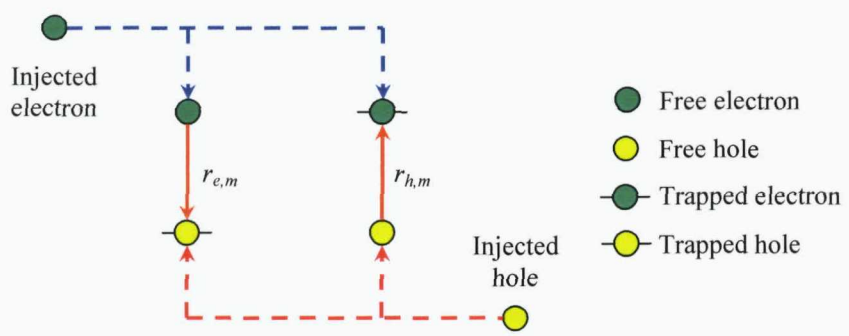

Figure 3.4: EL due to the bipolar recombination process between mobile and trapped charge carriers.

It should be noted as well that the recombination process will deplete the trapped charge densities. At the end of the time interval, the trapped electron charge density is reduced by an amount $q_h r_{h,m}$ and by $q_e r_{e,m}$ for the trapped hole density; where q_h and q_e are the charge on a hole ($1.6\text{x}10^{-19}$C) and an electron ($-1.6\text{x}10^{-19}$C) respectively. The remaining mobile charge is then trapped and the new amount of trapped charges available for the next iteration can be written as:

$$\rho_{e,t\,new} = \rho_{e,t\,old} + \rho_{e,m} - q_e r_{e,m} + q_h r_{h,m} \qquad \{3.28\}$$

$$\rho_{h,t\,new} = \rho_{h,t\,old} + \rho_{h,m} - q_h r_{h,m} + q_e r_{e,m} \qquad \{3.29\}$$

As no more mobile charges exist, both mobile charge densities $\rho_{e,m}$ and $\rho_{h,m}$ are equated to zero by the end of Δt. In the next time increment, a fraction of the injected mobile charge carriers will again recombine with charges that have accumulated in deep traps during the previous time intervals enabling the EL intensity to be calculated for the next time step. The calculations are repeated for each time step allowing the EL intensity to be simulated as a function of time.

3.3.2 Boundary Conditions and Analytical Solutions for Sinusoidal Applied Voltages

As the main objective of the model is to simulate EL emission in an alternating field, the applied voltage is therefore set to be sinusoidal and takes the form of:

$$V(t) = V_0 \sin(\omega t) \qquad \{3.30\}$$

where V_0 is the amplitude of the voltage applied, ω is the radian frequency and t is time. In addition to this boundary condition, two analytical solutions for time derivative of $E_0(t)$ and $j(t)$ can be derived under the special conditions of no charge injection and when saturation of $E_0(t)$ occurs. The first is determined by assuming that at any time there is insufficient electric field to inject significant charge carriers into the polymer to modify the injection field. In this case the current density is set to zero and hence Equation {3.9} is reduced to {3.31} and further integration with respect to time on both sides of the equation will lead to {3.32}:

$$\dot{E}_0(t) = \frac{\dot{V}(t)}{L} \qquad \{3.31\}$$

$$\therefore E_0(t) = \frac{V_0 \sin(\omega t)}{L} \qquad \{3.32\}$$

which is essentially the Laplacian field and is in phase with the alternating applied voltage. Secondly, if sufficient charge is injected such that the field at the injecting

electrode becomes constant then the time derivative of $E_0(t)$ will be zero. In the case of an initial injecting field of zero at time t=0 and that sufficient charge injection always occurs that the time derivative of the injecting field remains zero, then the current density, $j(t)$ will be given by Equation {3.9} with $\dot{E}_0(t) = 0$ giving Equation {3.33}. With Equation {3.30}, Equation {3.34} is obtained and hence if sufficient charge is always injected to reduce $\dot{E}_0(t)$ to zero for all time, then the current density will be in quadrature with the applied voltage.

$$j(t) = \varepsilon_0 \varepsilon_r \frac{\dot{V}(t)}{L} \qquad \{3.33\}$$

$$\therefore j(t) = \varepsilon_0 \varepsilon_r \frac{\omega V_0 \cos(\omega t)}{L} \qquad \{3.34\}$$

3.3.3 Simulation Algorithm

Based on the description of current density, charge density and recombination processes, the program to simulate EL phenomenon in a polymeric material has been developed. The program was written using MATLAB® programming language created by The MathWorks Inc. and the basic coding for the simulation is included in Appendix A.1.

The model operates by obtaining the solution for the electric field $E_0(t)$, and then calculating the corresponding current density $j(t)$ within a period of time. By using the solutions of these two equations, the numerical values for EL intensity, $I(t)$ are simulated assuming that light emission is proportional to this recombination rate due to the interaction of the mobile and trapped charges within the two defined space charge regions. The graphical outputs for $E_0(t)$, $j(t)$ and $I(t)$ can therefore be plotted separately for various inputs. A block diagram describing the algorithm for the overall simulation is shown by Figure 3.5.

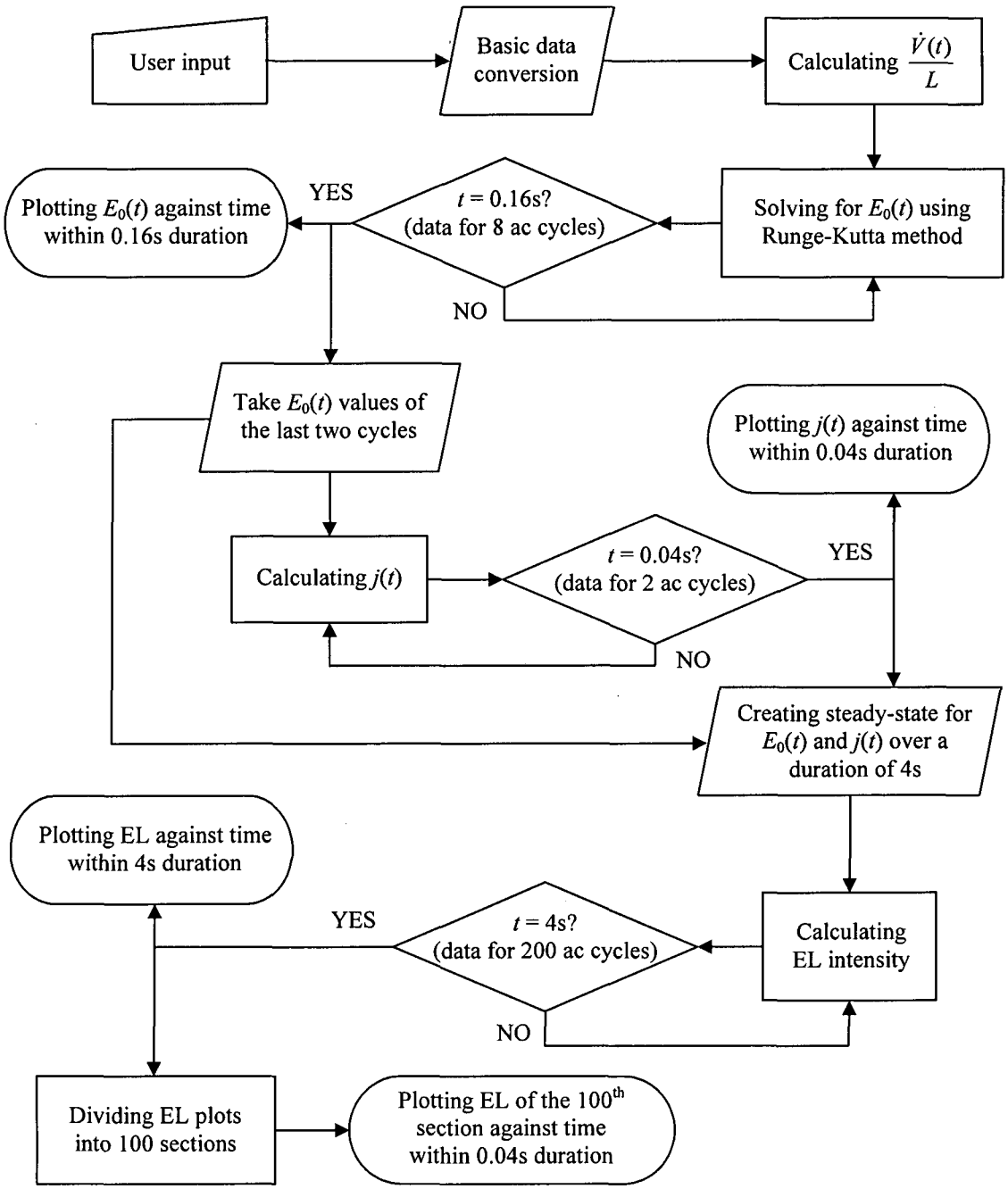

Figure 3.5: Flowchart describing the steps undertaken for modelling EL at the surface region of a polymer under a uniform ac field configuration.

3.4 Results of Computation

The determination for constants α and β of the current density equation can be obtained based on the linear approximation achieved by Hare [105]. The approximation, written as {3.35}, is in base 10 so by simply changing the base into natural logarithm the current density equation can be alternatively written as {3.36} and therefore the values of α and β may be estimated.

$$\log_{10}(j) = -4.5 + 3.0\times10^{-8}E \qquad \{3.35\}$$

$$\Rightarrow j = (3\times10^{-5})\exp((7\times10^{-8})E) \qquad \{3.36\}$$

Typical values of several other parameters used in solving the equations describing the iteration process must be defined prior to the initialization of EL modelling. They are defined in Table 3.1. Most of these parameters are those that were defined previously in [92] but for this simulation, the recombination coefficients $M_{e,h}$ and $M_{h,e}$ are set to be equal assuming that the emissions caused by electrons and holes are of the same magnitude. Similarly, the injection law for electrons and holes was also made the same by using the same values of α and β for the injection of both charge carriers.

Table 3.1: Pre-defined values of the EL simulation parameters.

Symbol	Definition	Value
α	Charge injection constant	$3\text{x}10^{-5}\text{Am}^{-2}$
β	Charge injection constant	$7\text{x}10^{-8}\text{mV}^{-1}$
Δt_1	Time increment for solving Laplacian field	10μs
Δt_2	Time increment for solving E, j and I	20μs
ε_0	Permittivity of vacuum	$8.85\text{x}10^{-12}\text{Fm}^{-1}$
ε_r	Relative permittivity	2.3
ω	Angular frequency of the applied voltage	100πHz
$M_{e,h}$	Mobile electron - trapped hole coefficient	$1.25\text{x}10^{12}\text{m}^3\text{C}^{-2}$
$M_{h,e}$	Mobile hole - trapped electron coefficient	$1.25\text{x}10^{12}\text{m}^3\text{C}^{-2}$
q_e	Charge of an electron	$-1.6\text{x}10^{-19}\text{C}$
q_h	Charge of a hole	$1.6\text{x}10^{-19}\text{C}$
A	Transmission coefficient at electrode 1	1
B	Transmission coefficient at electrode 2	0.8
L	Thickness of polymeric sample	100μm
X	Thickness of space charge region	0.01μm

3.4.1 Applied Fields Higher than 100kVmm^{-1}

Figure 3.6 (a) and (b) are typical computation results for the electric field at the injecting electrode E_0 and the current density j respectively, by applying sinusoidal voltage of peak values of 15kV, 20kV and 25kV. As the voltage applied is increased, the Laplacian field (i.e. the field in the absence of space charge) is perturbed (no longer sinusoidal) and the peak value becomes saturated. Increasing the applied voltage only increases slightly the saturated electric field as can be seen in Figure 3.6 (a). This is because by applying sufficiently large alternating voltage, there will be times during the cycle when sufficient charge is injected to significantly modify and limit the electric field at the injecting electrode such that $\dot{E}_0$ becomes close to zero. The current density during this time when field limiting occurs follows Equation {3.34} and by substituting {3.12} into this equation, the saturated electric field E_s is given by:

$$\alpha \exp(\beta E_s) = \varepsilon_0 \varepsilon_r \frac{\omega V_0 \cos(\omega t)}{L} \qquad \{3.37\}$$

$$\Rightarrow E_s = \frac{1}{\beta} \ln\left(\frac{\varepsilon_0 \varepsilon_r}{\alpha} \frac{\omega V_0 \cos(\omega t)}{L} \right) \qquad \{3.38\}$$

Equation {3.38} indicates that the saturation of electric field at the injecting electrode can only occur when the peak Laplacian electric field (given by V_0/L) is greater than E_s. With reference to Equation {3.38}, the saturation field is primarily determined by the injection coefficient β and due to the logarithm term, only weakly affected by the injection coefficient α and the peak value of applied voltage V_0. Figure 3.6 (b) shows the corresponding current density due to the significant charge injection during field limiting with increasing applied field. It is observed that the phase at which the current density peaks during each half cycle is shifted to an earlier phase angle as the applied voltage is increased.

The modelled EL emission over the first 200 cycles of the applied voltage is shown in Figure 3.7 and based on the numerical values calculated for E_0 and j for 200 cycles of the applied voltage shown in Figure 3.6. It can be seen from the simulated EL in Figure 3.7 (a) that the light intensity each half cycle increases with time and then achieves steady-state condition in less than 0.5s. The initial exponential increase in EL intensity is a consequence of the bipolar charge recombination model and is due to a corresponding increase in the number of deep trapped electrons and holes with time. Steady state is achieved when the amount of charge injected into deep traps each half

cycle is balanced by that lost due to recombination of the charge carriers each half cycle. Figure 3.7 (b) shows the EL intensity plotted for two cycles of the applied voltage. The similarity in the wave shape compared with that of the current density (as shown in Figure 3.6 (b)) demonstrates that the EL is proportional to j and that the phase corresponding to the peaks in the EL intensity are also shifted to earlier times (and hence, decreasing phase angles) when the applied voltage is increased.

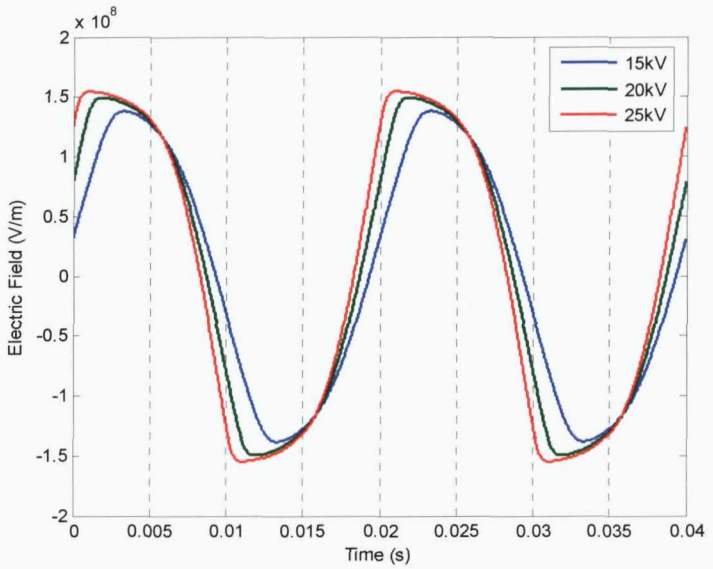

(a)

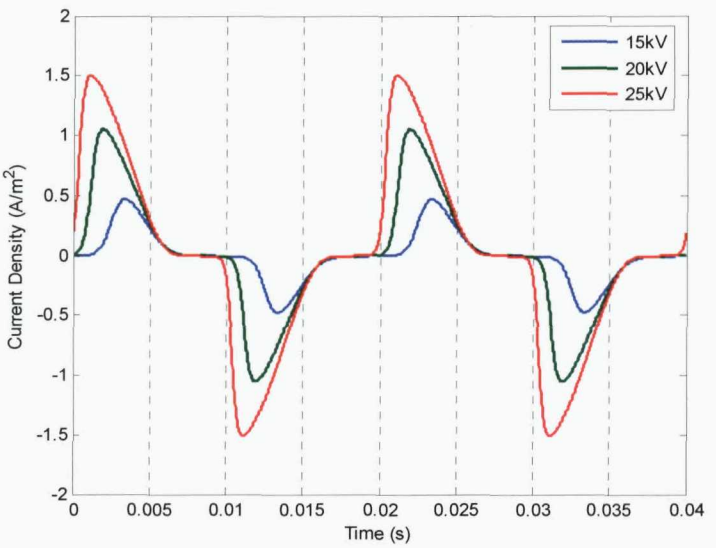

(b)

Figure 3.6: Graphical representation of the solutions obtained for (a) electric field at the injecting electrode, E_0 and (b) current density j for 50Hz alternating applied voltages of 15kV, 20kV and 25kV peak.

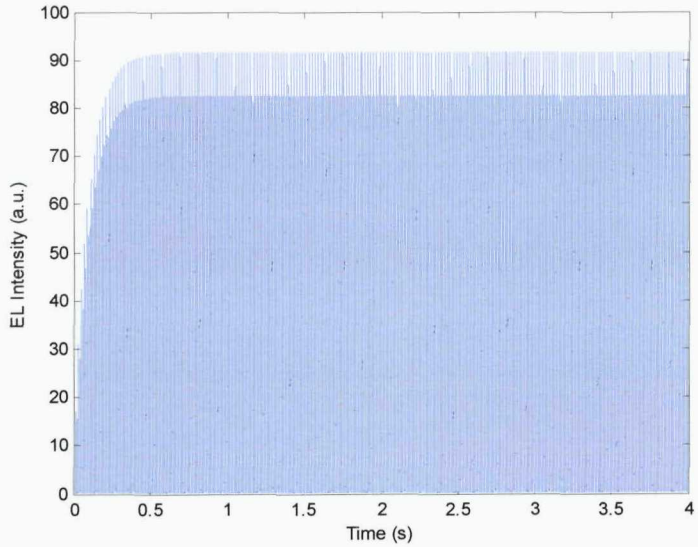

(a)

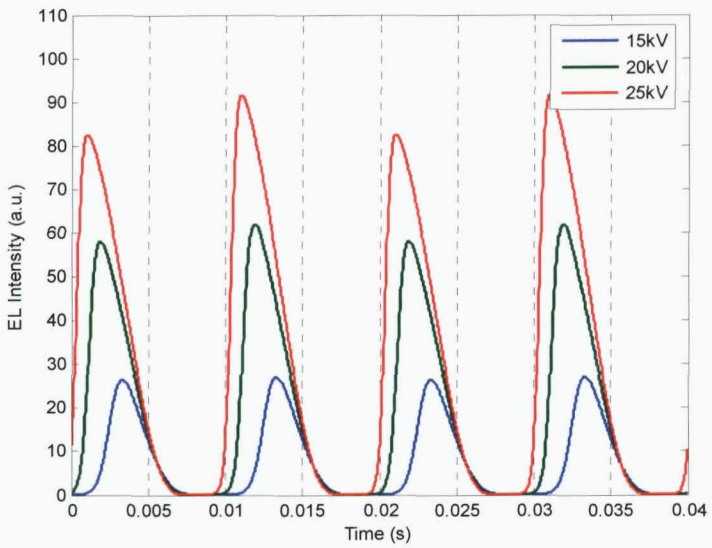

(b)

Figure 3.7: (a) Simulated growth of EL due to applied voltage peak of 25kV and (b) variation of EL emission with increasing electrical stresses.

3.4.2 Applied Fields Lower than 100kVmm^{-1}

Solutions for applied electric fields lower than 100kVmm^{-1} were also obtained and typical results are shown by Figure 3.8 and 3.9. The electric field distribution in Figure 3.8 (a) suggests that there is no significant change on the field at the injecting electrode so the plot matches the Laplacian field. From this observation, it can be deduced that the applied voltages are not high enough to inject significant amount of charges into the system to cause field alteration. This agrees with the numerical values obtained for the current density shown by Figure 3.8 (b). It can be seen that the corresponding current

density values are very small as compared to the maximum current limited by Equation {3.4}; therefore the resultant field will not saturate. This also explains the absence of changes in the phase angles of the current density peaks as the applied voltage is increased.

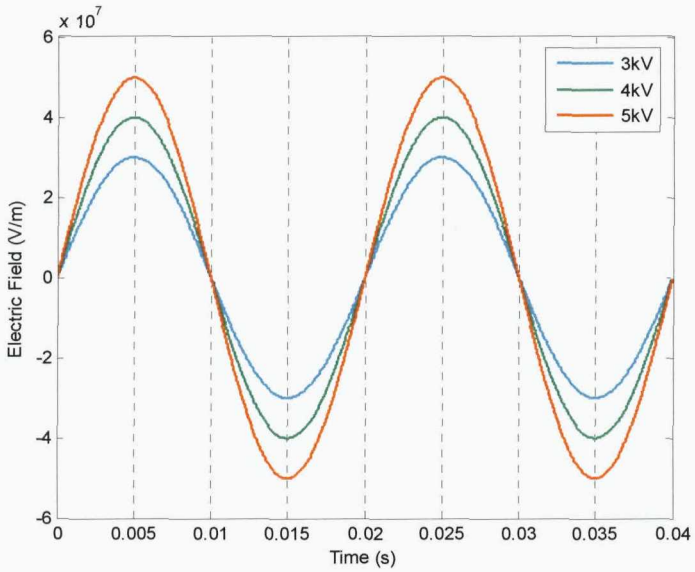

(a)

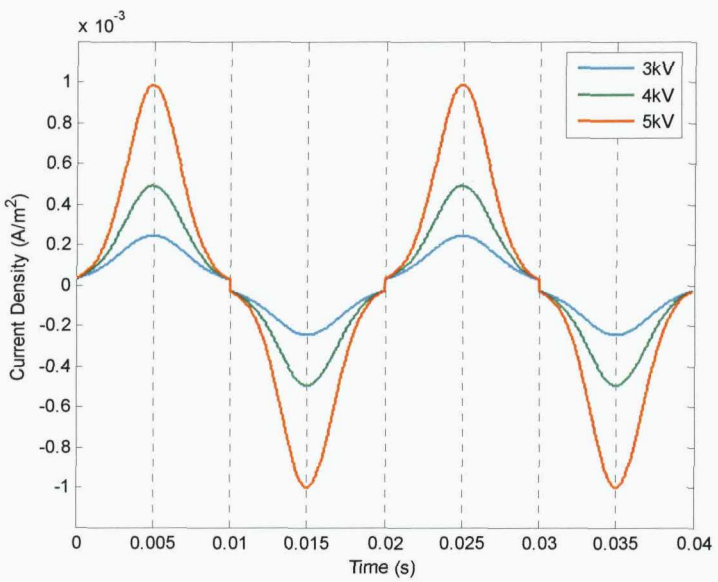

(b)

Figure 3.8: (a) Electric field distribution and (b) the corresponding current density by applying 30, 40 and 50kVmm^{-1} across the dielectric.

The simulated EL emission per two ac cycles using the same range of voltages is illustrated in Figure 3.9 (a). The result still follows the current density plot and there is not much difference in the position of the peaks when the applied voltage is varied.

Due to the fact that these applied fields are not sufficiently high to cause considerable charge injection, the simulated rise of the EL emission with respect to time before it achieves saturation becomes very slow as expected and is shown in Figure 3.9 (b).

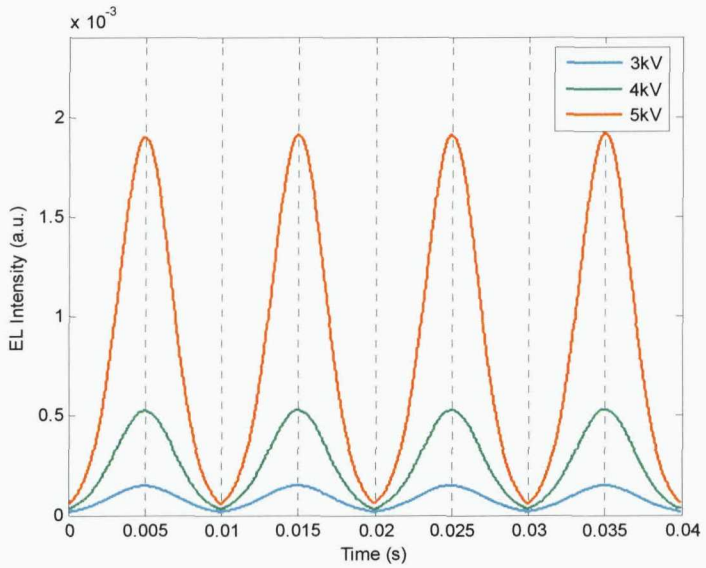

(a)

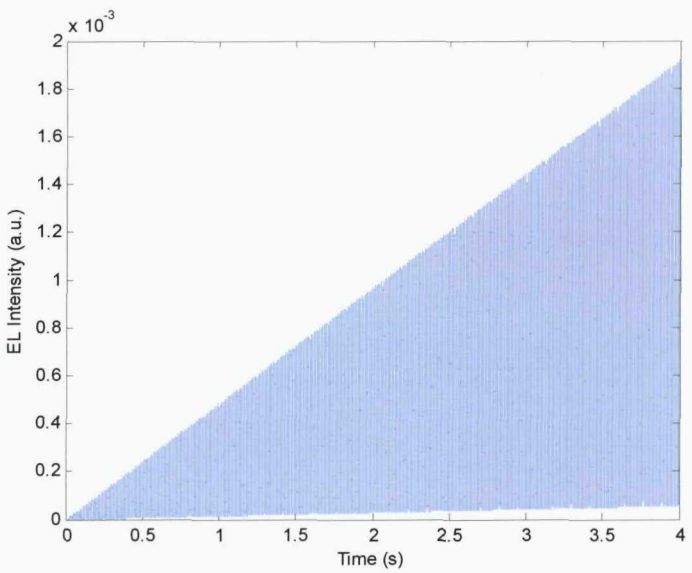

(b)

Figure 3.9: Simulated EL within a period of (a) 0.04s and (b) 4s by applying 30, 40 and 50kVmm^{-1} across the dielectric.

However, the coefficient for the recombination between mobile and trapped charges, which is a major parameter in the EL intensity calculations, used in the model was based on the values defined in Table 3.1. These values are from the original modelling work by Allsion *et al.* [92] which were derived from an experimental observation

[102]. Simulation was repeated for the same applied voltage but with different recombination density coefficients to check the effect of varying this parameter. The results are shown in Figure 3.10 and it can be seen that the growth of simulated EL is becoming faster with the increase of the recombination coefficient values. Thus it can be said that the time constant for the exponential rise of EL intensity is inversely proportional to the recombination coefficients.

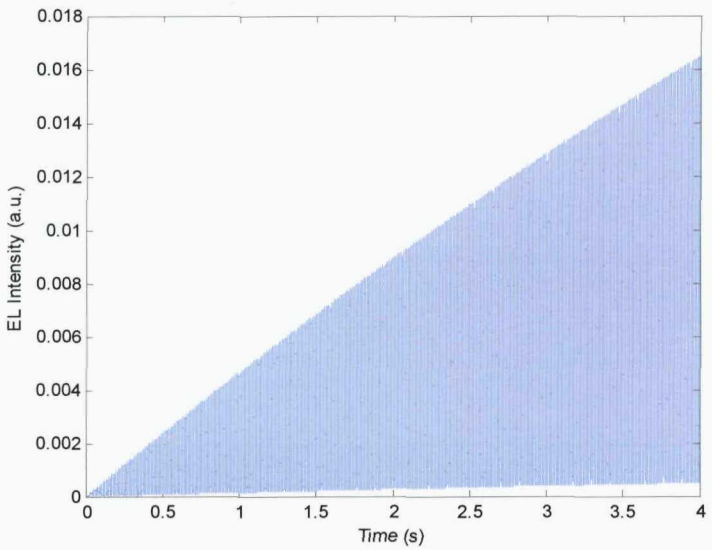

(a)

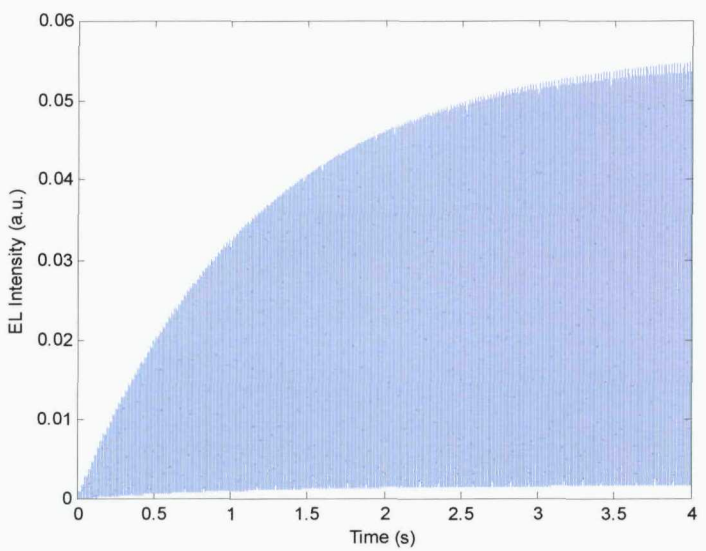

(b)

Figure 3.10: EL emission obtained by applying 50kVmm^{-1} with recombination coefficients set to the values of (a) $M_{e,h}$=$M_{h,e}$=1.25x10^{13}m^{3}C^{-2} and (b) $M_{e,h}$=$M_{h,e}$=1.25x10^{14}m^{3}C^{-2}.

3.4.3 Effect of Injection Law Parameters

So far, the constants α and β used in the injection law for electrons and holes have the values $3x10^{-5}Am^{-2}$ and $7x10^{-8}mV^{-1}$ respectively. These values chosen for the initial simulations were those found to be appropriate for the case of charge injection from a tungsten needle into epoxy resin [102]. However, in this work the materials under study were LDPE, PET and PEN, and the electrodes were formed by gold sputtering. The work function differences between tungsten and gold and the different electron affinity of these materials compared with epoxy resin are likely to make it necessary to modify the values of the injection law parameters for electrons and holes in order to be able to fit the simulation data with experimental data. In this section, the effect of varying the injection law parameters α and β for the injection of electrons and holes on the simulated charge injection and EL were examined. The voltage used for these simulations was 6kV peak at 50Hz, a typical value for the applied voltage used in the experimental work. These observations would therefore aid the process of fitting the simulations to the experimental data.

Figure 3.11 and 3.12 show the effect of varying α and β with a constant applied voltage lower than 10kV; in this case 6kV. All other parameters remain the same as defined in Table 3.1. From these results, it can be seen that the saturation of electric field and the significant increase in current density are achieved by changing the values of the current density constants. In addition, the effect of this field limiting process does not depend on one constant over another but instead a combination of both. This is understandable since both constants affect Equation {3.38} with different proportions. The variation of the values used for α and β in the calculation of Figure 3.11 and 3.12 is summarized in Table 3.2. The simulated EL emission plots corresponding to the numerical values given in Table 3.2 for the injection law parameters α and β are shown in Figure 3.13. Here the simulated EL can be seen to be proportional to the absolute value of the injection current as shown in Figures 3.11 and 3.12. The simulations of EL demonstrate that increases in the values of α and β enhance charge injection for a given voltage and increase the level of EL intensity. In addition, increasing α and β leads to a reduction in the phase angle corresponding to the peaks in the current density and EL intensity. The effect of increasing β is to produce a skewed intensity-phase distribution while increasing α maintains the symmetry in the EL-phase distribution.

Table 3.2: Different values of α and β used to compute the solutions for electric field, current density and EL emission due to the application of 60kVmm^{-1} across a polymer.

Figure	Curve	α (Am^{-2})	β (mV^{-1})	Figure	Curve	α (Am^{-2})	β (mV^{-1})
	1	3.0x10^{-5}	7.0x10^{-8}		1	3.0x10^{-5}	7.0x10^{-8}
3.11	2	3.0x10^{-5}	1.5x10^{-7}	3.12	2	5.0x10^{-3}	7.0x10^{-8}
	3	3.0x10^{-5}	2.0x10^{-7}		3	9.0x10^{-3}	7.0x10^{-8}
	4	3.0x10^{-5}	3.0x10^{-7}		4	2.0x10^{-2}	7.0x10^{-8}

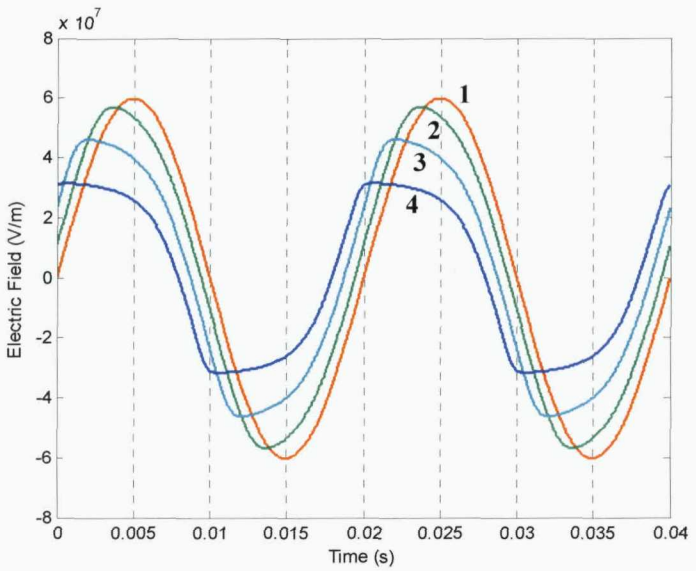

(a)

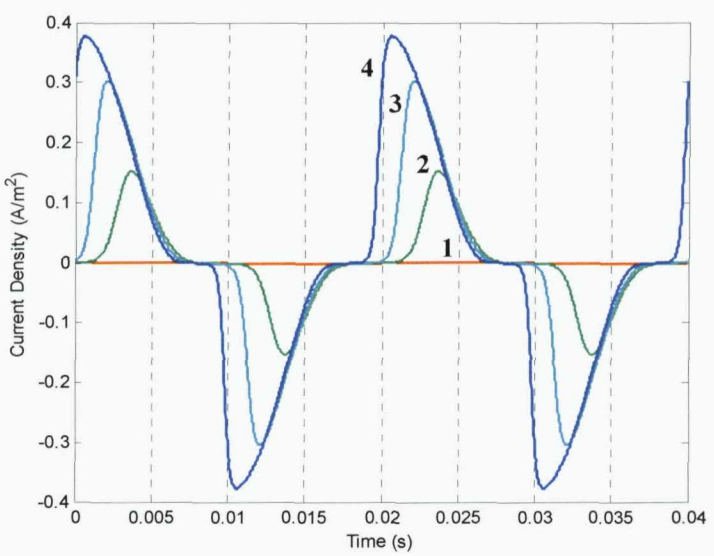

(b)

Figure 3.11: (a) Electric field and (b) current density plots by varying the constant β as defined in Table 3.2, with applied voltage peak fixed at 6kV.

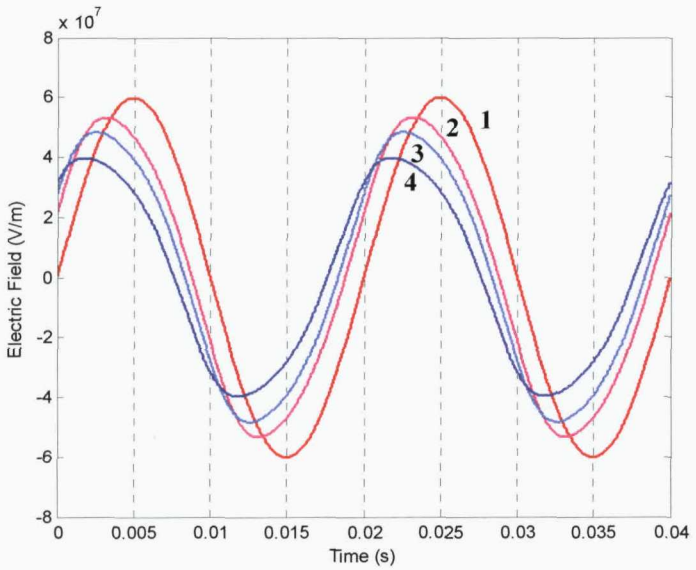

(a)

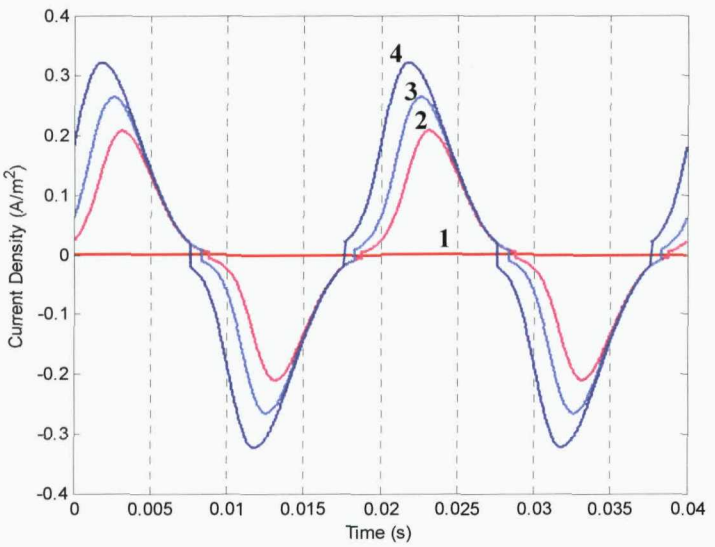

(b)

Figure 3.12: (a) Electric field and (b) current density plots by varying the constant α as defined in Table 3.2, with applied voltage peak fixed at 6kV.

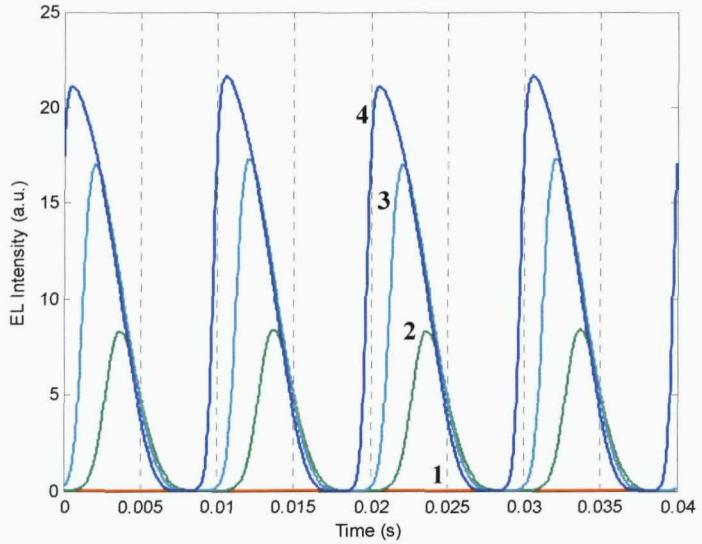

(a)

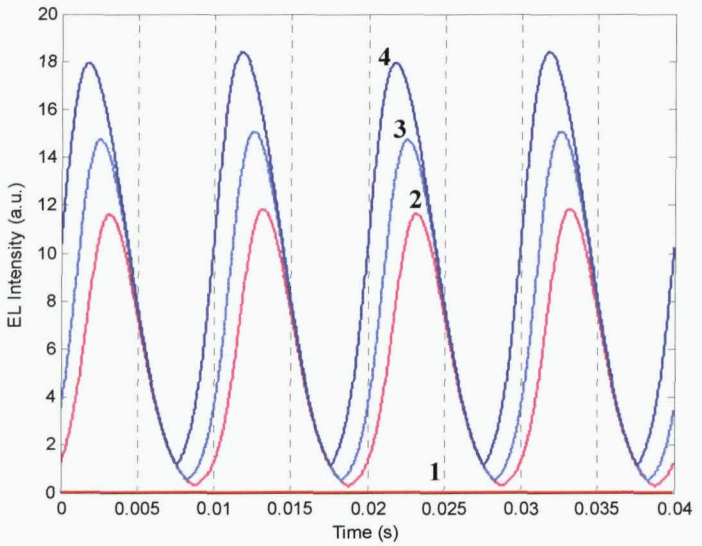

(b)

Figure 3.13: The corresponding simulated EL intensity with the variation of the constant (a) β and (b) α based on the values obtained from Figure 3.11 and 3.12 respectively.

3.5 Summary

To summarize, this chapter describes a simulation model of EL under uniform ac electrical stresses. The phenomenon is assumed to occur within a small region near the polymer surface, and the model is developed by incorporating the charge injection mechanism with the subsequent recombination processes between mobile and trapped charges inside the material. The simulation algorithm explains the necessary steps in simulating EL based on the numerical solutions obtained for the electric field strength and current density at the injecting electrode.

The simulation results obtained have shown that the EL phenomenon occurs within the first and third quadrants of the alternating voltages and it directly correlates to the injection current density values. In addition to that, the distribution of electric field is only modified when there is a sufficient flow of charges into the polymer, and this depends on the level of applied voltages as well as the constants that describe the charge injection mechanism. These variables have different degrees of influence on the computation of the electric field, current density and ultimately, EL emission.

Chapter Four

ELECTROLUMINESCENCE EXPERIMENTS

4.1 Introduction

An experimental arrangement was designed, built and then further developed to measure and monitor EL on insulating samples in a uniform field configuration at room temperature under ac stresses. This arrangement has been used previously for a range of measurements on typical dielectric materials [108-110]. Measurements are undertaken on a thin polymeric film that is sandwiched between two thin semi-transparent gold layers in order to allow a uniform electrical field to be applied. The setup is unique since it utilizes a Peltier cooled charge coupled device (CCD) camera as its detection mechanism, as opposed to using a conventional photomultiplier tube for measuring light intensity. This ensures that the measured light intensity is not due to another mode of discharge, for instance glow discharge or partial discharge. In

addition to temporal and spatial measurements, the system allows spectral analysis of the emitted light to be obtained using an optical filter wheel placed between the camera and the sample. The system can also be reconfigured to determine the phase angle relationship of EL with respect to the voltage applied. The software of the camera is triggered at the zero crossing of the positive half-cycle in order to synchronize the light emitted with the ac applied voltage.

4.2 Sample Preparation

The characteristics of EL were compared using three different insulating polymers obtained from Goodfellow; additive-free low density polyethylene (LDPE), biaxially-oriented polyethylene terephthalate (PET) and polyethylene naphthalate (PEN). LDPE was chosen since this material is widely used in high voltage cable applications, whereas the selection for PET and PEN films were based on the fact that the EL phenomenon is relatively better characterized in these materials [38]. A comparison of the measured EL characteristics between the three different types of polymer will be discussed in Chapters 5 and 6. The materials were supplied as thin films with thickness of 100±5μm for LDPE and PET, and 125±5μm for PEN. In order to allow a uniform electrical field across the polymer, both sides of these films were metallized with a semi-transparent layer of gold by cold sputtering using Emitech K550X coater (Figure 4.1). This method was chosen over the conventional thermal evaporation method in order to avoid sample heating.

To create circular gold electrodes on both sides of the sample, the polymer film was placed between two flat plates, each having a circular hole of 35mm diameter in the middle. The sample was then placed in the chamber at the coater's anode, facing the gold target which was connected to a negative voltage supply. In order to evacuate as much contamination as possible, the chamber was pumped down to a pressure around 0.1 mbar and subsequently, argon gas introduced automatically into the evacuated chamber until a stable pressure of 0.4 mbar was achieved. After that, a sputtering current of 25mA was applied to the cathode and this initiated glow discharge and ionization of the argon gas molecules. The accelerated ions then strike the target and remove gold atoms that are then deposited onto the surface of the film. The thickness of the gold layer depends on the duration of the sputtering process; so by fixing its deposition current to 25mA, the thickness of the electrode can be determined based on

the coater's sputtering rate shown in Appendix B.1. Sputter time of 2.5 minutes with ~20nm thick of gold layer was chosen for the entire experiment since it provides reasonable electrode conduction as well as good optical transmission for the detection system.

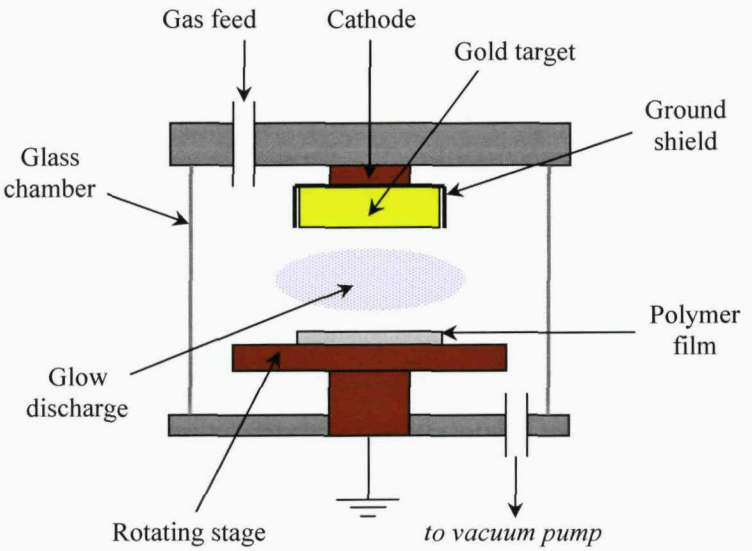

Figure 4.1: Cold sputtering using K550X sputter coater.

Once the sputter coating process was completed, silicone rubber was applied at the periphery of the metallized area. This is to reduce the likelihood of other forms of discharge and the corresponding production of light from a discharge site due to the intense electrical field strength created at the electrode edges when a high voltage is applied to the sample. An example of a prepared sample and its corresponding microscopic observation are shown in Figure 4.2 (a) and (b) respectively.

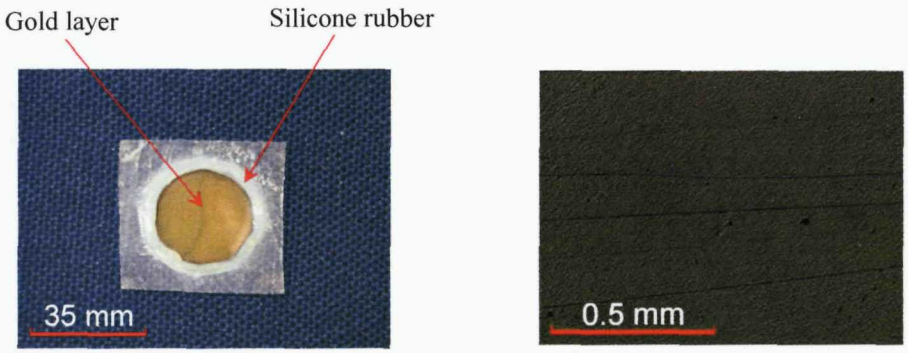

Figure 4.2: (a) The finished sample and (b) the gold layer surface as viewed under microscope with reflection illumination.

Using UV/visible spectrophotometer, the transmission of light through the LDPE, PET and PEN samples (with 20nm thick of gold layer on one side of the film only) was analyzed and results obtained are shown in Figure 4.3. The results show that the transmission spectra for PET and PEN are relatively higher compared to that of LDPE. All materials exhibit maximum transmission in the visible region with peaks occurring at ~500nm. This transmittance result is important for the calibration of EL spectral measurement, which will be discussed in Section 4.4.3. For other types of EL analysis; spatial, temporal and phase-resolved, no calibration is needed for the measured light intensity, as explained in Appendix B.2.

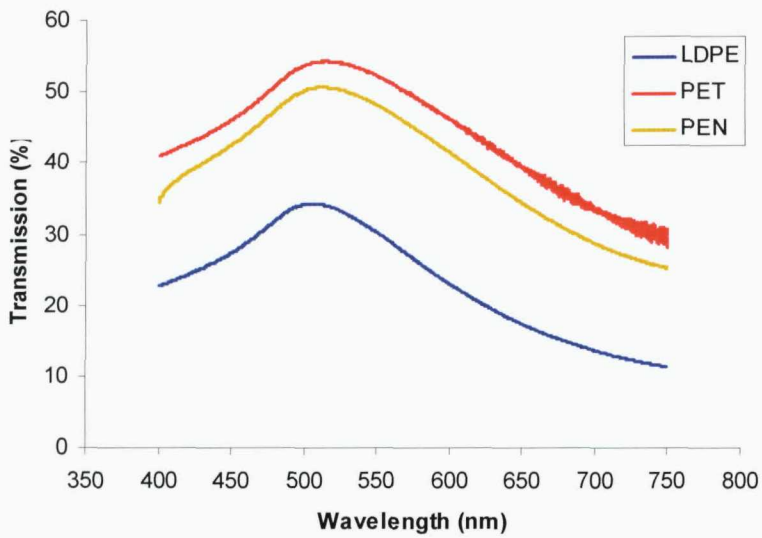

Figure 4.3: Transmittance response for LDPE, PET and PEN samples with 20nm thick of gold layer on one side of the film.

The prepared samples were sandwiched between two stainless steel electrodes with polished surfaces; one of which was a ring electrode to allow light to pass through to the CCD camera. The ring electrode was grounded and the other planar electrode, was connected to the high voltage supply. This configuration was chosen in order to minimize the effect of corona discharges. If the electrodes are connected the other way around, the sharp edge of the ring electrode would produce a more intense electrical field that can cause electrical discharges and disrupt the light emission measurement. The two electrodes were then clamped together using a plastic holder and a paper cover with a square window ($8x8mm^2$) was placed over the aperture of the sample holder in order to produce a square image of EL. Figure 4.4 shows the overall design of the sample holder.

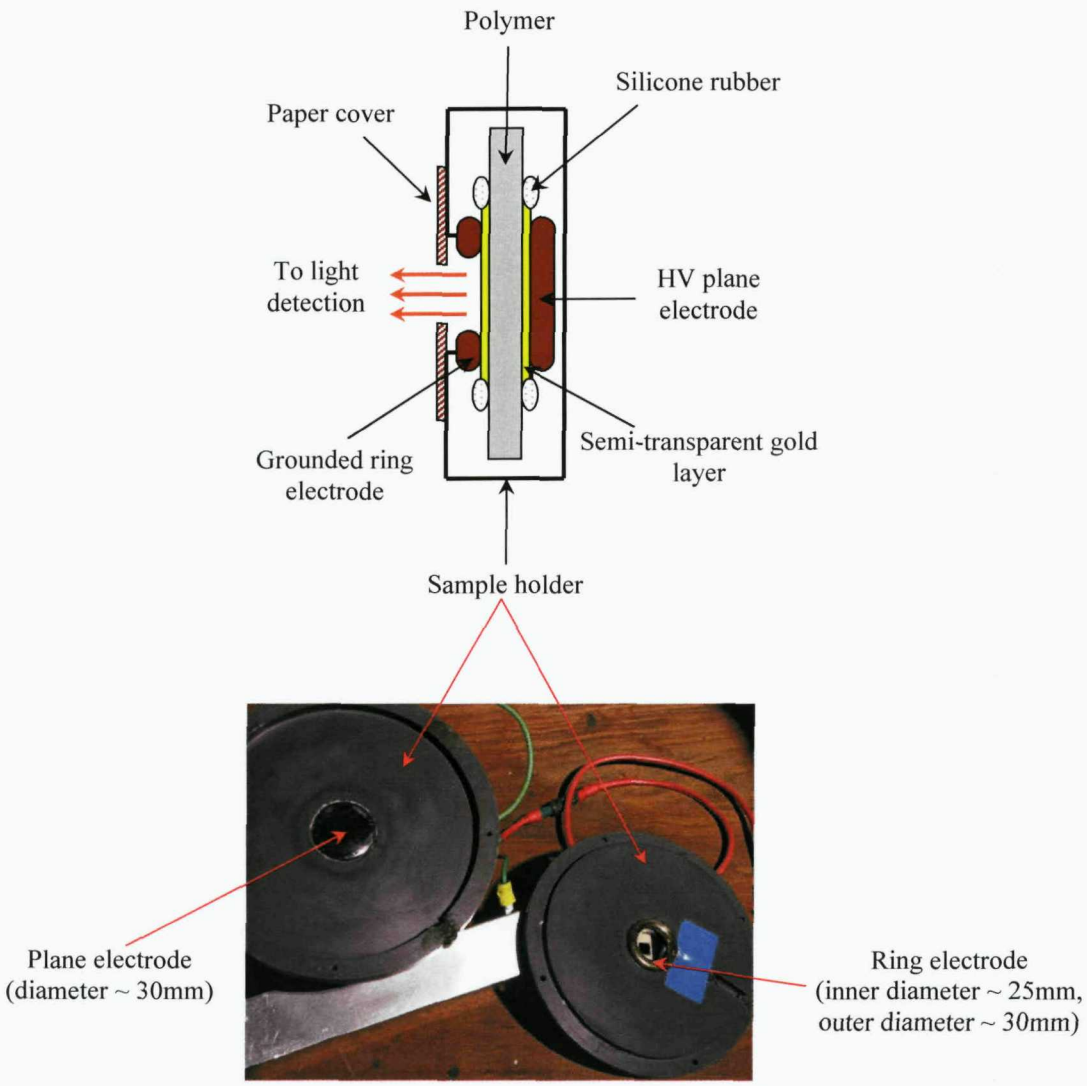

Figure 4.4: The configuration of the polymeric sample and its holder.

4.3 Experiment Setup

The arrangement for EL measurement is shown in Figures 4.5 and 4.6. The main part of the system was placed in a Faraday cage to exclude external light and all power supply connections through the box were filtered in order to minimize the influence of external noise that can be detected by the sensitive CCD camera. The sample holder was placed on top of a motorized movable stage to align the sample accordingly so that EL images could be taken at the desired position. A lens of 50mm diameter was used to focus the light emitted onto the CCD array and is made of fused quartz, allowing transmittance in the range of wavelength required (300-900nm) [111]. The whole system was also star-point grounded in order to avoid earth loop interference.

All samples were tested inside a vacuum/gas chamber that could be pressurized under atmospheric, low or high pressure conditions. It is 300mm in diameter and was constructed using a borosilicate glass pipeline component manufactured by QVF Ltd. The transparency of the chamber allows visual monitoring of the sample displacement during positioning of the sample. The walls of the chamber comprised two stainless steel plaques with a fused silica window attached to them to allow light to pass through a lens to the camera. A rubber strip, applied with silicone grease was used as a seal at the periphery of the class chamber entrance as it helps to prevent gas leakage when the chamber is under vacuum or in a pressurized condition. The chamber was also connected to a turbo molecular pump system to evacuate air and humidity before it is pressurized with gas. To monitor the gas pressure level inside the chamber, the system was fitted with Pirani gauge which was steered by Edwards automatic controller.

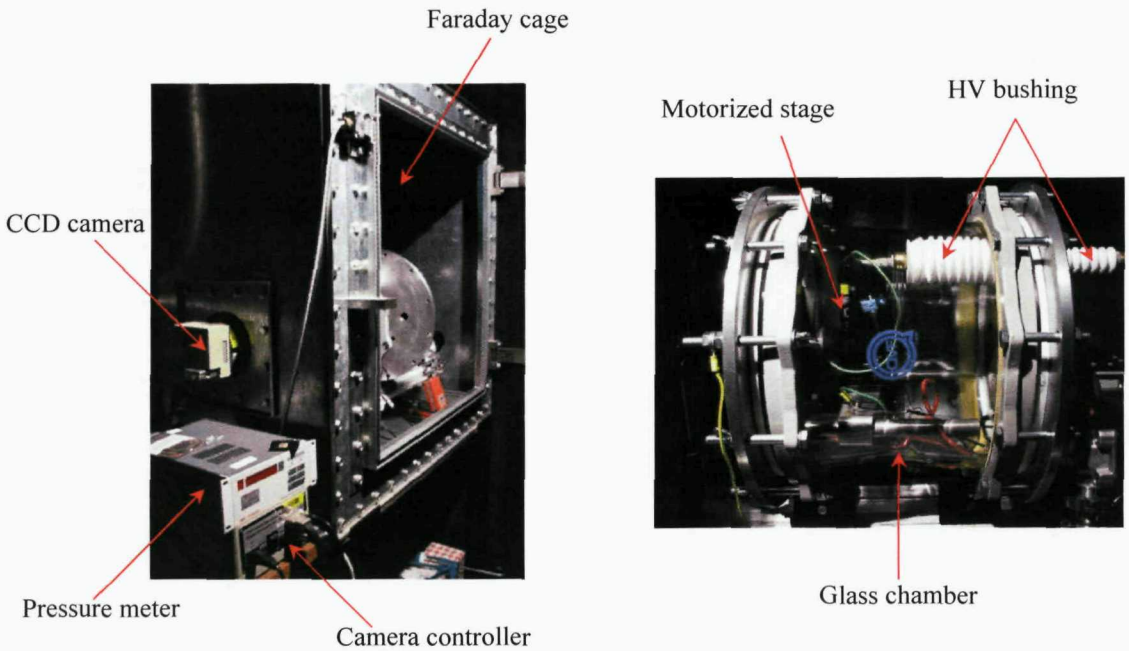

Figure 4.5: Setup to measure EL in insulating polymers at room temperature.

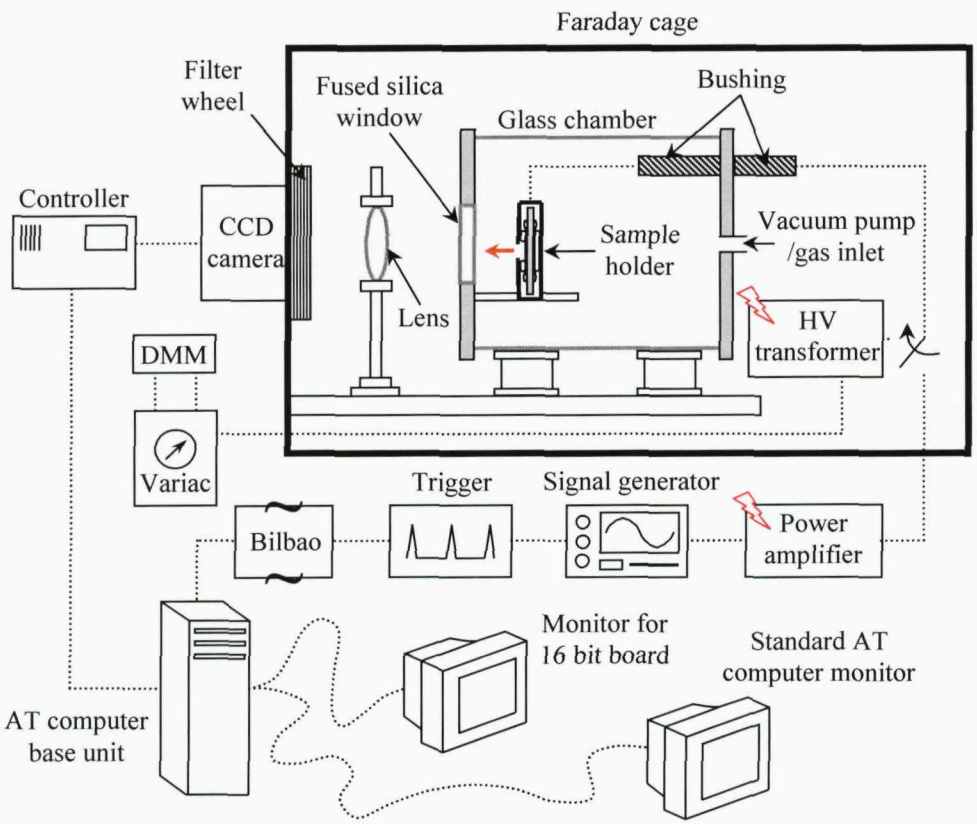

Figure 4.6: Schematic diagram for the overall EL measurement.

4.3.1 High Voltage System

The polymeric samples were subjected to high electrical stresses via two approaches. Originally, all EL tests were performed using a step up transformer that was rated at 20kV maximum for secondary voltage. It was first calibrated using a high voltage voltmeter in order to control the voltage applied to the samples using Variac from the outside of the cage. A calibrated digital voltmeter was used to measure the output from the Variac and the corresponding calibration measurement is shown by Figure 4.7. To allow high voltage to pass safely into the vacuum/gas chamber, a bushing built from polytetrafluoroethylene (PTFE) was employed as it eliminates any possible discharge current at the normal working voltages applied during the experiment.

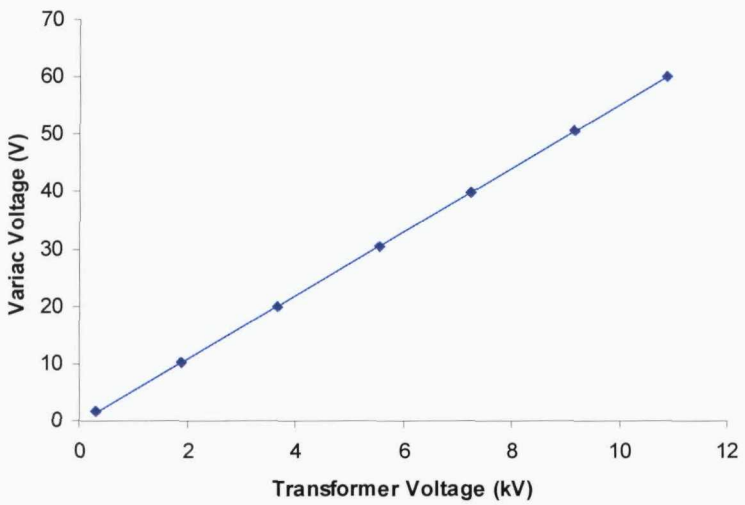

Figure 4.7: Calibration of the Variac and transformer high voltages.

The existing high voltage system has been further improved in order to get a more accurate reading for the EL experiments, particularly for the phase-resolved measurement. In the current system, the voltages for the step up transformer and trigger are fed from different ac mains thus there might be a slight time difference between the signal for the trigger and the actual voltage applied to the polymeric sample. In addition to this, frequency discrepancies may occur as a result of occasional load fluctuations from the main ac supply. Although it can be argued that these discrepancies are negligibly small, the long duration in measuring phase-resolved EL (around 20 minutes per measurement) may amplify this effect, leading to inaccurate intensity readings with respect to time.

A signal generator was incorporated into the experimental setup to allow more control in producing the voltages to be applied across the sample. To generate the high voltage source, a HV power amplifier with a gain of 1:2000 and up to 20kV peak-to-peak voltage was used. This new system will ensure that the frequency of the applied voltage remains constant throughout the measurement. The signals for the trigger and power amplifier came from the same source so the possibility of time variation in applying the voltage and initiating light intensity measurement may be eliminated. Phase-resolved EL measurements can also be conducted by applying voltages other than the typical sinusoidal; such as periodic square and triangular waveforms. This may provide some further insight into the charge injection mechanism relating to the occurrence of EL under alternating electrical stresses.

4.3.2 Optical Filter Unit

The wavelength distribution of the light emission was analyzed using a set of interference optical filters. The unit consisted of a rotating filter wheel with 6x50.8mm^2 standard sized filters and was fixed inside the Faraday cage; between the camera and the lens. Six narrowband (~50nm) interference filters centred at the wavelengths of 450, 500, 550, 600, 650 and 700nm were used to obtain the spectra of light emission. The filter unit was controlled independently by the computer to resolve specified wavelengths of light. Using UV/visible spectrophotometer, the transmission profile for these filters is obtained and shown in Figure 4.8.

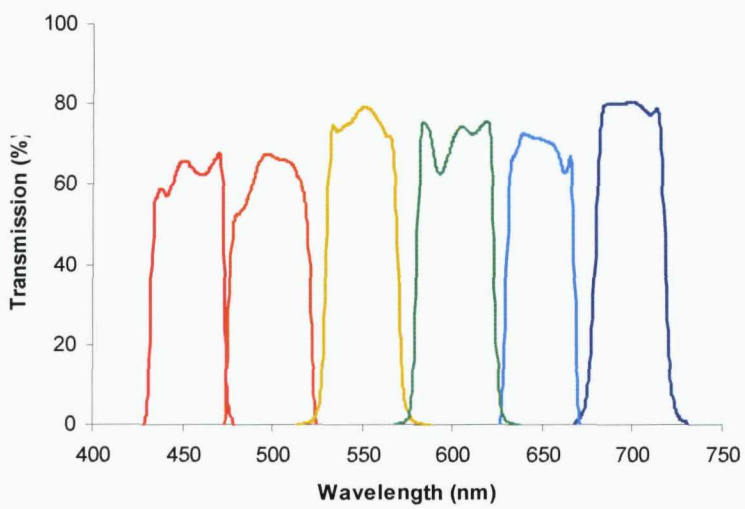

Figure 4.8: Transmission of filters at 450, 500, 550, 600, 650 and 700nm wavelength.

4.3.3 AT1 System

The AT1 System, manufactured by Wright Instruments, is a Peltier CCD imaging system designed for low light level and precision optical imaging in scientific applications. The comprehensiveness and versatility of the AT1 System software allows the system to be used in a wide variety of applications involving both one and two dimensional imaging. Specific application areas include astronomy, Raman and other spectroscopy, fluorescence and luminescence imaging and microscopy, and streak and phosphor screen readout.

The CCD has been chosen for the detection of EL over the traditional use of a photomultiplier tube (PMT) since the CCD has higher quantum efficiency, broader spectral range [112] and allows images of the emitted light to be obtained. A CCD is an integrated circuit containing an array of potential wells each capable of trapping electrons. In imaging CCD, photons incident on the surface of the device during the exposure produce photoelectrons in the potential wells. The number of photoelectrons produced depends on the wavelength of incident light, the intensity and the exposure time. During readout, the charge accumulated in the potential wells are then moved, one pixel at a time, to an output amplifier. The output of the amplifier has a voltage which is proportional to the charge in each pixel. An analogue to digital converter then digitizes the voltage signal for each pixel so that the intensity information can be read into a computer. By reading out the intensity information in all pixels of the CCD array in a sequential manner allows an image of the intensity distribution of light falling onto the CCD array to be produced.

The high sensitivity Peltier cooled CCD camera used for the light detection achieves an operating temperature of 200K using a heat pump and air cooling for waste heat removal and gives low dark current level of 4.5×10^{-3} e^-/pixel/second. In addition to this, the readout noise due to A/D conversion and electronic bandwidth for this particular camera is 15.6 and 7.8 electrons rms at high speed and low speed respectively. The camera is equipped with a CCD chip that has high quantum efficiency over the spectral range used for EL measurement, as shown in Appendix B.3. Quantum efficiency is defined as the ratio of the electrons generated over the photons incident with the CCD chip. Its CCD pixel array has 512 horizontal by 455 vertical pixels with each pixel having a physical size of $19 \times 19 \mu m^2$.

In addition to this, the camera is able to add the whole accumulated charge on the CCD arrays to produce a single light intensity reading. This action is termed as pixel 'binning', where rectangular groups of pixels are combined to effectively become single larger pixels. The charges on the CCD pixel array are then moved down in parallel, one row at a time into the serial register and after all photoelectrons are moved, they are subsequently summed and moved to the amplifier to produce a single value. The camera also has a variable gain amplifier that determines the relative signal gain of the camera electronics. This particular camera uses only gains of one and four (10 photoelectrons per count at a gain of one and 2.5 photoelectrons per count at a gain of 4). Throughout the experiment, the camera gain was set to one.

4.3.4 Bilbao System

In order to determine the phase angle relationship of EL with respect to the applied alternating voltage, an additional system was built and integrated [113] into the original experimental setup [114]. The system, which comprises a software program and a synchronization module, controls the movement of photoelectrons on the CCD pixel array. The software was written using Borland Delphi programming language and it allows the communication between the CCD camera and the computer; including several input parameters that can be defined by users via its graphic user interface (GUI). Table 4.1 and Figure 4.9 show the functions of the input parameters of the software and its corresponding GUI respectively.

Table 4.1: User-defined input parameters for EL phase-resolved measurement.

Input Parameter	Function
Vertical Pixels	Number of vertical pixel rows averaged to produce single light intensity measurement
Points Per Trigger	Number of light intensity measurement for each trigger pulse
Number Triggers	Number of triggers required to average the light intensity measured

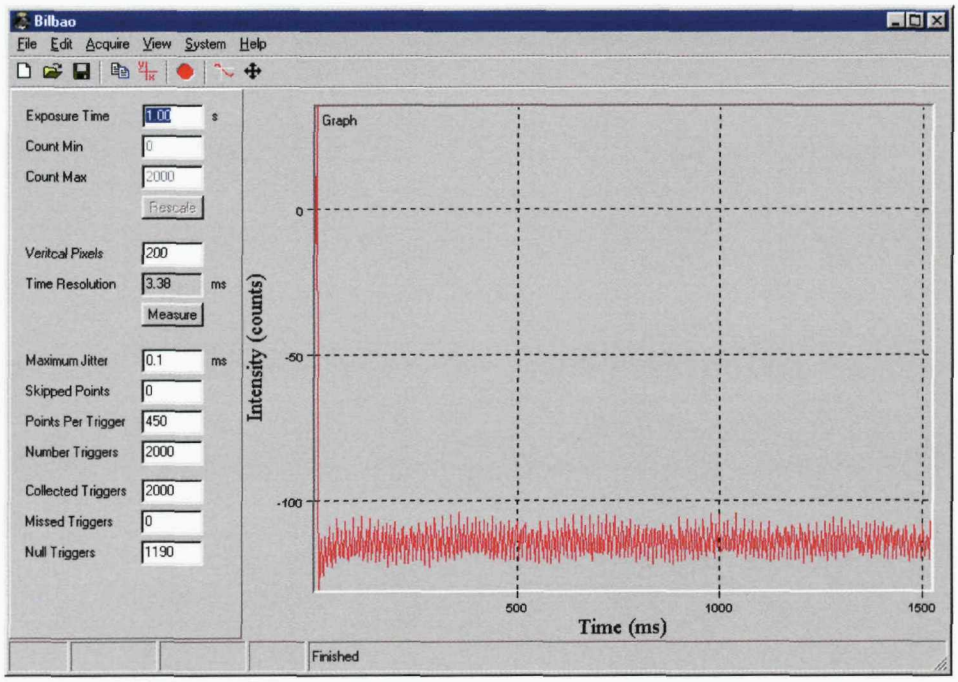

Figure 4.9: Graphic user interface (GUI) for the point-on-wave measurement.

In addition to the input parameters, the GUI also displays several other variables. The Measure button is used to initiate the calculation for the time resolution of clocking out the light intensity from the number of total vertical pixels chosen, and the result is displayed in the Time Resolution box. The Maximum Jitter is the maximum time allowed for between receiving a trigger signal and the initiation of the readout procedure by the camera. Since the software runs under a Windows system, instructions are not executed immediately so the computer will discard all data when the timing jitter is more than a specified value. In conducting the phase-resolved EL experiment, the value is set as 0.1ms and the number of triggers that exceed this maximum allowed time is displayed as Missed Triggers. The Collected Triggers box corresponds to the number of triggers that have been performed whereas Null Triggers represents the number of triggers that fail to provide any intensity result during measurement.

On the other hand, the external Bilbao electronic board is used to synchronize the light emission with the ac voltage. It is connected to the Wright Instruments interface card, allowing it to send trigger signals to the computer when a zero crossing point of the positive half cycle of the ac voltage is detected. Refer to [114] for a more detailed description of the Bilbao system and circuitry.

4.4 Experimental Procedures

After positioning the sample, the glass chamber was sealed and air evacuated using a vacuum pump until a pressure around 0.5 mbar was achieved. Then the chamber was pressurized with 1 bar of dry nitrogen (N_2) or sulphur hexafluoride (SF_6) gas in order to suppress the complicated effect of oxygen on EL [87] and to avoid corona discharges within the chamber due to the application of high voltages. The chamber was re-pressurized manually from time to time throughout the experiment to ensure a constant pressure reading. The CCD camera was then switched on and allowed to cool down to its normal operating temperature of 200K.

In order to ensure that the sample is at the correct position, a series of images was taken prior to measurements. The Faraday cage door was opened slightly, allowing weak light to enter the cage. Images were then obtained with 10 seconds exposure time and the position of the square window of the paper cover was noted. The lens, the glass chamber and the sample holder (using the motorized movable stage) were positioned accordingly until the square image was formed somewhere in the middle of the CCD array. After the desired position of the sample was achieved, the Faraday cage was closed completely, voltage was applied and EL measurements were taken. The procedural steps to conduct the various types of measurement using the AT1 software are summarized in Appendix C.

4.4.1 Imaging of Light Emission

Images of light emission were taken before and after measurements in order to ensure that the measured intensity originated from the sample and not from corona activity within the glass chamber. A constant magnitude of 50Hz ac voltage was applied to the sample; starting at 1kV rms and then was increased in 1kV rms steps after an interval of 10 minutes. At each voltage step, an image of the light emission was obtained using the CCD camera with an exposure time of 600 seconds. The AT1 software also facilitates the analysis of the image spatial distribution so the effect of different gas environments on EL could be examined more accurately.

4.4.2 Temporal Behaviour Measurement

A preliminary temporal measurement was made on a 125μm PEN sample in order to examine the stability of light emission due to the application of high electrical stress. The light intensity over the whole image was integrated using the 'binning' function and it included the readout and thermal noise of the CCD camera. The exposure time was set to 2 seconds per measurement point and the intensity is expressed as the number of counts over 2 seconds. The voltage was increased manually to 4kV rms after 4 minutes of measurement and the temporal light was detected for nearly an hour. From Figure 4.10, it can be seen that the light emission is stable throughout the whole measurement. This is one of the important characteristics for EL phenomenon as the stable emission proves that there were no other light emission events from for example, discharges detected by the CCD camera.

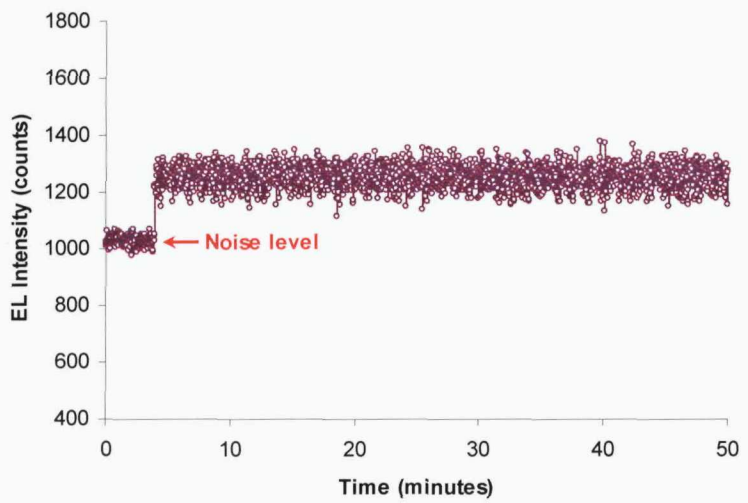

Figure 4.10: Preliminary EL temporal measurement for PEN under 4kV ac applied voltage.

To investigate the voltage and time dependence of EL in the three different polymeric samples, measurements of EL emission were obtained by measuring the integrated light intensity over the whole EL image with increasing applied voltage of 1kV rms steps. At each step the magnitude of the applied voltage was kept constant for 4 minutes and repeated measurements of the light intensity using a 2 seconds exposure were made during this period. Figure 4.11 shows the typical result for this type of experiment, obtained from a PET sample.

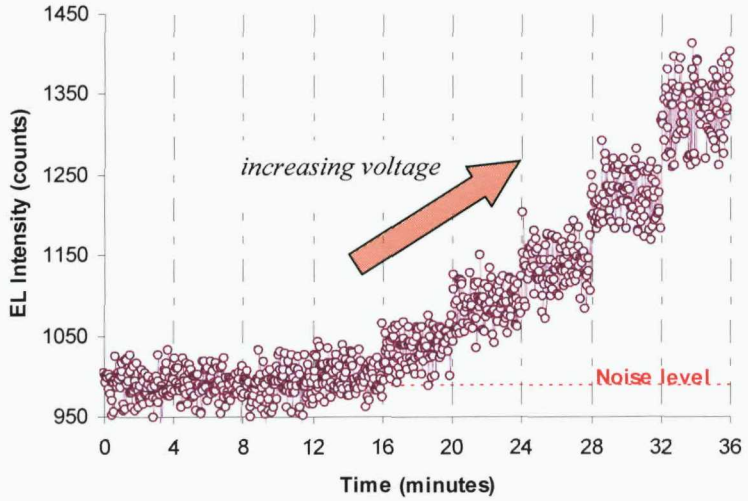

Figure 4.11: Temporal EL behaviour with increasing applied voltages across a 100μm PET sample.

4.4.3 Spectral Analysis of Light Emission

The spectral characteristics of the observed EL were obtained by measuring the light intensity with 15 seconds exposure time using six interference filters. The filters, which were placed in the optical path, have centre wavelengths ranging from 450-700nm. For each filter setting, 10 or 12 measurements were taken in order to obtain the average intensity of EL and the whole procedure was repeated with different values of ac electrical stresses. In obtaining each spectrum, corrections were made for the transmission through each filter, absorption due to the gold layer and the spectral response of the CCD camera. Table 4.2 shows the calibration of the optical response for the different materials and their overall efficiency at each filter wavelength.

Table 4.2: Calibration of EL emission for LDPE, PET and PEN with respect to CCD quantum efficiency, filter transmission and sample response.

Wavelength (nm)	Quantum efficiency (%)	Filter transmission (%)	Sample response (%)			Overall optical response (%)		
			LDPE	PET	PEN	LDPE	PET	PEN
450	60.6	65.9	27.4	46.1	42.6	10.9	18.4	17.0
500	68.6	67.0	34.2	53.7	50.2	15.7	24.7	23.1
550	70.6	79.2	30.2	52.3	48.2	16.9	29.2	27.0
600	68.5	71.4	23.1	46.2	41.5	11.3	22.6	20.3
650	66.4	71.0	22.9	39.2	34.4	10.8	18.5	16.2
700	57.9	80.4	13.7	33.3	28.7	6.4	15.5	13.4

4.4.4 Phase-Resolved Measurement

The Bilbao system was used to investigate the occurrence of EL with respect to the applied alternating voltage waveform. Only a number of pixel rows from the CCD array adjacent to the output array were exposed to the light emission by means of a paper cover and they were then summed to give a single EL intensity measurement at a particular point of the voltage waveform. The time resolution (or the time taken for measurement readout) was calculated automatically by the software based on the number of pixel rows chosen for analysis. For this experiment, 100 pixel rows were selected and the calculation for the total readout time by the Bilbao software was made as follows:

Number of vertical pixels x vertical transfer time,	100x16μs/row = 1600μs
Number of horizontal pixels x horizontal transfer time,	512x0.3μs/column = 153.6μs
Pixel read time (low speed),	34.5μs
TOTAL READOUT TIME =	1.7881ms

Since a 50Hz ac voltage has a period of 20ms, around 20ms/1.7881ms = 11 EL intensity measurements were obtained for every cycle. The number of points per trigger was chosen as 450 and these measurements were then averaged over 1000 separate acquisitions. As 450 data points were taken for each acquisition, there were 450/11 = 41 cycles of ac voltage altogether per trigger. A stable, repetitive signal was detected with the exception of the first two 20ms cycles, which were ignored in the subsequent calculations. This is due to the accumulation of photoelectrons and thermal electrons on the CCD array prior to EL detection. The rest of the phase-resolved measurements on the other hand, were cascaded over one cycle of the applied alternating voltage.

Nonetheless, an adjustment to the time for these measurements was necessary due to the time taken to clock out all photoelectrons of the CCD pixel array. Based on the readout speed testing previously undertaken by Ing Wong [114, 115] shown in Appendix B.4, the time taken to process data from each pixel row was found to be 18.2μs. To correct the delay caused by this readout time, all phase-resolved measurements were advanced by 18.2μs times n, where n is the number of pixel rows

selected. Figure 4.12 summarizes the necessary steps to be taken for the point-on-wave EL measurement. Since the system also allows different types of ac waveform to be applied to the samples, the phase-resolved measurement was also performed using alternating triangular and square voltage shapes in addition to the typical sinusoidal.

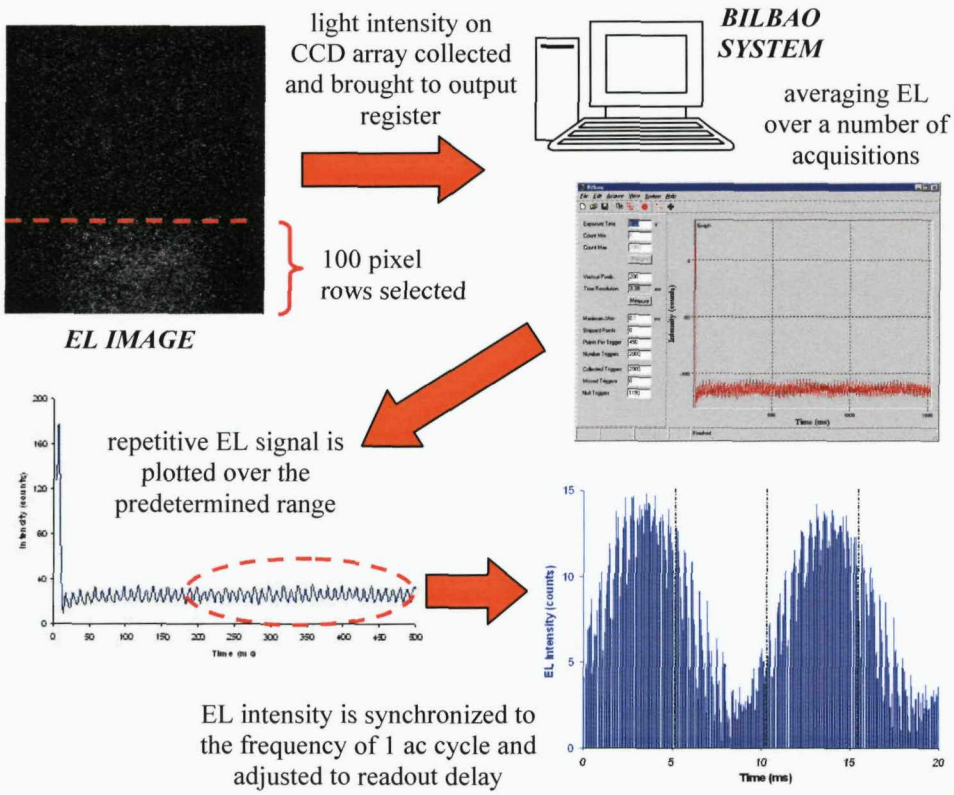

Figure 4.12: Computation of light emission measurement with respect to the alternating applied voltage.

4.5 Summary

This chapter describes the EL experiments used within this research project. Sample manufacture, experiment setup and the types of measurements that can be undertaken to investigate EL phenomenon have been outlined. The insulating samples used for the study were from LDPE, PET and PEN polymers since they are typically found in high voltage engineering applications. The experiment enables the different types of EL analysis to be conducted such as imaging, spatial distribution, temporal behaviour, field dependence, spectral characteristics and phase resolved measurement of EL. The wide variation of experiment for EL investigation using a common detector allows a more conclusive insight on the nature of this phenomenon under ac conditions to be made.

Chapter Five

EXPERIMENTAL RESULTS

5.1 Introduction

Overall, 173 samples (98 LDPE, 30 PET and 45 PEN films) were manufactured in order to examine EL phenomenon when polymers are subjected to high alternating electrical stresses. Extra care was taken in preparing the samples since it was discovered that impurities and unwanted particles, such as dust, affect the emitted light being observed. Although silicone rubber was applied at the edge of the gold layer as part of the sample preparation procedure, most of the breakdowns were detected near this region rather than in the middle part of the sample; indicating that the electric field is still high enough to cause serious degradation. Figure 5.1 shows an example of failed sample and the point of location of breakdown. Nevertheless, only 18 samples failed before any measurements could be conducted and good reproducibility was achieved in examining EL from the remaining samples.

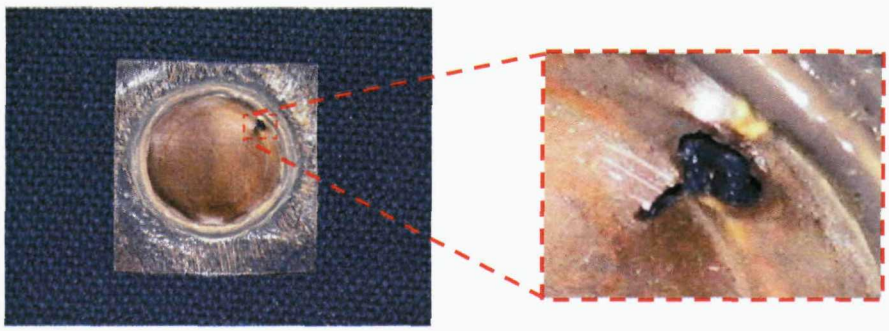

Figure 5.1: Failed sample with magnification of the breakdown point near the electrode edge.

The following results presented in this chapter essentially represent typical ones obtained from a series of measurements undertaken using different test samples. Where applicable, some of other results are included in the Appendices section as supplementary evidence of the general outcome.

5.2 EL Imaging

Typical EL images obtained by applying ac electrical stresses across the different polymeric samples are shown in Figure 5.2. Each image was produced using 10 minutes exposure time for the CCD camera and they were constructed using the same grey level in order to compare the relative intensities of the emitted light from different samples. In general, the light emission observed can be classified as homogeneous or inhomogeneous. The presence of bright spots superimposed on the homogeneous emission may be due to surface defects such as parallel lines caused by manufacturing processes involved in producing blown films and point defects that were observed from microscopic examination of the gold layers, as previously reported and shown for a typical specimen in Figure 4.2 of Chapter 4. In addition to this, the images appear to be square in shape; confirming that the light emission measured only comes from the centre of the sample under test and not from any other form of electrical discharge with the apparatus. Table 5.1 highlights some of the common EL imaging results that were obtained from the three materials subjected to various voltage levels.

The AT1 system enables the measurement of light intensity within a pre-defined area from the total emission. Since the main interest of this research focuses on EL phenomenon due to charge injection from the metal electrode into the polymer, measuring the intensity in the region where homogeneous emission occurs is the main

priority, rather than the light caused by impurities on the surface of the specimen. It was observed that the presence of bright spots is reduced significantly when the surface of the polymer is cleaned using dust removal spray prior to the sputter coating process.

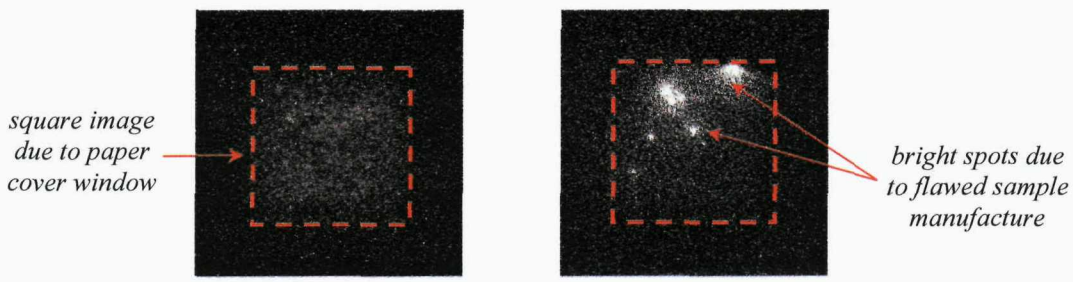

Figure 5.2: (a) Homogeneous and (b) inhomogeneous EL emission.

Table 5.1: Classification of EL images from three types of polymer under various ac rms voltages.

Homogeneous EL		Inhomogeneous EL	
LDPE subjected to 4kV	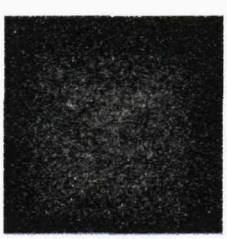	LDPE subjected to 4kV	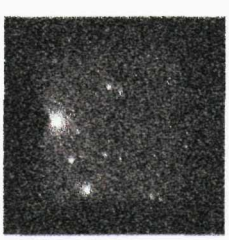
LDPE subjected to 4.5kV		LDPE subjected to 5kV	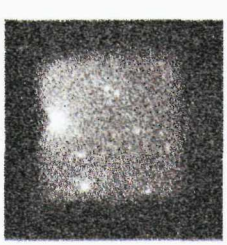
PET subjected to 4kV	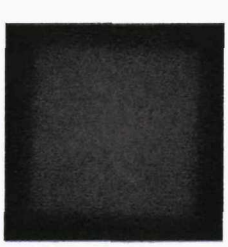	PET subjected to 3kV	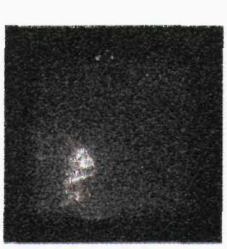
PEN subjected to 5kV	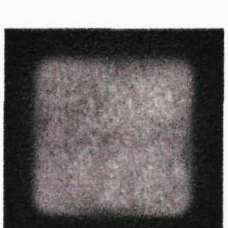	PEN subjected to 4kV	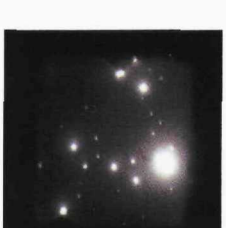

5.3 EL Characteristics from Different Polymers

In order to investigate the extent of EL as an indicator for electrical degradation of polymer insulation, the phenomenon was observed using LDPE, PET and PEN films [69, 116]. Although PET and PEN are not generally used in high voltage cable insulation systems, their application in electrical engineering especially their use in capacitors is well-recognized. More importantly, both materials exhibit high reliability in optical investigations of light emission [117-119]; therefore they are dependable sources of reference when measuring EL from other types of polymer such as LDPE. The main feature of PET and PEN polymers is their aromaticity, in which the carbon elements bond together to form a hybrid structure of a 'ring'. Figure 5.3 shows the molecular structures of both types of material and it can be seen PEN has two aromatic rings in its structure. The increase in rigidity which this structure possesses indicates that PEN can be up to twice as stiff as PET [120].

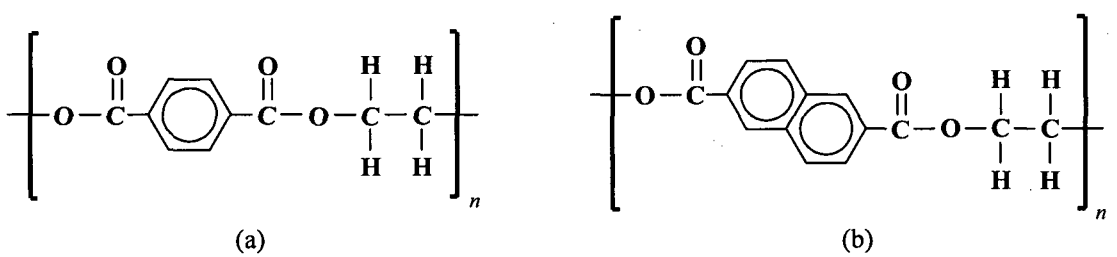

(a) (b)

Figure 5.3: Molecular structure of (a) polyethylene terephthalate (PET) and (b) polyethylene naphthalate (PEN).

5.3.1 Voltage Dependence of EL

EL measurements for LDPE, PET and PEN samples during a stepped increase of 1kVrms in applied voltage are shown by Figures 5.4, 5.5 and 5.6. The 'noise level' in these figures corresponds to the sum of readout noise and dark current level when no voltage was applied. Basically, all intensity measurements from the different materials exhibited the same behaviour of emission against time as the ac voltage was increased. The light emitted started at a threshold voltage and increased with increasing applied voltage. Under constant voltage conditions over a time period of 4 minutes, the EL intensity was found to be stable with the steady fluctuations and this behaviour demonstrates that light measured by the CCD camera is due to EL emission, not from sporadic discharge events. The observed fluctuations can be examined by the following simple analysis.

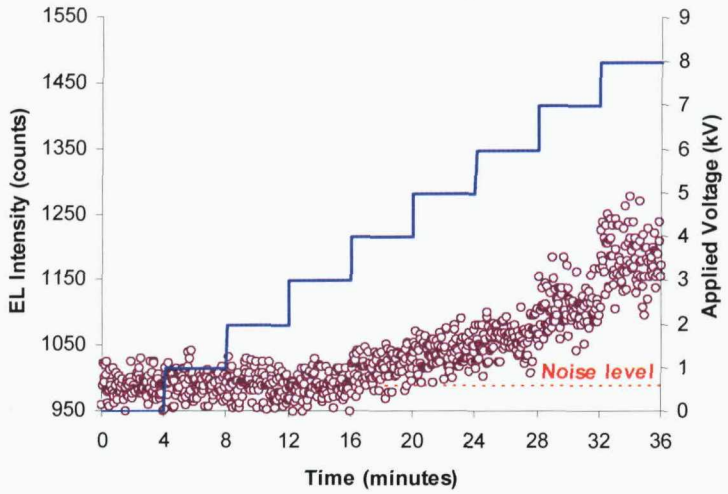

Figure 5.4: Measurement of EL for a 100μm LDPE sample over a range of applied voltages.

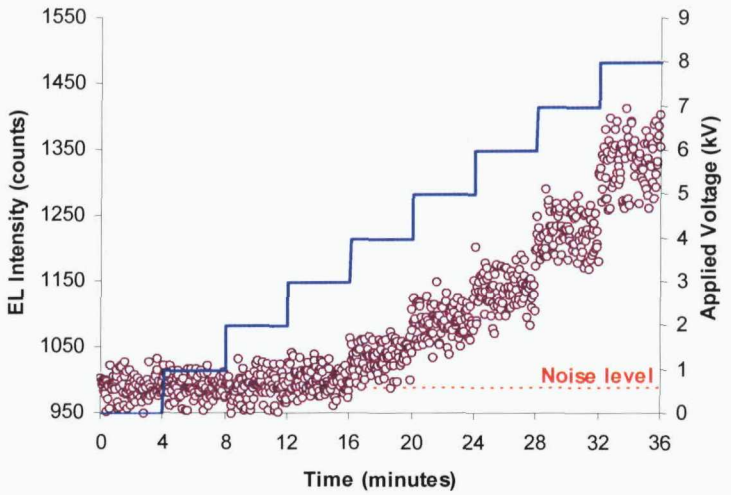

Figure 5.5: Measurement of EL for a 100μm PET sample over a range of applied voltages.

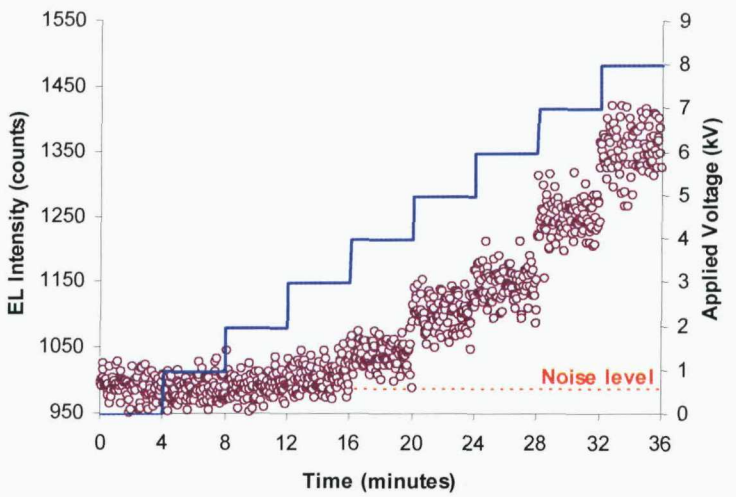

Figure 5.6: Measurement of EL for a 125μm PEN sample over a range of applied voltages.

In measuring EL by the CCD camera, the number of photons and hence the number of detected photoelectrons in a particular time interval is governed by Poisson's statistics [121, 122]. The uncertainty (or fluctuation in each intensity measurement) is equal to the square root of n, where n is the average number of photoelectrons detected per time interval. Thus the expected fluctuation for each individual measurement by applying a constant voltage over a 4 minutes period can be determined according to the Poisson's distribution. Table 5.2 shows the expected uncertainty obtained from the averaged EL intensity minus the noise level for a range of applied voltages whereas Table 5.3 summarizes the calculated standard deviation derived from the intensity measurements.

Table 5.2: The expected uncertainty of the measured EL intensity according to Poisson's distribution.

Applied Voltage (kV)	Expected Uncertainty (counts)								
	LDPE Sample			PET Sample			PEN Sample		
	I	II	III	I	II	III	I	II	III
4	4.69	4.37	3.92	4.49	5.57	6.05	6.36	5.61	7.21
5	5.92	5.89	5.09	7.94	8.15	7.88	9.41	8.65	9.67
6	7.32	6.95	6.96	10.89	9.94	9.94	11.91	10.12	11.73
7	8.98	8.91	8.82	13.13	12.26	12.26	14.25	13.06	14.07
8	11.46	11.41	11.23	15.48	14.67	14.67	17.23	15.52	16.29

Table 5.3: The calculated standard deviation of the measured EL intensity.

Applied Voltage (kV)	Observed Uncertainty (counts)								
	LDPE Sample			PET Sample			PEN Sample		
	I	II	III	I	II	III	I	II	III
4	19.58	19.59	17.81	17.57	20.36	20.26	21.33	18.20	20.73
5	20.69	20.22	19.31	23.12	22.87	20.04	21.58	24.29	22.86
6	24.43	21.81	22.78	26.94	26.43	25.39	25.08	24.47	22.98
7	26.95	28.45	27.81	29.01	28.20	33.72	30.57	27.19	29.79
8	34.03	37.80	37.94	39.09	38.30	32.22	40.52	34.01	41.04

Comparing the results from these two tables, it can be seen that the measured EL fluctuates within a wider range than the calculated fluctuation based on the photon counting statistics. Nevertheless, it was also found that the standard deviation for the measurement with 0V applied (the noise level) is around 18 counts and this is much

larger that calculated fluctuations of EL intensity in Table 5.2. Thus the measured noise is dominated by the uncertainty of the noise level although photon counting statistics makes up a significant fraction of the observed fluctuations at higher voltages. Other temporal behaviour and voltage dependence of EL observed from different samples are shown in Appendix D.1.

5.3.2 Spectral Analysis

The spectral characteristics obtained from the three different types of polymer exhibiting homogeneous EL emission are shown by Figures 5.7, 5.8 and 5.9. At each wavelength, the light emission intensity measurements were corrected for the transmission loss of the filters and sample, as well as the spectral sensitivity of the CCD camera. The readout noise and thermal noise of the CCD camera were also subtracted from all measurements. The error bars are plus and minus one standard deviation for 12 EL measurement points. The total light intensity was observed before and after the spectral measurement in order to ensure that the light level was stable and there was no significant change to overall EL intensity during the data acquisition process.

The EL spectra obtained from the three materials, LDPE, PET and PEN have a number of common characteristics. The EL intensity at 450nm was very low and independent of voltage for the LDPE and PEN materials suggesting that the emission intensity was below the noise floor. All three materials show evidence for a peak in the EL intensity at approximately 600nm particularly at the higher voltages. The size of this peak is dependent on the material being greatest for LDPE and PEN. The peak at 600nm also becomes more prominent as the applied voltage increases. There is also evidence for another peak that lies beyond 700nm particularly evidenced in the LDPE and PET materials. The spectral characteristics are therefore dependent on the material as well as the applied voltage and reflect differences in the recombination energies of excited charge carriers that not only relate to the chemical composition of the materials but are also influenced by the applied voltage. These issues will be discussed in more detail in Chapter 6.

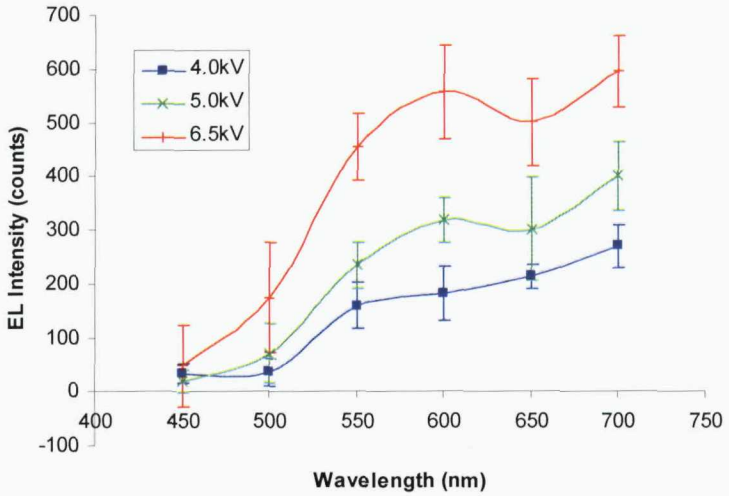

Figure 5.7: Spectral analysis for a 100μm LDPE sample.

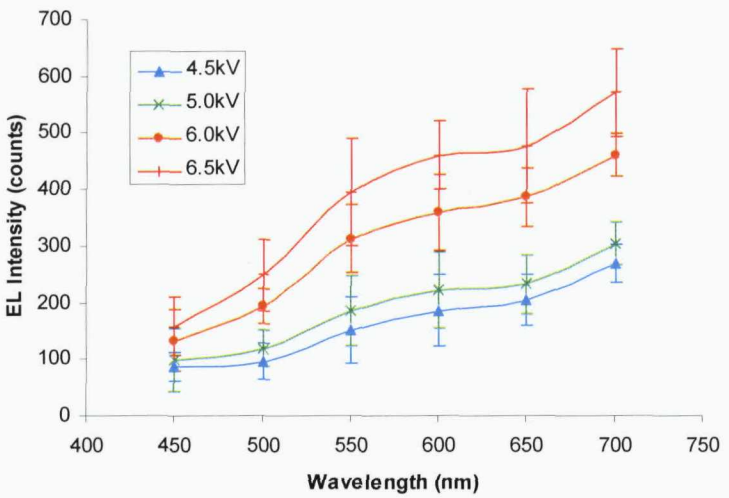

Figure 5.8: Spectral analysis for a 100μm PET sample.

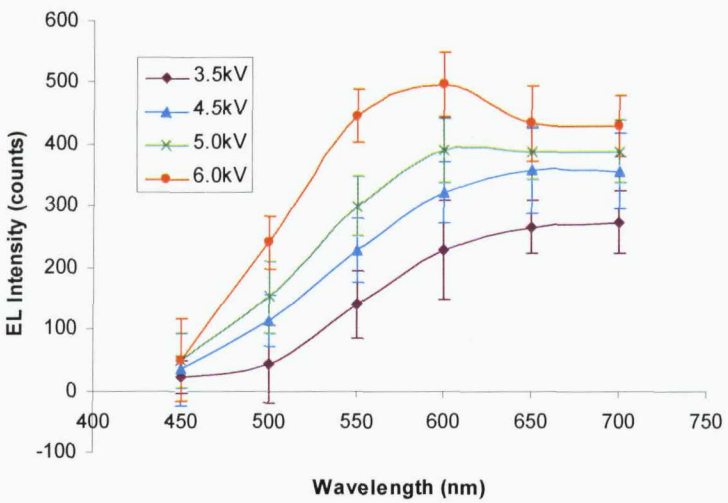

Figure 5.9: Spectral analysis for a 125μm PEN sample.

5.4 Effect of Gas Environment on EL

Since the area of this research work focuses on the material commonly used as insulation in high voltage cables, the following experiment was undertaken using LDPE films only. The influence of gases on the EL phenomenon has been observed by many researchers [87, 90] through deliberate impregnation of gases into polymeric samples and most of these works implemented a divergent electric field configuration. Although experiments using thin films were typically conducted under vacuum [123-125], nitrogen (N_2) [37, 126, 127] or sulphur hexafluoride (SF_6) [66, 128, 129] gas environments, no work has been done so far to compare EL characteristics under such conditions. Therefore the main objective of this part of experiment is to examine the role, if any, of gas diffusion into the surface or bulk of the polymer on the processes leading to EL [130, 131].

5.4.1 Spatial Distribution

The effect of different gas environments in relation to the EL intensity was examined by comparing the spatial distribution that can be derived from the emission images. This was achieved by defining a specific area from the overall image using the software and analyzing the intensity level within this region. The lens gives the magnification of 35μm/pixel; therefore the width of the square window of the paper cover corresponds to ~230 pixels in length. In the case shown by Figure 5.10 (a), an area of 30 pixel rows was chosen from the homogenous emission image obtained by applying 4kV rms across a 100μm LDPE sample. The intensity was then averaged over the selected area to give the spatial measurement at each pixel column. A comparison on the effect between the two gases in terms of the material's EL is shown in Figure 5.10 (b). From the result, it can be seen that the light intensity is relatively higher in N_2 as compared to SF_6 gas.

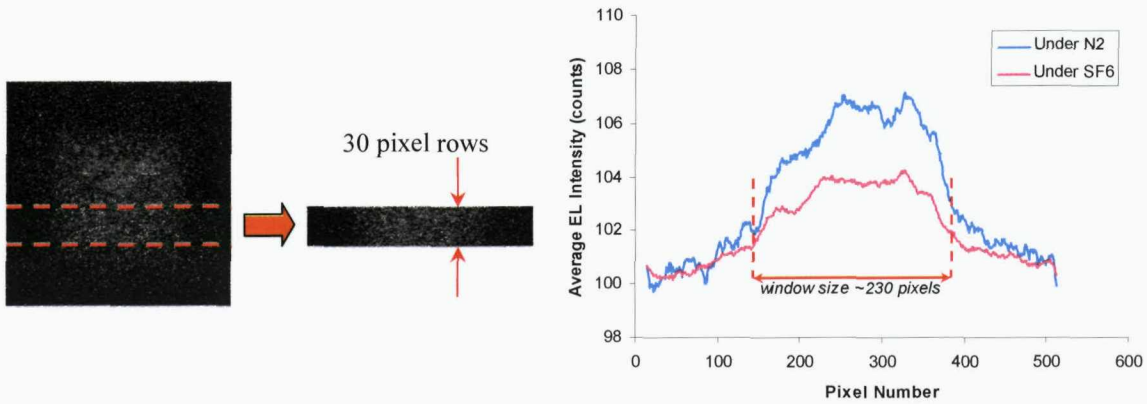

(a) (b)

Figure 5.10: (a) A selection of area to be analyzed and (b) its corresponding spatial distribution of EL under N_2 and SF_6 gas environments and an applied voltage of 4kV rms.

It has been shown earlier in Section 5.2 that the observed light emission in general has two different spatial characteristics; homogeneous and inhomogeneous emission. Whilst it can be said that homogeneous emission is due to the interaction of the injected charge carriers with the molecules of the polymer, the existence of bright spots was found to be as a consequence of imperfect sample manufacture leading to the presence of impurities and surface defects. In addition, it has been shown previously [114] that inhomogeneous emission is characterized by a greater EL emission in the visible wavelengths around 550nm than that found in samples emitting homogeneous EL; suggesting that at bright spots, charge may have been injected further into the bulk of the material and trapped in deep states much more representative of the bulk polymer. Nevertheless, both inhomogeneous and homogeneous emissions are due to the injection of charges into the material from the electrode and so the presence of electronegative gas is likely to affect the emission of both provided that the gas is able to permeate into the bulk of the material.

The same procedure was repeated using measurement data from another LDPE sample that exhibited inhomogeneous EL. 40 pixel rows were selected (Figure 5.11 (a)) in order to examine the effect of the different gas environments on the inhomogeneous EL. The result, as shown in Figure 5.11 (b) also agrees with the analysis obtained for homogeneous emission where EL intensity is found to be higher under the influence of N_2 gas than that of SF_6 gas. Other examples on the effect of gas environments on

spatial distribution of EL can also be seen in Appendix D.2. Thus the presence of gaseous molecules could play a crucial role in the occurrence of EL as they could affect the excitation and recombination of surface or interfacial states of the polymeric sample. It could also be argued that the difference in this intensity level may be due to absorption of light by the gas molecules. However Tomkiewicz *et al.* [132] has reported that light absorption by N_2 and SF_6 gas only occurs in the wavelength region below 300nm at 1 atmospheric pressure; therefore EL discrepancy between the two cases are more related to the influence of gas molecules on the excitation and recombination of excited states within the polymer rather than the fact that the light is being absorbed by the gas.

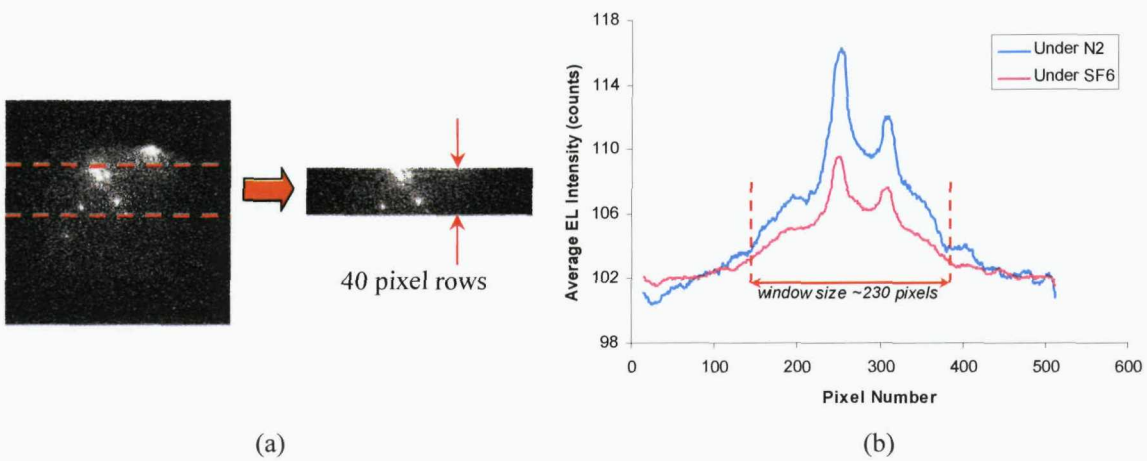

Figure 5.11: (a) 40 pixel rows from an inhomogeneous EL region are chosen and (b) the comparison of EL intensity in two different gas environments is made.

5.4.2 Spectral Analysis

The spectral characteristics for EL emission under N_2 and SF_6 gas environments were also examined in order to understand the mechanism that causes the differences in the spatial distribution results. Typical spectral measurement results are shown in Figure 5.12 for N_2 and Figure 5.13 for SF_6. Although the general trend of the spectra (increasing EL from 450 to 700nm wavelength) remains the same, it can be seen that the intensity is noticeably higher in N_2 compared to SF_6. The same observation can also be seen from the results included in Appendix D.3.

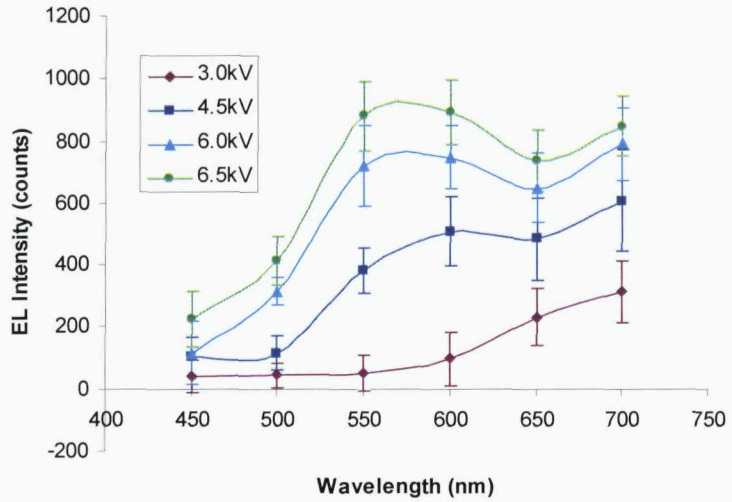

Figure 5.12: Spectral measurement for an LDPE sample under nitrogen (N_2) gas.

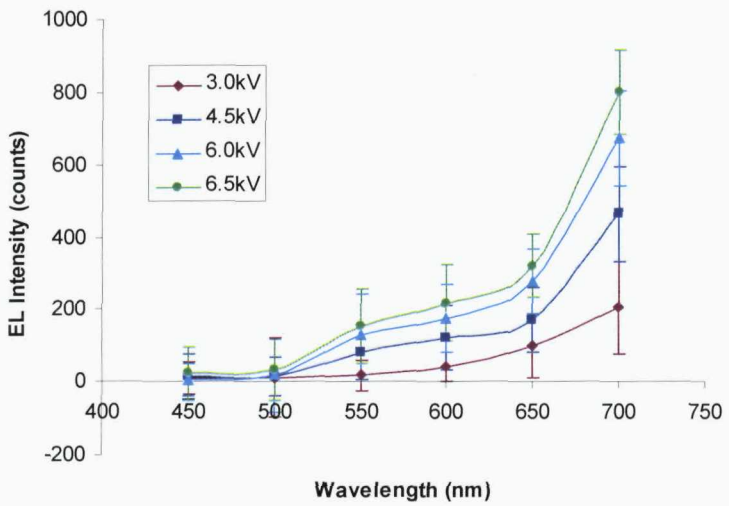

Figure 5.13: Spectral measurement for an LDPE sample under sulphur hexafluoride (SF_6) gas.

The EL spectra obtained for LDPE in N_2 and SF_6 are significantly different. The peak in the EL spectra at approximately 550 to 600nm that is observed in the N_2-conditioned specimen is almost completely suppressed when the sample is conditioned in SF_6 atmosphere. However the EL intensities at 700nm appear to be identical and therefore not affected by the gas environment. This observation suggests that SF_6 is able to influence the recombination process that gives rise to EL at 550 to 600nm but not that which gives rise to emission at 700nm. These observations and possible reasons for the observed differences in the EL spectra obtained under the different gas environments will be discussed in more detail in Chapter 6.

5.5 Phase-Resolved EL Measurements

Although EL phenomenon in polymeric materials has been widely investigated under dc fields [79, 133], the understanding about its behaviour due to ac electrical stresses is still far from conclusive. In an alternating field, charge carriers are being injected and extracted continuously so the processes leading to the observation of EL is not so straightforward. Excitation of excited states may be due to hot electron impacts within the material or due to recombination of opposite charge carriers in the case of bipolar charge injection. One of the ways to comprehend the nature of this phenomenon in an ac field is through the phase-resolved, also known as the point-on-wave, measurement.

5.5.1 Influence of Gas Environment and Polymer Material

Point-on-wave EL measurements were undertaken using 1 bar of dry nitrogen (N_2) or sulphur hexafluoride (SF_6) [131]. Sinusoidal ac stresses were applied across the polymeric samples and the typical results are shown by Figure 5.14 (a) and (b) for N_2 and SF_6 gas conditions respectively. The plots show that there is detectable light emission (indicated by arrows) occurring in the first and third quadrant of the applied alternating voltage when N_2 was used as the environmental gas whereas no light emission above the noise level when the chamber was pressurised with SF_6. Similar observations can also be seen in the graphs presented in Appendix D.4. This supports the theory that in the presence of electronegative gas such as SF_6, the absorbed gas molecules within the polymer suppress the processes resulting in EL leading to significantly reduced EL intensity. Due to the difficulty in obtaining phase-resolved measurements on samples within an SF_6 environment, remaining phase-resolved measurements of EL were carried out on samples under a N_2 environment.

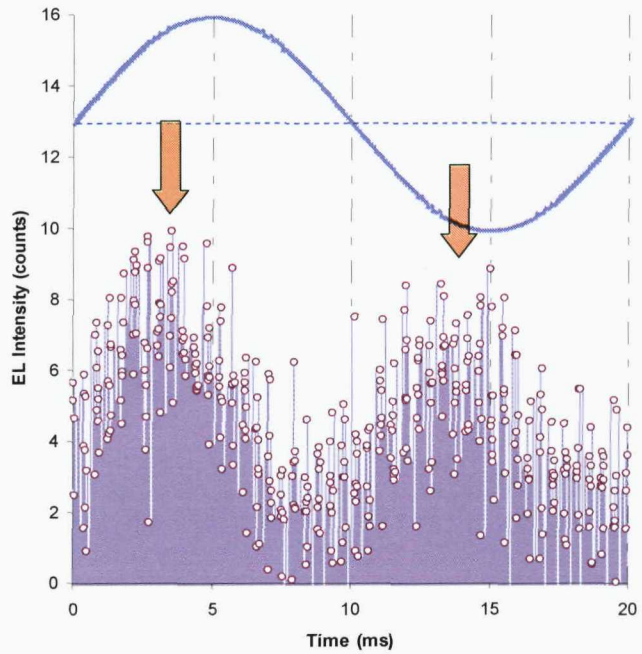

(a)

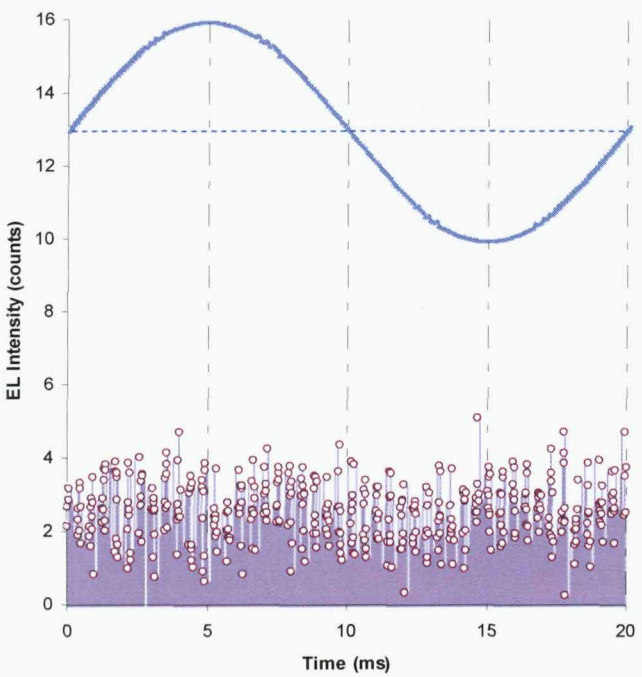

(b)

Figure 5.14: Phase-resolved EL measurement when an LDPE sample was subjected to 3.5kVrms applied voltage under (a) N_2 and (b) SF_6 gas environments.

To analyze further the occurrence of EL with respect to the applied alternating stresses, some form of data-processing mechanism needs to be applied on the measurements taken. The measurements were first corrected by subtracting the noise levels (measurement without any voltage applied across the sample). Then polynomial regression lines have been added to the graphs for every half cycle in order to determine the time where EL is a maximum during one cycle of ac voltage. As shown by Figure 5.15 (a) and (b), there are two points where the light intensity measured is highest, and these peaks occur prior to the positive and negative peaks of the alternating voltage waveform. It can therefore be hypothesized that charge injection during each half cycle may be the main cause responsible for the occurrence of EL when the polymer is subjected to ac fields. For analysis purposes, the phase difference between EL maxima with the positive and negative peaks of the ac voltage is denoted as φ_p and φ_n respectively.

The plots in Figure 5.15 also reveal that the magnitude of light intensity measured from a PEN sample is relatively higher than an LDPE sample for the same magnitude of electric field [134]. This can be explained by the presence of aromatic molecular backbone in PEN molecules which acts as chromophores in the repeat units of the polymer chain. The same reason may also explain why the intensity distribution is more well-defined for PEN as compared to that of LDPE.

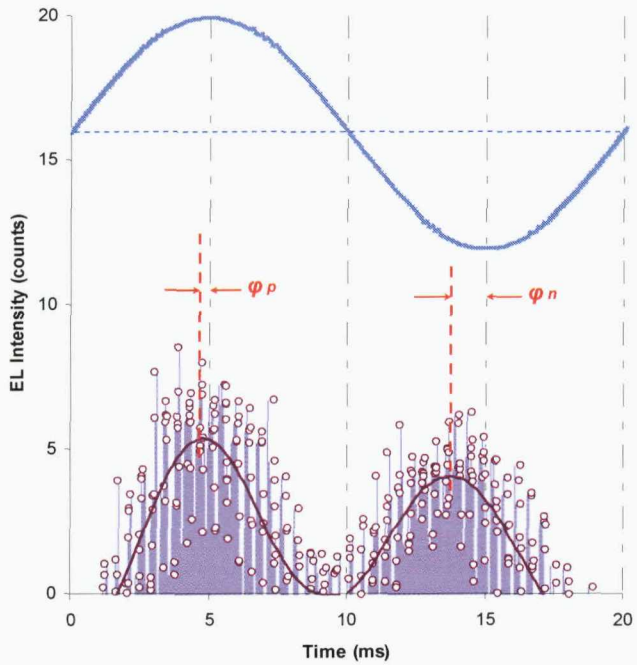

(a)

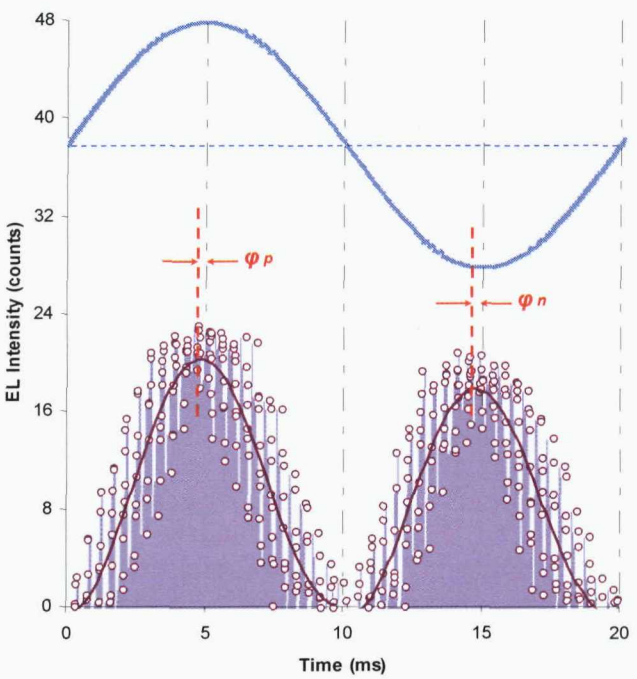

(b)

Figure 5.15: Point-on-wave EL for (a) LDPE and (b) PEN materials subjected to 4kVrms under N_2.

5.5.2 EL Behaviour under Typical Sinusoidal AC Voltage

Since there is a possible reduction of light emission intensity when SF_6 molecules are present, all phase-resolved results presented were obtained from samples in a pressurised N_2 environment. The graphs are simplified using regression lines and the raw data for the plots can be seen in Appendix D.5 to D.9. Figure 5.16 (a) and (b) illustrate the phase-resolved EL emission for various applied voltages using LDPE and PEN samples. Both figures show that the magnitude of the light intensity detected by the CCD camera increases with the rise of electric field across the polymeric samples [134]. By increasing the voltage applied, more electrical charges are injected into the bulk of the material and this will lead to an increase in the number of recombination processes. In addition to this, it can be seen that all maximum EL points for both types of polymer occur just before the peaks of the positive and negative applied voltages. Table 5.4 summarizes the phase difference approximation obtained from three samples and it can be deduced that there is no obvious pattern relating the changes of EL peak with increases in the applied voltage. This is probably related to the uncertainty in determining the exact phase angle at which peaks occur in the experimental data at these low applied voltages.

Table 5.4: Phase difference comparison of three tested samples subjected to increasing electrical stresses.

Sample Material		LDPE (Sample I)			LDPE (Sample II)			PEN		
Applied Voltage (kV)		3.0	3.5	4.0	3.0	3.5	4.0	3.5	4.0	4.5
Phase Difference	φ_p	19.7	3.62	4.12	12.2	11.6	11.4	0.92	2.72	4.59
(degrees)	φ_n	0.22	7.78	7.52	7.78	15.3	8.28	0.68	7.13	7.47

It can also be seen from these figures that there is a small discrepancy between the EL intensity distribution for the two half cycles. As shown by Ing Wong [114], the intensity was found to be asymmetric for the phase-resolved inhomogeneous emission samples. Nevertheless, when both surfaces are equally emitting light, then an almost equal intensity in the two half cycles would be expected and the slight difference is due to some transmission loss of the light through the sample when the light is emitted from the side furthest from the CCD camera. The asymmetry shown in Figure 5.16 may be due to light being preferentially produced at one electrode or that there are regions on the sample where the light emission is slightly inhomogeneous.

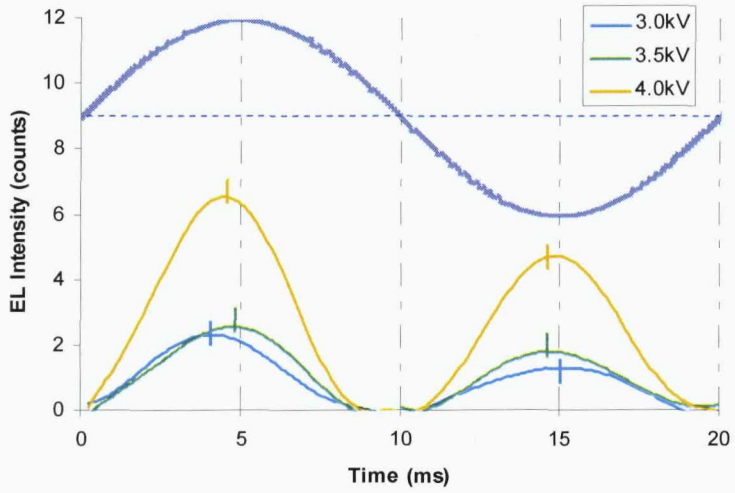

(a)

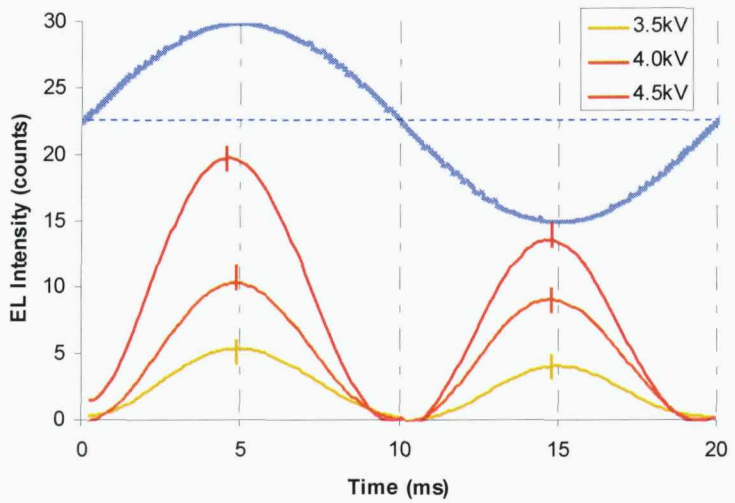

(b)

Figure 5.16: Comparison of phase-resolved EL measurements on (a) LDPE and (b) PEN samples subjected to various voltage levels.

When the applied voltage is increased at higher levels (i.e. more than 5kV), a more obvious relationship between the phase angle and the electrical field stress is observed, as both φ_p and φ_n are shifted significantly as the voltage is increased. An example of this can be seen from the results obtained from conducting phase-resolved EL measurements on two different samples, shown by Figure 5.17. These results are in agreement with the simulations of the phase resolved EL described in Chapter 3 and hence also in agreement with the simulations of Alison *et al.* [92]. Simulations of charge injection, recombination and EL have shown that the phase distribution of EL is dependent on the magnitude of the applied voltage as well as the parameters describing the current density at the injecting electrode.

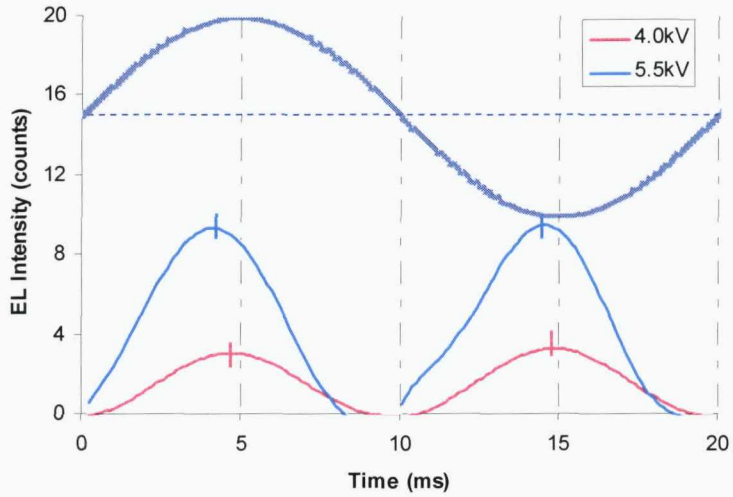

(a)

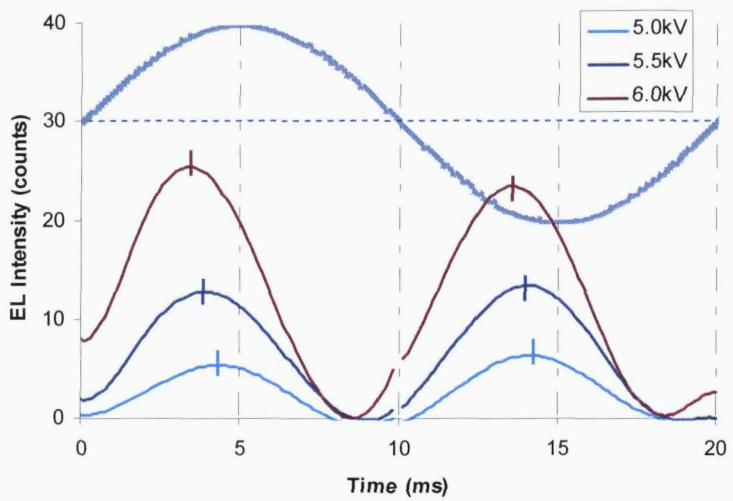

(b)

Figure 5.17: Phase difference shift at voltage levels more than 4kVrms as observed from measurements undertaken using (a) LDPE and (b) PEN samples.

5.5.3 Comparison of EL under Different Voltage Waveforms

The phase-resolved EL measurements were also conducted by applying square and triangular voltage waveforms. For this part of the experiment, the frequency was fixed to 50Hz and all measurements were conducted using LDPE samples. A comparison comprising typical phase-resolved EL measurements undertaken using sinusoidal, triangular and square applied voltages can be seen in Figure 5.18. EL was observed by applying 5.66kV voltage peak across the polymer film and the difference between the maximum and minimum intensity levels for each type of waveform is denoted as ΔEL

in the graphs. It can be seen that EL intensities for sinusoidal and triangular applied voltages are significantly lower than the emission caused by the square voltage. Nevertheless all plots exhibit the existence of two EL peaks for every ac cycle; confirming that EL phenomenon is an effect due to the interaction of the injected charge carriers with their opposite counterparts at or near to the surface states of the polymer. The EL distributions of the two half cycles for sinusoidal and triangular voltage waveforms appear to be almost symmetrical whereas the phase-resolved EL emission for square voltage waveform is asymmetric.

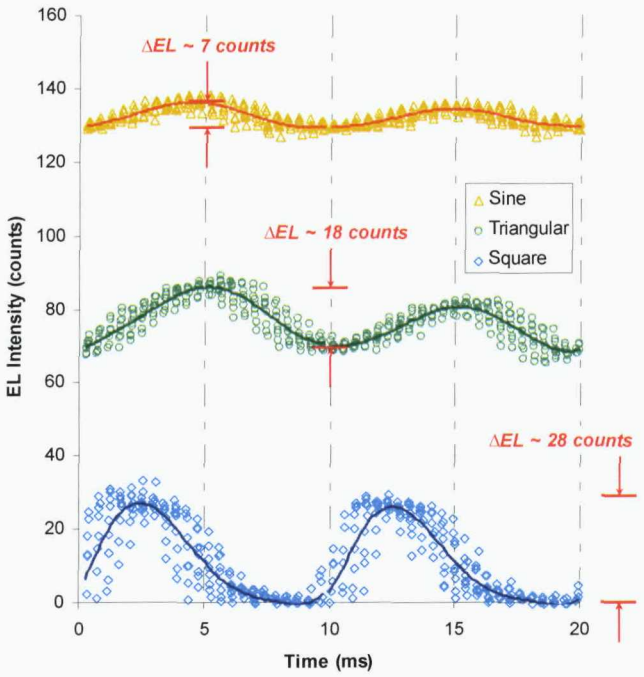

Figure 5.18: Comparing EL intensity level for one cycle of sinusoidal, triangular and square ac voltages.

Further analysis on the effect of voltage waveforms on EL can be made by comparing the corresponding time where the emission peaks each cycle. As shown by Figure 5.19, it can be seen that EL is maximum prior to the voltage peaks of the sinusoidal voltage applied. This is in accordance to the observations made by several other researchers [78, 81-83] using different experimental arrangements conducted on various types of polymeric material. In contrast, EL peaks for the triangular voltage waveform were found to occur after the peaks of its positive and negative voltage applied, but its EL intensity distribution appears to be almost symmetrical and is very similar to the measurement obtained for sinusoidal voltages. The distribution of EL for the square applied voltage on the other hand, is not as symmetrical as that of the other two waveforms. The increase in light intensity occurs very rapidly and after reaching

its maximum point, EL decreases at a relatively slower rate. The difference in EL maxima in these three types of waveform may be due to their respective charge injection characteristics, which will be discussed thoroughly in Chapter 6.

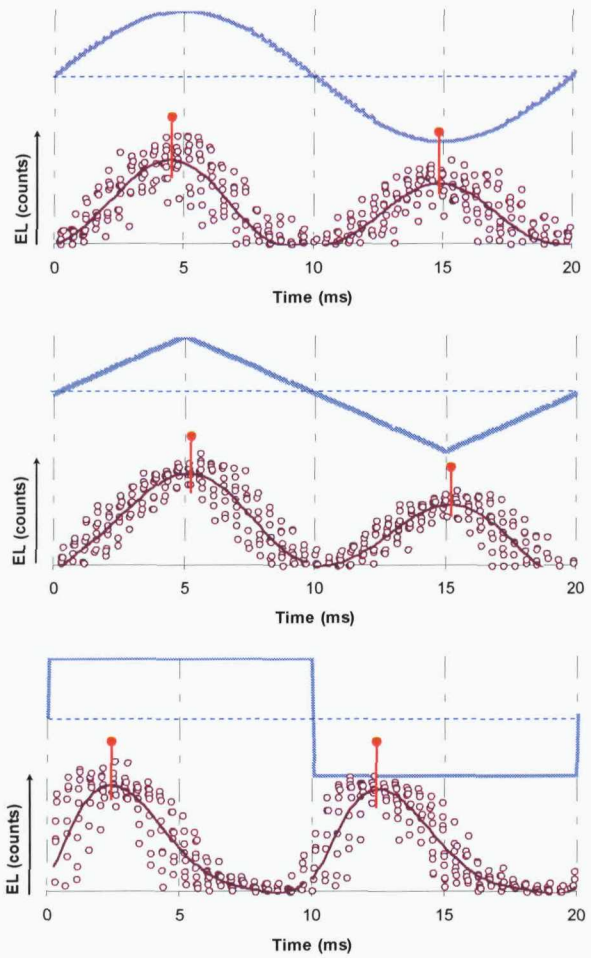

Figure 5.19: EL peaks comparison under different alternating waveforms with ~5.66kV voltage peak applied to an LDPE sample.

As the applied voltage peak is increased, EL maximum points for triangular and square waveforms do not change significantly as shown by Figure 5.20 (original plots are included in Appendix D.10). This is probably because the voltage applied is not sufficient enough to cause significant charge injection to modify the field at the injecting electrode and therefore the phase angles of the EL peaks remain unchanged. Thus they remain more or less the same with increasing electrical stresses, similar to the observation found for sinusoidal wave shape presented in Figure 5.16 (a).

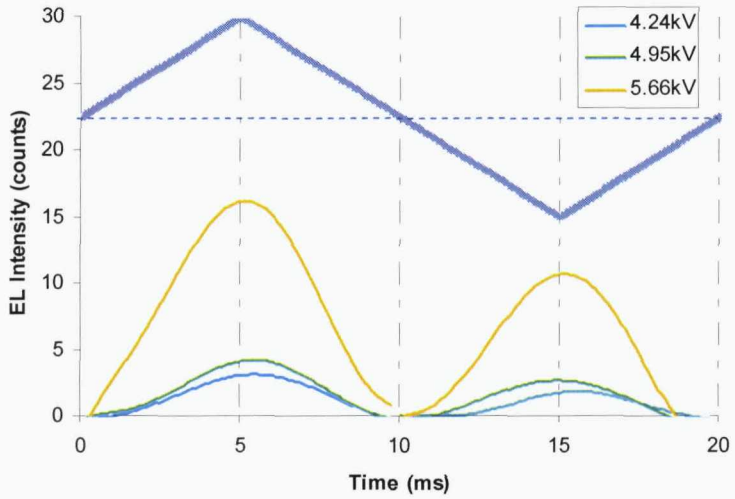

(a)

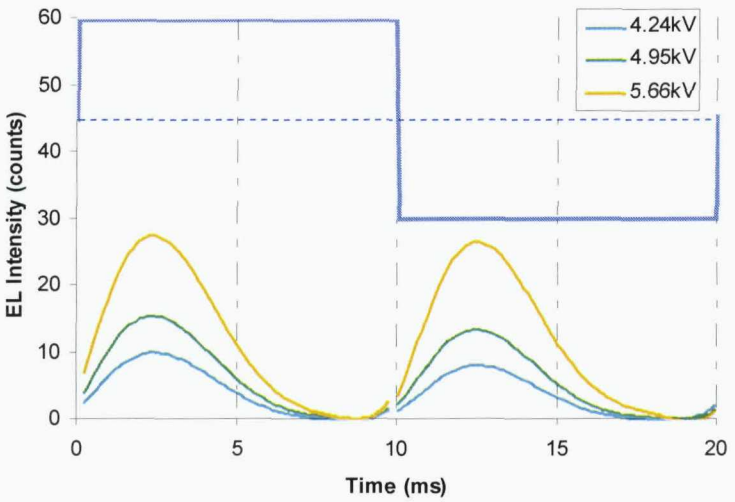

(b)

Figure 5.20: The effect of increasing applied voltages on EL maxima for (a) triangular and (b) square waveforms.

5.5.4 Effect of Voltage Symmetry on EL

Phase-resolved EL measurements were also undertaken by varying the symmetry of the applied voltage waveforms. The objective of this part of the experiment is to see how EL peaks change when the positive and negative maxima of the applied voltages are shifted in phase without changing the magnitude of the voltage peaks. The measurements were obtained by applying 4.24kV and 4.95kV peak voltage an LDPE sample for sinusoidal and triangular waveforms and the resultant EL are shown in Figure 5.21 (a) and (b) respectively. From the graphs, the phase resolved behaviour in both cases are similar and demonstrates that the phase of the maximum points of EL

intensity changes with the position in phase of the applied voltage peaks. EL was found to be highest near the voltage maxima for all measurements.

Close inspection of Figure 5.21 (b) demonstrates that the EL peaks for the triangular applied voltage waveform always occur immediately after the corresponding voltage peaks. However, this is not the case for sinusoidal applied voltage, where the peaks in the EL intensity may occur before or after the corresponding voltage peak depending on the waveform's symmetry. Table 5.5 and 5.6 summarize the phase difference, φ_p and φ_n with respect to the related peak for sinusoidal and triangular voltage wave shape. The 'plus' (+) and 'minus' (-) signs are added in order to indicate whether the EL maximum point is leading or lagging its corresponding applied voltage peaks. Although it can be argued that the position in time for these peaks may depend on the accuracy of the data obtained, the occurrence of EL maxima for the 50% symmetry of the sinusoidal applied voltage was found to be identical to the observations obtained from the previous measurements using the conventional high voltage transformer, as shown by the results in Figures 5.15 (a), 5.16 (a) and 5.17 (a). Thus the fact that the highest emission takes place just before the sinusoidal applied voltage maxima still holds true. In addition, the asymmetry of the sinusoidal and triangular applied voltage waveforms also affects the relative intensities of the two EL distributions that occur each cycle. In both cases, sinusoidal or triangular, the EL peak having the highest intensity always follows that part of the applied voltage waveform where the rate of change of voltage, *dV/dt* is greatest.

Table 5.5: Phase difference analysis for sinusoidal waveform under different voltage peak levels.

Applied Voltage Peak (kV)		4.24			4.95		
Waveform Symmetry (%)		25	50	75	25	50	75
Phase Difference	φ_p	+19.1	-8.3	-27.9	+19.1	-9.0	-19.8
(degrees)	φ_n	-17.1	-3.0	+18.0	-22.5	-9.0	+16.9

Table 5.6: Phase difference analysis for triangular waveform under different voltage peak levels.

Applied Voltage Peak (kV)		4.24			4.95		
Waveform Symmetry (%)		25	50	75	25	50	75
Phase Difference	φ_p	+19.4	+8.1	+18.9	+36.7	+26.1	+18.9
(degrees)	φ_n	+17.1	+27.0	+34.2	+17.1	+27.9	+34.2

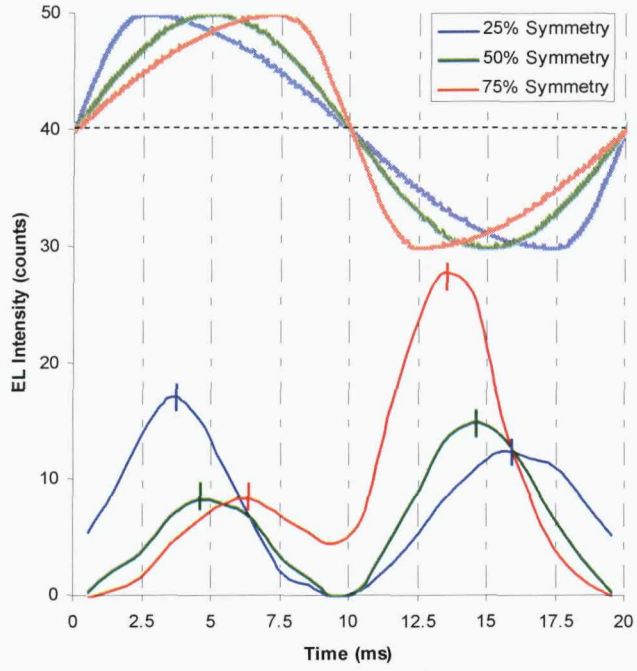

(a)

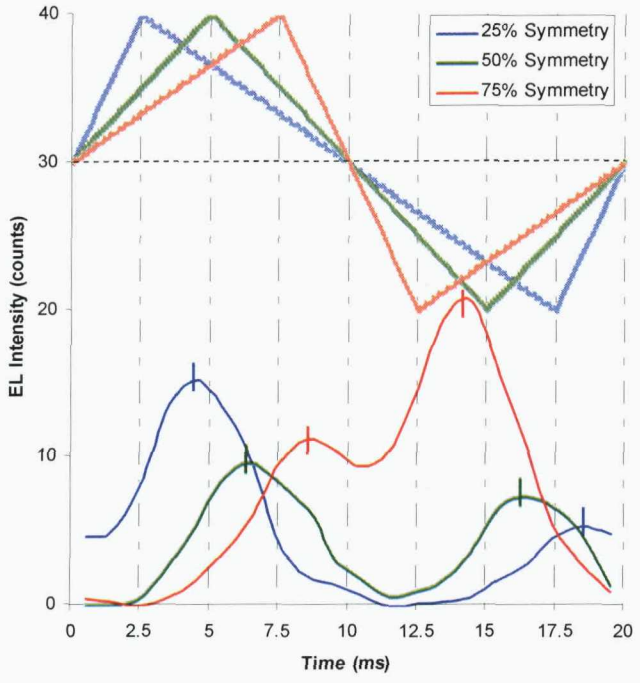

(b)

Figure 5.21: The effect of voltage symmetry on EL under (a) sinusoidal and (b) triangular waveforms with peak voltage of 4.95kV.

EL measurements were also conducted using a square wave applied voltage waveform with different symmetries (mark-space ratios) to determine the effect of abrupt changes to the applied voltage as well as the relative times of constant positive and negative applied voltage on the resultant EL intensity. EL measurements obtained using peak voltages of 4.24kV and 4.95kV peak and a range of symmetries are shown in Figure 5.22 for an LDPE sample. The EL emission begins after the sudden change from positive to negative applied voltage or vice versa. After the EL reaches a maximum intensity, there is a gradual decrease in the EL intensity while the applied voltage remains at a constant value and before the voltage sign suddenly changes again. The decrease in EL intensity may be due to stored charge in the space charge region gradually reducing the amount of charge injected or that subsequent recombination events while the applied voltage is constant are depleting the amount of trapped charge of opposite sign in the space charge region. The phase at which the peaks in the EL intensity occur each cycle appears to be independent on the magnitude of the applied voltage and when the symmetry is changed. The phase delay between the reversal of the applied voltage polarity and the peak in the EL intensities also remains constant as shown in Table 5.7.

Table 5.7: Phase difference analysis for square waveform under different voltage peak levels.

Applied Voltage Peak (kV)		4.24			4.95		
Waveform Symmetry (%)		25	50	75	25	50	75
Phase Delay	φ_p	+54.0	+54.2	+46.8	+63.5	+63.9	+63.0
(degrees)	φ_n	+46.8	+52.2	+45.0	+46.3	+54.0	+61.2

Similar to sinusoidal and triangular voltage waveforms, the relative intensity of the EL peaks for square voltages was also found to be dependent on its symmetry. It appears that the EL peak with the maximum intensity follows the parts of the applied voltage cycle where the duration of constant voltage is a minimum. The raw data and other adjusted phase-resolved EL results for all three waveforms are included in Appendix D.11 to D.16.

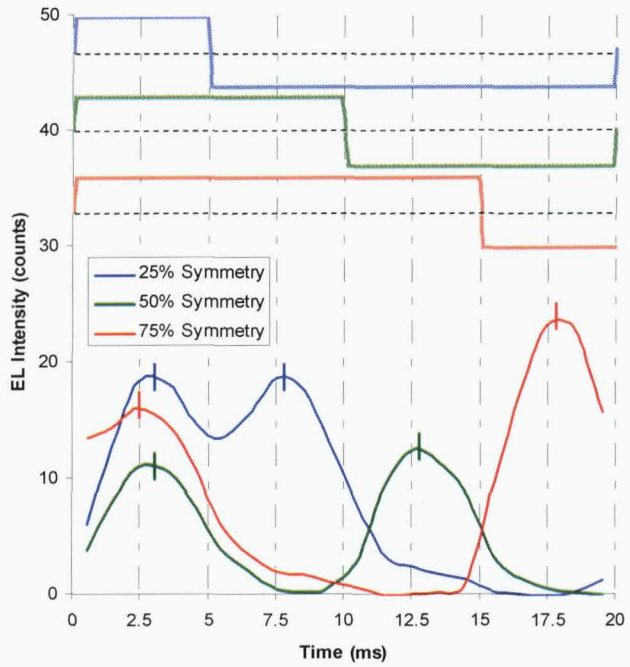

(a)

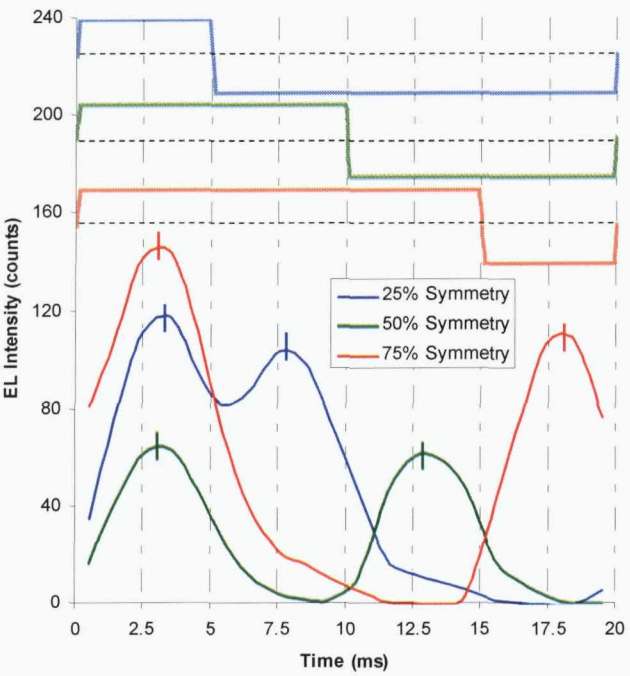

(b)

Figure 5.22: EL variation with waveform symmetry as a result of applying (a) 4.24kV and (b) 4.95kV voltage peaks across an LDPE film.

5.6 Summary

The experimental results obtained to investigate EL phenomenon in polymeric insulating materials have been detailed and discussed in this chapter. In general, EL emission can be classified as homogeneous or inhomogeneous and the difference in the images obtained relates to how well the samples are prepared. Three types of polymers were used in the experiment and they are of low-density polyethylene (LDPE), polyethylene terephthalate (PET) and polyethylene naphthalate (PEN) films.

It was observed that light emission coming out from PET and PEN samples have relatively higher intensities compared with LDPE and this is probably because of the aromaticity feature present in the two types of material. The behaviour of EL phenomenon under different gas environments was also investigated. The chamber was filled with 1 bar of dry nitrogen (N_2) or sulphur hexafluoride (SF_6) in order to study their effects on EL. The light emission was significantly reduced under the influence of SF_6 gas and this correlates to its strong capability in capturing the free electrons emitted from the metallic electrode.

Since the main objective of this research is to examine EL phenomenon under alternating applied voltages, the original experimental setup was developed further in order to perform the phase-resolved measurements. The occurrence of EL with respect to the ac voltage was determined and it was found that the light emission is at maximum near the peaks of the applied electrical stress. In addition to the typical sinusoidal waveform, EL measurements were also conducted by applying triangular and square voltages across the sample under test.

Chapter Six

DISCUSSION

6.1 Origins of the Detected Light Emission

In analyzing the occurrence of EL phenomenon in insulating materials, it is crucial to understand the physics encompassing the characteristics of a simple polymer such as polyethylene. The material has a very wide band gap so the movement of charge carriers is not as simple as for semi or fully conducting materials. The existence of traps, especially at the surface region of polymers, allows charge carriers to be 'implanted' within the vicinity of the dielectric. At room temperature, electrical charges are injected from metallic electrode into polymer via Richardson-Schottky or Fowler-Nordheim mechanisms; depending on the level of electric field applied. Then these injected charges will either collide with the molecules of the dielectric material or recombine with the charge carriers of opposite polarity, both of which can lead to excited molecular states. Regardless of the type of excitation mechanism, subsequent

relaxation process will cause the release of photonic energy and this is essentially EL emission.

As explained earlier in Section 3.2.2, the occurrence of EL is strongly related to the current density of the charge carriers injected into the polymer. Since the experiment was carried out by applying electric fields in the range of several tens of $kVmm^{-1}$ across the sample, it was shown in Section 3.4 that the theoretical injected current density (and therefore EL emission) is an exponential function of the electric field applied. Figures 6.1, 6.2 and 6.3 show the averaged natural logarithm of EL measured against a series of applied voltages for LDPE, PET and PEN samples respectively; the data being derived from those shown in Figures 5.4 to 5.6. 120 points were averaged per voltage level and the error bars correspond to plus and minus one standard deviation of the calculated values of EL natural logarithm. From these figures, it can be seen that detectable EL emission starts at a voltage of approximately 3 to 4kV. It is difficult to ascertain whether the range corresponds with the actual process of charge injection since no simultaneous measurement for current were taken and the detection may be limited by the sensitivity of the camera. Nevertheless, the detection of EL at a voltage of around 3kV for any sample suggests that the measurements in examining the phenomenon should be performed with applied voltage levels greater than this value. In addition to this, it has been demonstrated that the natural logarithm of EL is linearly proportional to the voltage applied as predicted from the injection law characteristics, described by Equation {3.36} in Section 3.4.

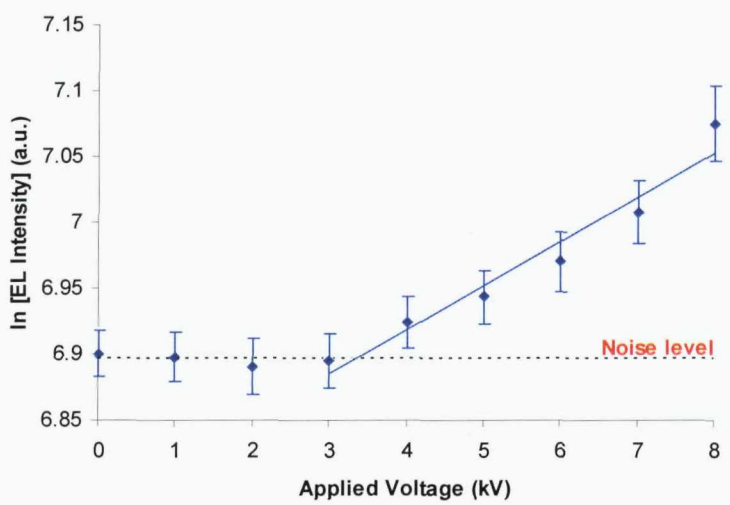

Figure 6.1: The averaged natural logarithm of EL intensities as a function of applied voltages for an LDPE sample.

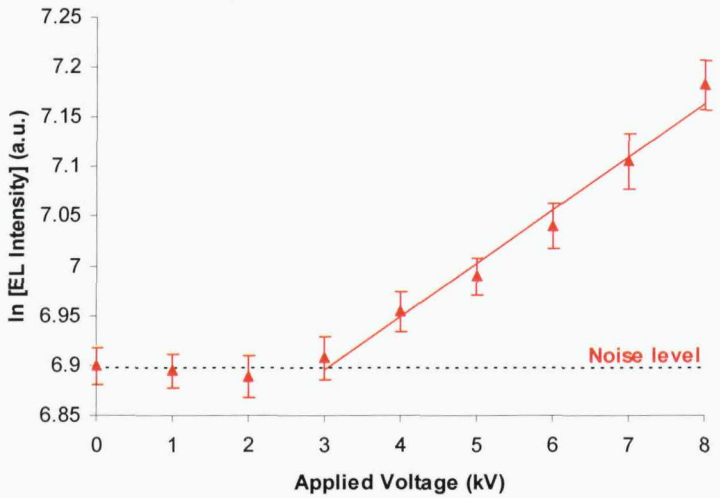

Figure 6.2: The averaged natural logarithm of EL intensities as a function of applied voltages for a PET sample.

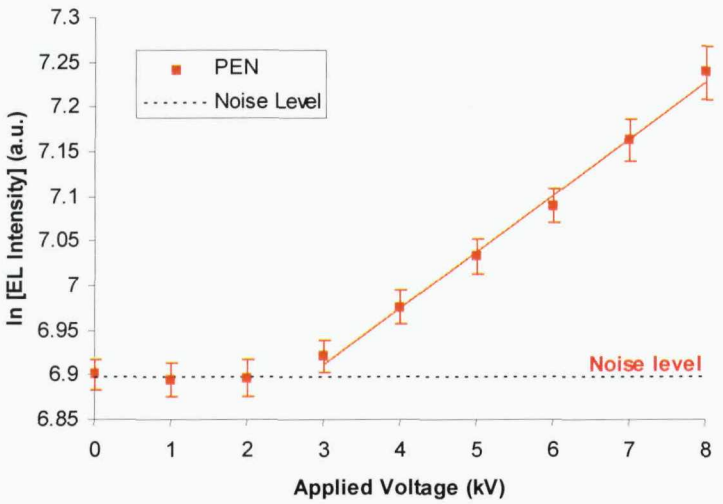

Figure 6.3: The averaged natural logarithm of EL intensities as a function of applied voltages for a PEN sample.

The threshold voltages obtained by extrapolating the EL intensity to the noise level for the three materials were 3.3kV ± 0.5kV for LDPE, 2.8kV ± 0.4kV for PET and 2.6kV ± 0.4kV for PEN. These values correspond to threshold electric fields of 33kVmm^{-1} ± 5kVmm^{-1}, 28kVmm^{-1} ± 4kVmm^{-1} and 21kVmm^{-1} ± 3kVmm^{-1} for LDPE, PET and PEN respectively. Hence, the threshold fields for the occurrence of EL were found not to be significantly different for these materials.

Figure 6.4 compares the averaged EL intensity as a function of voltage levels for the three types of polymer after subtraction of the dark noise. It was found that the EL intensity from PET and PEN films are more or less similar with both have significantly higher intensity compared with LDPE samples for voltages of 5 to 8kV. The difference in intensity levels is due to the existence of an aromatic backbone in the repeating units of PET and PEN molecules, but not for LDPE. This feature acts as chromophores where light is being emitted as the delocalization of electrons present in the ring structure allows more excited states to be produced and supports the conjecture of Mary *et al.* [135].

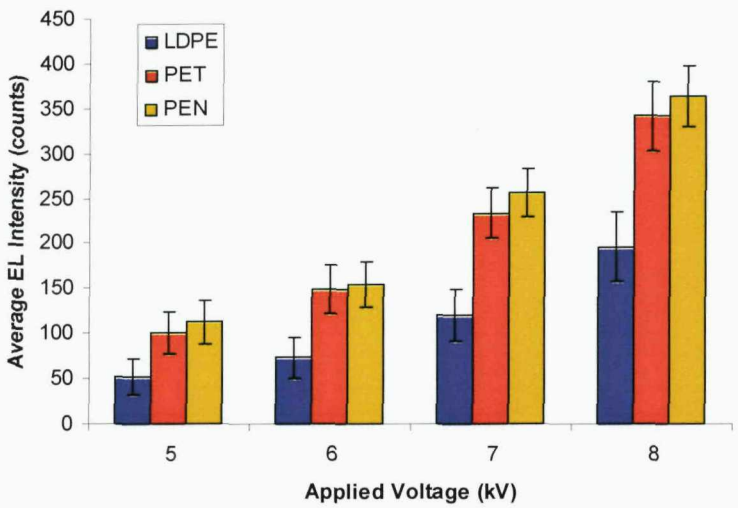

Figure 6.4: Averaged EL intensity after subtracting the noise level for three different polymeric materials subjected to 5 to 8 kV rms.

6.1.1 Effect of Material Chemical Composition

The general trend for all spectra of the three polymeric materials is increasing EL intensity from 450nm towards 700nm wavelength as shown by Figures 5.7, 5.8 and 5.9. The relatively low level of emission near the ultraviolet range compared to the other spectrum region indicates that the light is not due to partial discharge activity since this phenomenon occurs with energies beyond 4eV [85] and light emission of wavelength corresponding to the near UV region. In addition to this, it can be seen that the emission is significantly high in the infrared region for all voltage levels. Previous studies have shown that this finding was only observed under a uniform field [108, 135, 136] but not under divergent field conditions [56, 137, 138]. It has therefore been suggested by Teyssedre *et al.* [139] that the significant contribution from the red

component observed in this measurement could originate due to the formation of surface plasmon through the metallic layer. Generally speaking, surface plasmon is a radiative effect due to the decay of electromagnetic waves that propagate along metal surfaces as a result of collective electron gas oscillations within the metal [140]. The strong fluctuations of current density at the boundary of metal and polymer due to polarity reversal make this effect specially evident under ac stresses as opposed to the dc condition where injection is space charge limited [139].

In order to see more clearly the changes in EL emission within regions of the spectrum where they are less affected by the surface plasmon, the effect may be suppressed by normalizing all data points with respect to the intensity values at the 700nm wavelength. The normalized data at point i, X_{iN} can be calculated using the formula:

$$X_{iN} = \frac{X_i - X_{\min}}{X_{700} - X_{\min}} \qquad \{6.1\}$$

where X_i is the intensity value to be normalized, $X_{\min}$ is the minimum intensity and X_{700} is the intensity at 700nm from the series of data for one spectral measurement per voltage applied. The effect of the normalization can be illustrated by Table 6.1 and the results from other samples are presented in Appendix D.17. From these results, it is obvious to see that there is a gradual increase in light intensity in the visible region (500 to 600nm) as applied voltage is increased, whereas the changes near the ultraviolet wavelength remain negligibly small. These findings indicate that on increasing the electrical stress, charge is injected further into the material and recombines in regions more representative of the bulk material and this will lead to the increasing contribution of emission at wavelengths of 500 to 600nm; which corresponds to energy level of around 2eV. The interpretation of such finding has been reported by several other researchers [58, 59, 141] and that this level of energy may just be sufficient to break the intermolecular bonds of the polymer and create reactive radicals that can cause further degradation.

The comparison of EL characteristics between LDPE, PET and PEN materials has provided some insight into this phenomenon. The presence of aromatic backbone in PET and PEN results in significantly higher total light intensity compared to LDPE, and the small discrepancy observed from the spectral analysis of these three materials suggests that they have slightly different recombination mechanisms leading to EL in the range 500 to 600nm.

Table 6.1: Normalizing the spectral measurement of Figures 5.7, 5.8 and 5.9.

Material	Normalized result
LDPE	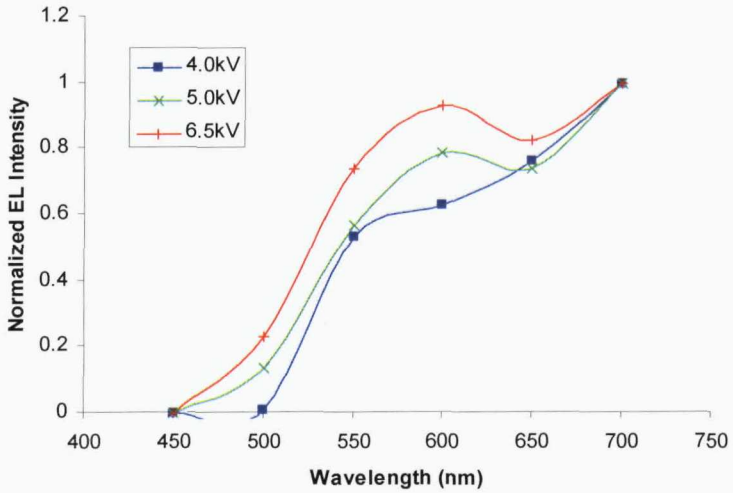
PET	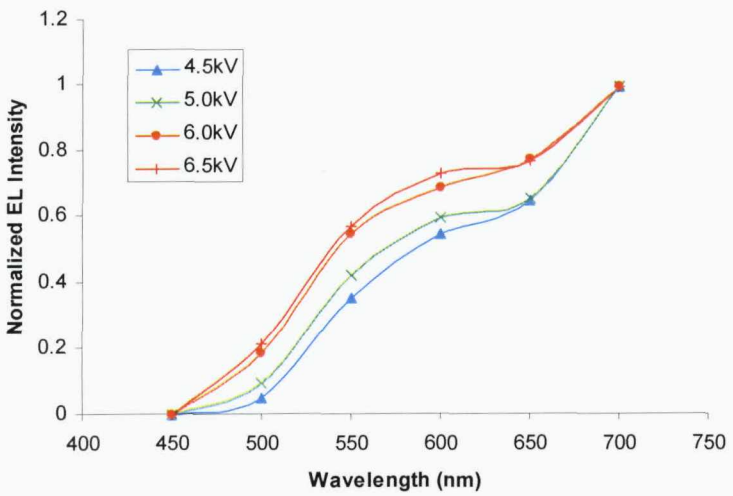
PEN	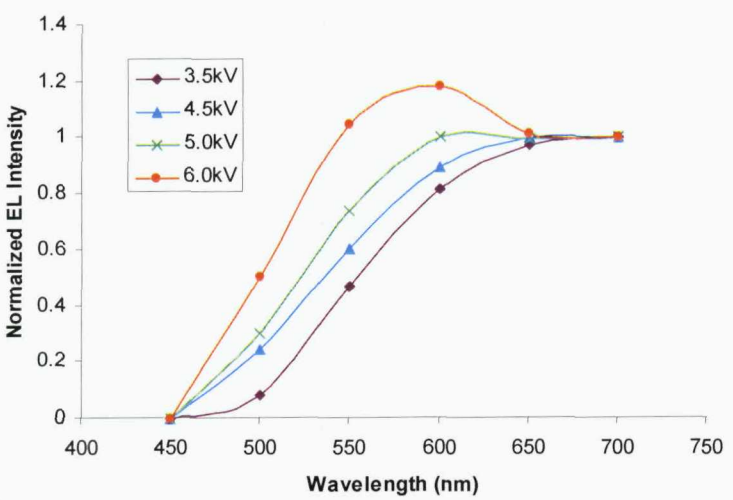

6.1.2 Impact of Gas Molecules

It is interesting to see that the intensity levels near the infrared region for both N_2 and SF_6 gas environments (shown in Figures 5.12 and 5.13) are more or less the same. EL intensity at the 700nm wavelength obtained from testing three LDPE samples subjected to various electrical stresses under the influence of N_2 and SF_6 gases are compared and shown in Figure 6.5. Although having slightly lower intensity in SF_6, the average level of EL at this particular wavelength falls between the plus and minus one standard deviation of the intensity measured under N_2. This indicates that the presence of gaseous molecules may have greater impact on the emission processes that occur within the bulk of the polymer rather than on the surface (interfacial) states or the formation of surface plasmon on the electrode. Therefore the relative increase in EL intensity with the rise of applied voltage can be compared by normalizing all data points with respect to their corresponding values at 700nm wavelength.

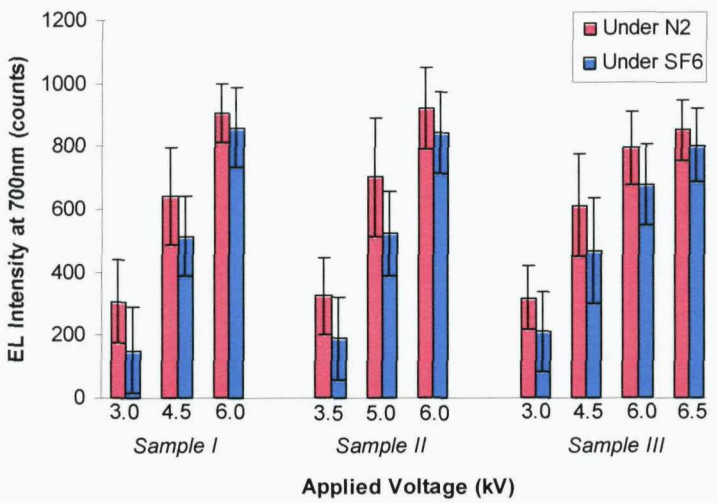

Figure 6.5: Comparing EL intensities near the infrared region under N_2 and SF_6 gases.

Using Equation {6.1}, the normalized plots for two sets of measurements are constructed as shown by Figure 6.6; which is based on the results presented in Figure 5.12 and 5.13, and Figure 6.7; which is based on the results shown in Appendix D.3 from a different sample of the same material. These figures show that in increasing the voltage applied on the same sample, EL emission in the 500 to 600nm region increases more apparently when the chamber is pressurized with N_2 rather than SF_6 gas. Since no absorption of light by the gases should occur within this wavelength range, it can therefore be argued that the significant reduction in EL intensity at 550nm of samples

within a SF_6 environment is due to the influence of the gas on the excitation and recombination of electronic states within the bulk of the polymer. The polymeric samples are vacuum treated by pumping down the chamber containing the samples at room temperature to a pressure of 0.5 mbar for a long period of time (40 to 60 minutes) to allow existing gas molecules within the samples to diffuse out of the material. When re-pressurising the chamber to 1 bar using N_2 or SF_6, these gas molecules may diffuse into the bulk of the polymer. Gas molecules may be situated at the metal dielectric interface and may introduce new localized electronic states that could further affect the charge injection characteristics of charge carriers across the interface [87].

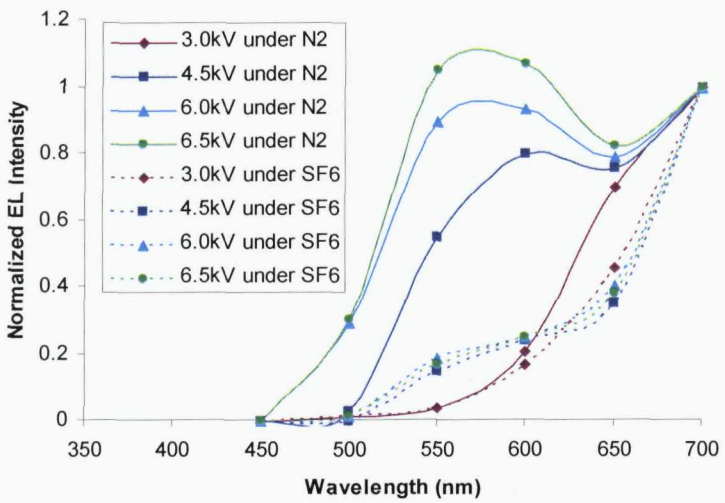

Figure 6.6: Comparing the effect of gas environment on EL emission from LDPE sample I.

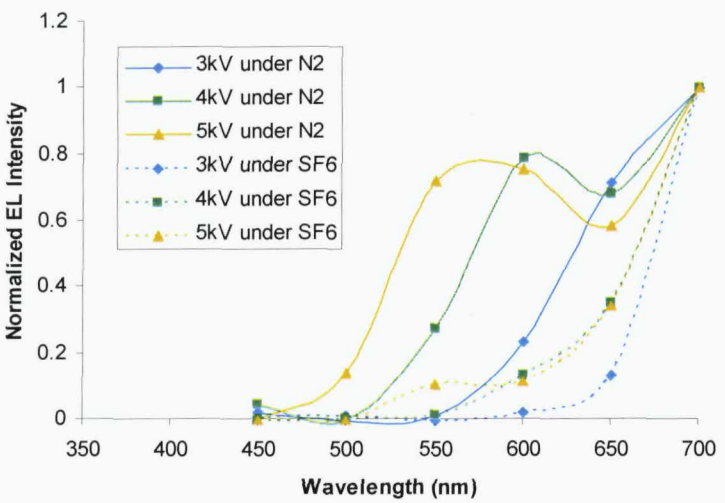

Figure 6.7: Comparing the effect of gas environment on EL emission from LDPE sample II.

Thus it can be argued that the difference of light intensity in the visible wavelength under the two types of gas environment correlates to the chemical characteristics of the gas itself. SF_6 is an electronegative gas so its molecules can interfere with the formation of the excited states by capturing the injected electrons due to its high electronegativity. This will eventually decrease the light emission since there will be less radiative recombination available. Similar reduction of EL was also obtained by Laurent *et al.* [84] using oxygen (O_2), which is another type of gas with strong electronegativity. N_2 on the other hand, is a chemically inert gas so its molecules will not interact with any other elements including the injected carriers from the metal. Therefore it can be said that the EL emission observed under N_2 gas environment is more likely to represent the actual processes of excitation, recombination and trapping that are intrinsic to the material. This statement could be confirmed by testing samples under vacuum; however this presents a significant experimental problem in that under low pressures, a glow discharge is set up in the chamber making it impossible to detect the EL from the samples.

From this study it can be concluded that the presence of gas molecules plays a crucial role on the formation of EL in polymer materials. It was found that the presence of gases with high electronegativity would suppress the processes leading to the formation of EL and hence could be used as a means of suppressing ageing in polymeric materials. However, the absence of EL does not necessarily mean that ageing no longer occurs as charge injection and recombination could still occur but that the recombination is no longer radiative resulting in energy dissipation via the formation of phonons (quanta of vibrational energy) which could still lead to material ageing. Hence it is important to identify exactly how electronegative gases can suppress excitation or modify the recombination process.

6.2 Occurrence of EL with respect to Alternating Applied Voltage

The occurrence of EL with respect to the alternating applied voltages was determined through the phase-resolved measurements. In conducting this part of experiment, the light intensity was measured within a small timescale over a large number of acquisitions in order to get reliable signal to noise ratio. The experiment was initially performed using the typical sinusoidal applied voltage obtained using a step-up HV

transformer. It was found that the EL reaches its maximum point just before the voltage peaks, and it advances in phase as the applied voltage is increased. This observation is similar to the results obtained from other researchers [82, 84].

Employing a signal generator and HV amplifier enabled phase-resolved measurements to be conducted using triangular and square voltage waveforms in order to understand the role of charge injection in causing EL emission. The results show that the EL distribution for sinusoidal and triangular voltages are almost symmetrical, with the difference being the point where EL peaks occur with respect to voltage maxima. The discrepancy of the peaks in relation to the voltage maxima may possibly correspond to the difference in the saturation mechanism for both waveforms. The phase-resolved results using square voltages on the other hand, show that EL increases rapidly to its maximum value when the voltage peak changes and then gradually decreases during times of constant applied voltage. In addition, phase-resolved EL measurements were also conducted by varying the alternating voltage symmetry, and the results obtained clearly indicate that the emission peaks are dependent on the positions in phase of the positive and negative maximum levels of the applied voltage.

6.3 Comparing Phase-Resolved Experimental Results with EL Simulations

The results obtained from various phase-resolved EL measurements allow comparisons to be made with simulations of the phenomenon. Using the same parameters defined in the simulation work by Alison *et al.* [92], it was found that the saturation process occurs for applied electric fields greater than 100kVmm^{-1} where significant phase shift in the EL peaks occurs as a result of increasing field. For fields lower than this value, saturation was found to be negligibly small and therefore no shift in EL peaks can be seen as applied voltage is raised. In the phase-resolved EL measurements on the other hand, the phase angle between the EL and applied voltage peaks is quite evident even at fields lower than 100kVmm^{-1}. Although the phase angles do not change drastically when voltage is increased from 3kV to 5kV, the shifts become more obvious when the applied field is in the range of 60kVmm^{-1} and above; suggesting that the field limiting process occurs at slightly lower fields than the simulated values. There are a number of reasons that can possibly explain the difference between the experimental and simulation results.

The parameters for the charge injection defined by Equation {3.12} used in the simulation were based on the work specifically for injection in a pin-plane configuration [105]. Thus it may be argued that it might not be true for the case of plane-plane electrode geometry sample where the injection field may be much lower. In addition to this, the choice of material used for EL analysis may also contribute to the differences. The values for α and β approximated by Hare [105] may only be appropriate for the injection from a tungsten pin into an epoxy resin whereas the experimental work for this research was undertaken using polymers with gold sputtered onto the surface. This will then lead to a discrepancy in the barrier height for the charge injection mechanism due to the different work function of the metallic electrode and electron affinity of the dielectric. Therefore by adjusting the values of parameter α and β describing the charge injection mechanism, a better agreement between the modelling results and experimental data could be achieved. In modifying these values, several outcomes from the experimental results must be taken into consideration:

1. EL peaks occur just before the peaks of the sinusoidal applied voltages so it can be deduced that field saturation does occur albeit very small.
2. The shift in the EL peaks does not occur drastically with the increase of applied voltages from 3kV to 5kV rms but tends to become more obvious as voltage is raised above 5kV rms.
3. Although the changes of the phase angles of the EL peaks were observed with the increase of applied voltage beyond 5kV rms, the distribution of the emission does not change significantly and appears to remain almost symmetrical.

As discussed in Section 3.4.3, the changes on charge injection mechanism (and therefore simulated EL emission) rely on the values of α and β with different proportions. The phase angles observed experimentally changes evidently but the EL distribution's skewness does not change drastically so it may be plausible to increase the value of α in order to allow field saturation. Figure 6.8 (a) and (b) shows the simulation results obtained for various applied voltages with $\alpha=3\text{x}10^{-3}\text{Am}^{-2}$ and $\beta=7\text{x}10^{-8}\text{mV}^{-1}$ for the injection law parameters. From these figures, it can be seen that by increasing the value of α by two decades from the approximated value obtained by Hare [105] will cause EL peaks to occur just before the applied voltage maxima and minima as a result of field saturation. This is in accordance to the experimental results presented in Chapter 5.

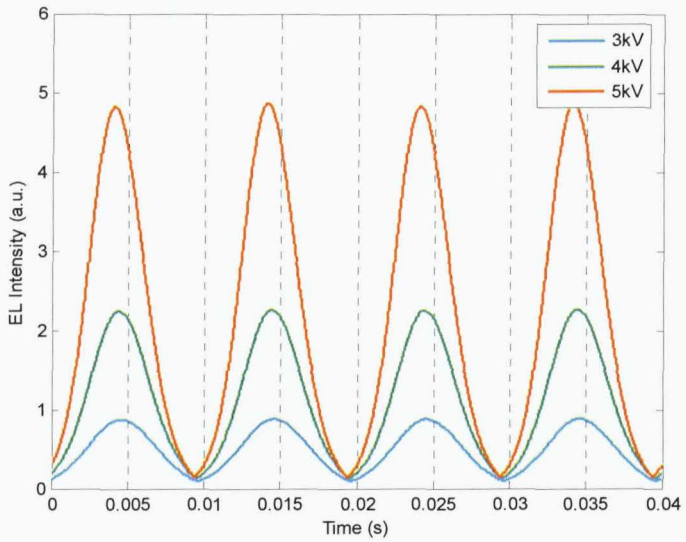

(a)

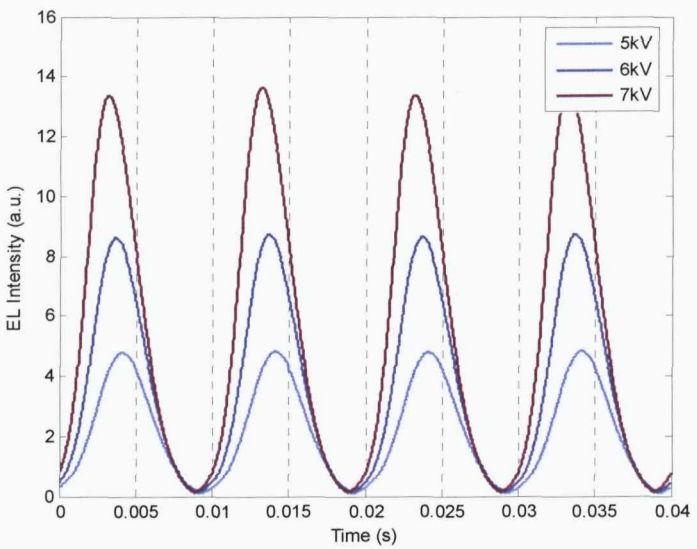

(b)

Figure 6.8: Simulation of EL as a result of applying sinusoidal voltage with peak values of (a) 3, 4 and 5kV, and (b) 5, 6 and 7kV with injection law parameters α=3x10^{-3}Am^{-2} and β=7x10^{-8}mV^{-1}.

It must be noted however that the simulated emission does not decrease to zero for any applied voltage since the minimum value for the injected current density equation described by {3.12} will essentially equal to the value of α. This is not the case for the phase-resolved measurements where EL was found to be zero at certain times. It can be argued that the emission is too small for the CCD camera to detect and therefore the results obtained experimentally are limited to the sensitivity of the detection system. In addition to this, it can be said as well that the lack of accuracy in the measurement system could be responsible for the phase difference between EL peaks and the applied voltage maxima and minima, not because of the saturation of field per se. This argument can be validated by comparing the simulation of EL with different waveform symmetries under field saturation (α=3x10^{-3}Am^{-2}) and non-saturation (α=3x10^{-5}Am^{-2}) conditions.

Figures 6.9 (a) and (b) compare the simulation results obtained by applying 5kV voltage peak with different sinusoidal waveform symmetries under field saturation and non-saturation conditions respectively. The simulated EL emissions in both cases have shown that the position of EL peak is dependent on the relative position of the applied voltage maximum and minimum values. During field limiting however, the relative EL intensity is also a function of the applied voltage symmetry and this agrees with the observation obtained in the phase-resolved experiment. EL peak was found to be the highest when the rate of change of the voltage applied, *dV/dt* is the greatest. Therefore it can be deduced that the measurements of EL were undertaken during field saturation process, and the difference in phase angles corresponds to this effect, not because of inaccuracy in intensity reading. Hence the simulations with α=3x10^{-3}Am^{-2} are in accordance with the measured data.

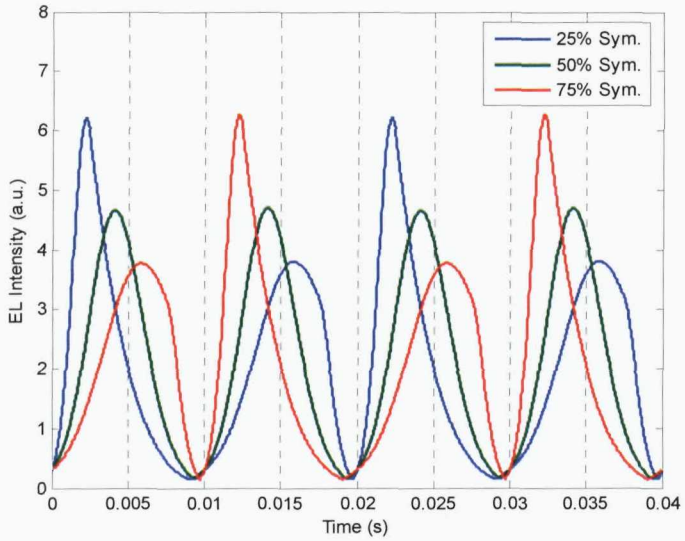

(a)

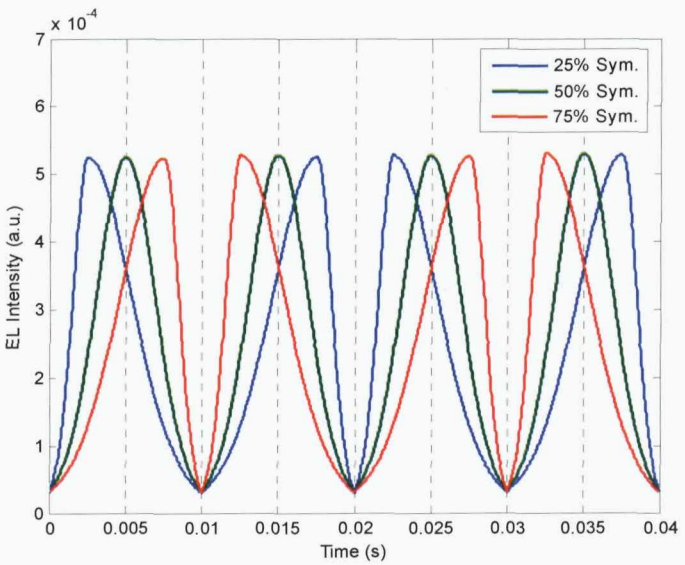

(b)

Figure 6.9: Simulated EL emission by applying sinusoidal voltage with a peak value of 5kV under different waveform symmetries with charge injection parameter α set to (a) $3x10^{-3}Am^{-2}$ and (b) $3x10^{-5}Am^{-2}$.

6.3.1 Modifying the Model to Accommodate EL Simulation using Triangular and Square Applied Voltages

Since the phase-resolved EL experiments were also conducted using triangular and square applied voltages in addition to the typical sinusoidal, the model has been modified to incorporate both waveforms into the simulation. This is to analyze further the effect on the charge injection mechanism due to the different applied field waveforms. The alterations can be seen in Appendix A.2 (for triangular voltage) and

Appendix A.3 (for square voltage), and all graphical outputs were obtained using the same parametric values as defined in Table 3.1 except for α, which is set to the new value of $3x10^{-3}Am^{-2}$ to allow saturation of field to occur. In modifying the applied voltage following a triangular waveform, the voltage is set to increase at a constant rate before reaching its maximum and minimum points. Modelling using a square wave applied voltage nevertheless, is not as straightforward as voltage does not increase abruptly from zero to its maximum and minimum values realistically speaking. Instead, voltage increases gradually within a short period of time and thus the simulation was developed based on a trapezoidal voltage waveform rather than a perfect square. In modifying the original program, the 50Hz triangular and 'square' voltages are allowed to ramp up and down to its maximum and minimum points in 5ms and 2ms respectively; as shown by Figure 6.10.

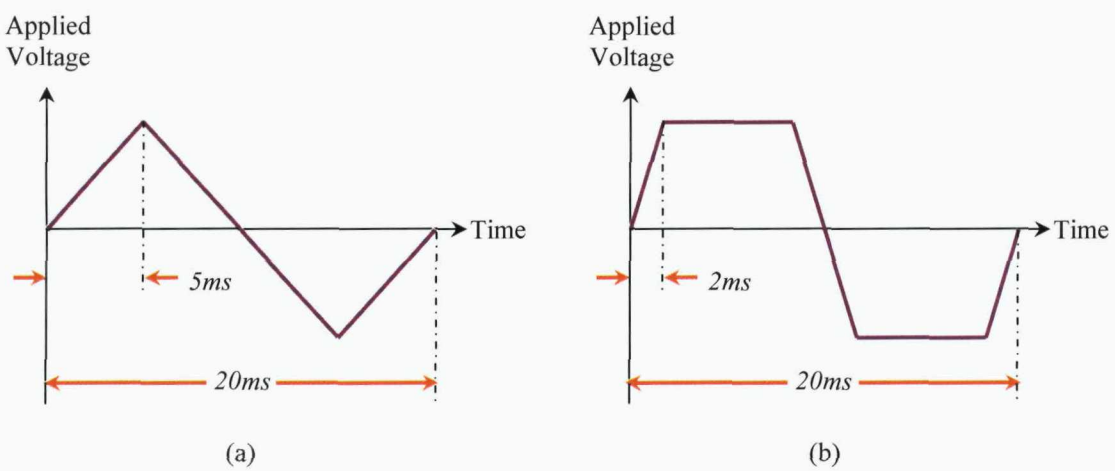

Figure 6.10: The voltage profile to simulate EL emission under the influence of (a) triangular and (b) 'square' voltage waveforms.

The results shown in Figure 6.11 (a) and (b) represent the simulated EL emission by applying triangular and square applied voltage waveforms respectively; with peak values of 3, 4 and 5kV. With the new value of α, the computed EL emission due to triangular applied voltages does not exactly match its corresponding experimental result and this is most probably due to the fact that in the experimental measurements of EL, the data was subject to a ~2ms time averaging filter, and this will be explored later in this section. The phase angle of the EL peak also remains the same with increasing applied voltages; indicating insufficient charges were injected to cause significant saturation of field for the peaks to shift. The simulated EL emission for

square voltage waveforms on the other hand, shows a high degree of saturation occurs even at low fields and the emission result obtained is in very good agreement with the results observed experimentally. The slight discontinuity shown in Figure 6.11 (b) is due to the non-zero current density when the electric field is low as a result of using a relatively high value for α. Nevertheless, the striking resemblance observed in the distribution of EL in both simulation and experimental work has further validated the occurrence of field saturation during the measurement of EL with a square wave applied voltage even for applied fields lower than 60kVmm^{-1}.

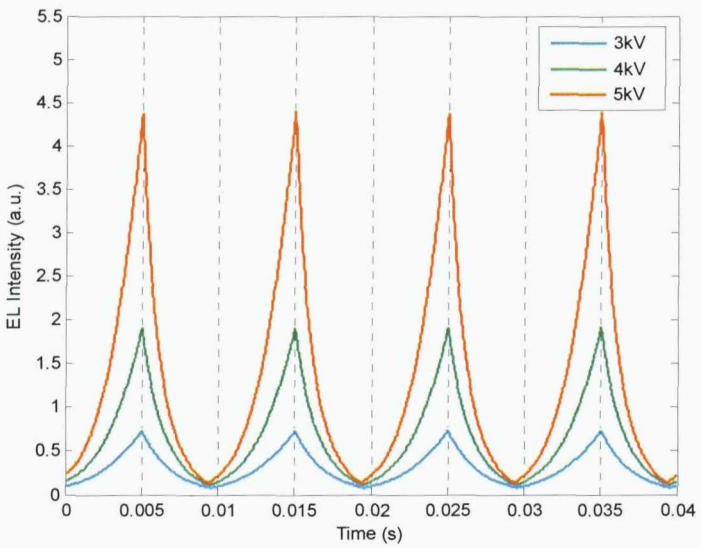

(a)

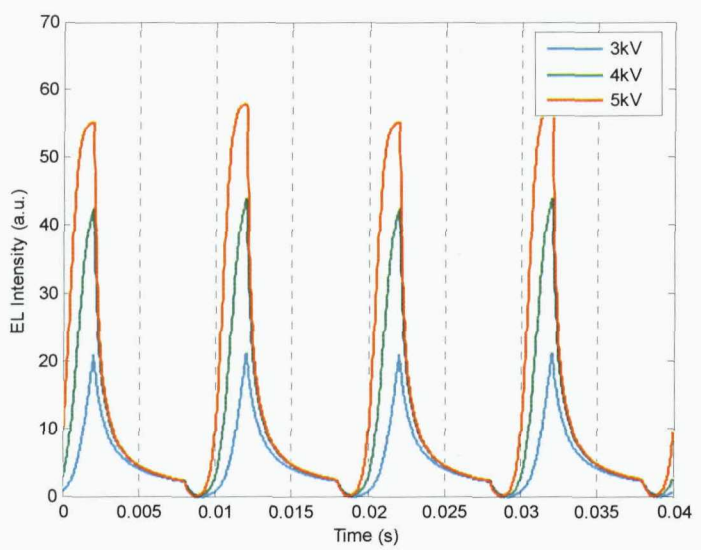

(b)

Figure 6.11: Simulated EL emission due to (a) triangular and (b) 'square' waveforms for various applied voltage peaks.

The simulated EL emission under sinusoidal, triangular and square waveforms with applied voltage peaks of 5kV are compared in Figure 6.12. From this figure, it is obvious to see that EL peaks under square voltages are relatively much higher than those for sinusoidal and triangular waveforms. In addition, it can also be seen that the phase angles are different for each voltage waveform where EL emission with square voltage has the smallest angle, followed by that of sinusoidal and then triangular voltages. These two outcomes are consistent with the comparison made for phase-resolved experimental results using the three types of applied voltage waveforms, as shown in Figures 5.18 and 5.19. Since the magnitude of EL peak and its corresponding phase angle are highly dependent on the applied voltage waveforms, it can therefore be said that the occurrence of the phenomenon is a function of the rate of change of voltage applied, *dV/dt*. This argument can be validated by analyzing the simulated EL emission by varying the waveform symmetries. Figure 6.13 shows the effect of varying the symmetries of the triangular and square applied voltages with peak value of 5kV. Similar to the results obtained using sinusoidal voltage waveform, it can be seen that the relative EL peaks and their phase angles are significantly different for each voltage symmetry; further supporting the fact that the occurrence of EL depends greatly on the rate of change of the applied voltage as long as saturation of field condition is achieved.

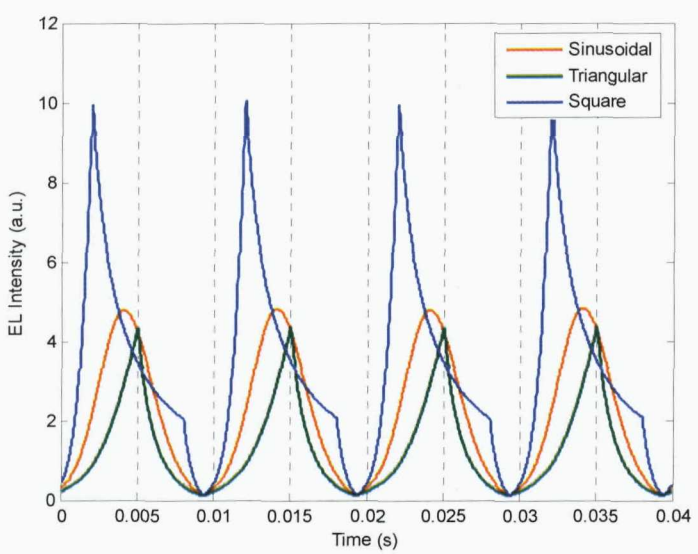

Figure 6.12: Comparing the simulated EL emission for sinusoidal, triangular and square applied voltage waveforms.

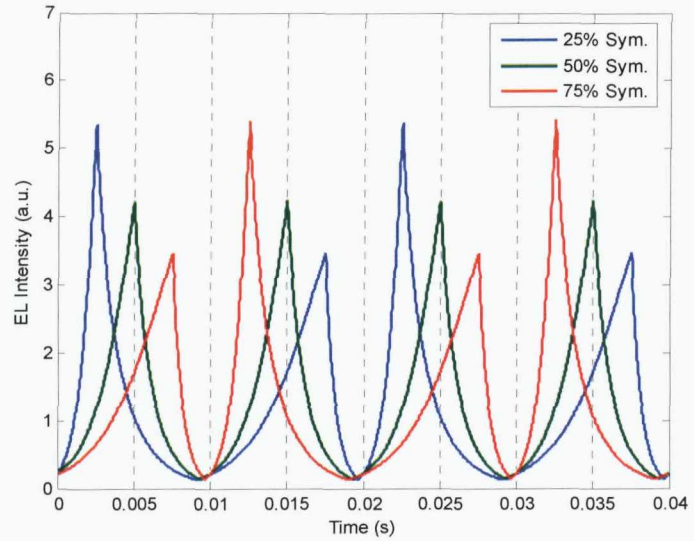

(a)

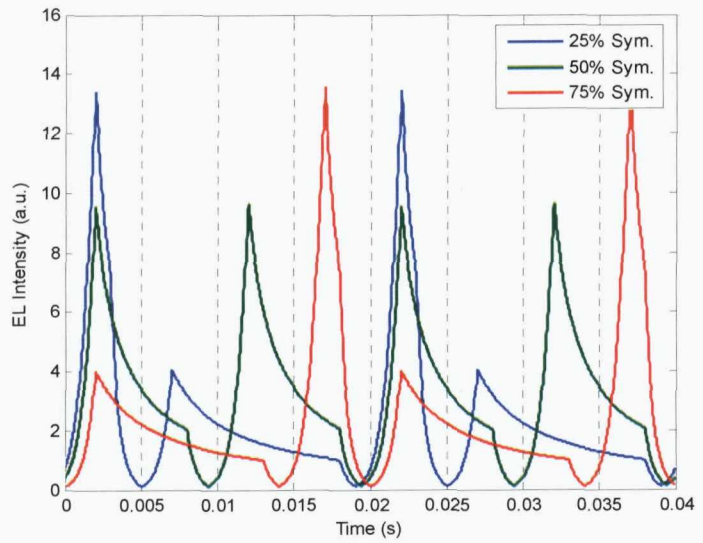

(b)

Figure 6.13: The effect of varying the voltage symmetries for (a) triangular and (b) square waveforms with peak value fixed at 5kV.

Although a fairly good agreement has been achieved between the simulated results and the experimental data in terms of the magnitude of EL peaks and their corresponding phase angles there is a quite noticeable difference in their distribution shape per ac cycle and this is due to the time resolution of the experimental data. In measuring EL intensity for one cycle of a 50Hz applied voltage, the intensity was taken for every 1.79ms (as explained in Section 4.4.4) whereas the time taken to simulate the EL emission per ac cycle is set as 0.02ms. The vast difference in time resolution is responsible for the sharp edges observed for simulation results but not for experimental data. Therefore applying a time averaging filter of duration 1.79ms to the simulated

results should smear out any sharp edges and thus produce output similar to the measurement data. Figure 6.14 compares the phase-resolved experimental observations with the EL simulation data averaged per every 1.79ms time window for sinusoidal, triangular and square waveforms with voltage peak of 5kV. It can be seen that the sharp edges observed evidently in modelling EL using triangular and square voltages have been smoothed out and the plots resemble very much to the results shown in Figure 5.19.

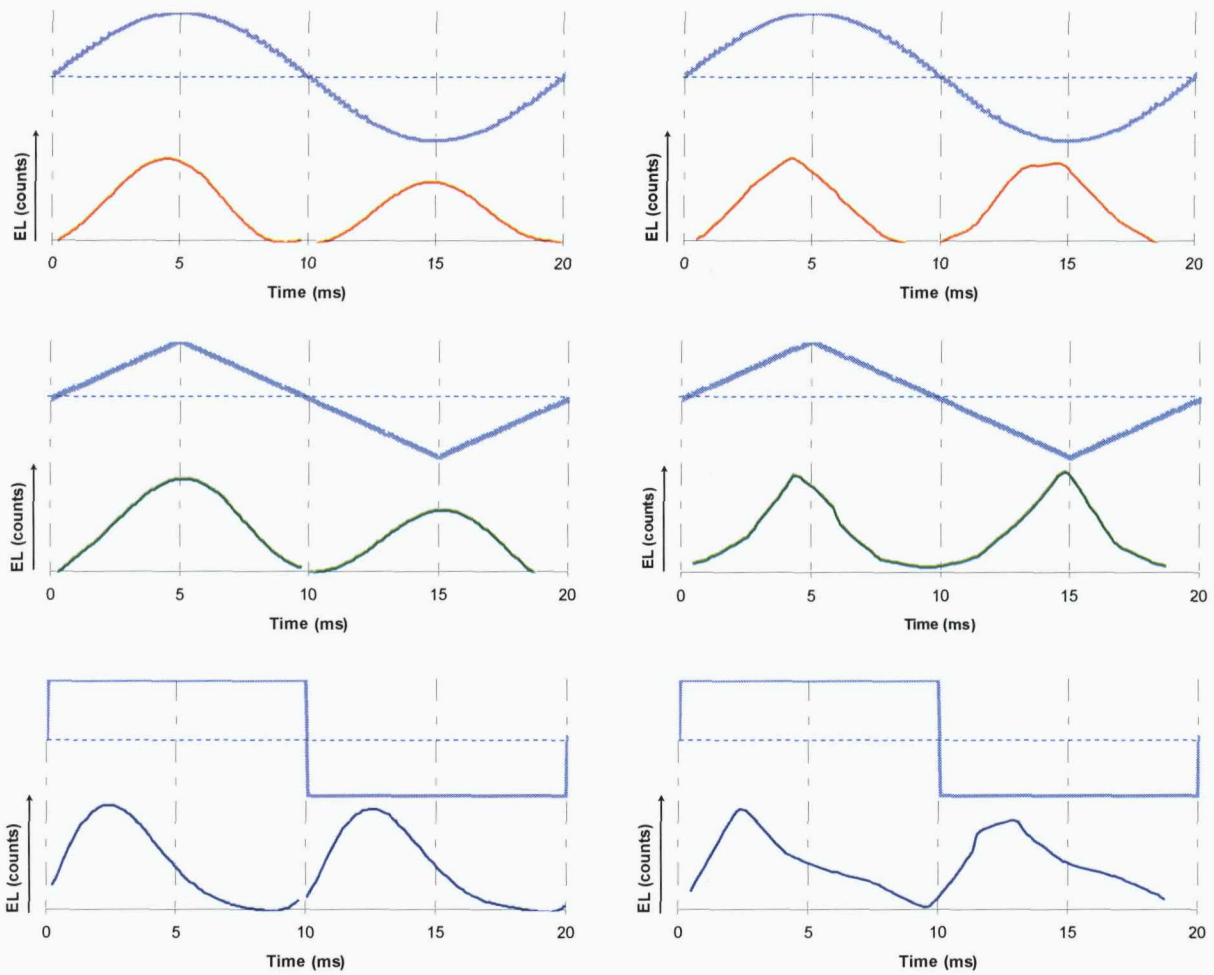

Figure 6.14: (a) The phase-resolved EL measurements and (b) the simulation results averaged to 1.79ms time window. The plots for the experimental observation are obtained by cascading 40 cycles of measurement data whereas the modelling results consist of two cycles of simulated data.

6.4 Summary

This chapter discusses the general outcome from the series of EL experiments undertaken and compares the results with simulation outputs. The causes of the phenomenon were determined by comparing the EL results from the different types of polymer and gas environments. It can be deduced that the difference in EL intensity not only depends on the level of voltage applied, but also the chemical composition of the polymeric material. In addition to this, the presence of gas molecules also affects the occurrence of EL depending of the chemical reactivity of the gas concerned. It has been suggested that the presence of electronegative gases such as SF_6 or O_2 could prevent light from being emitted from the sample since the charge carriers from the metallic electrode are captured by these gaseous molecules.

Based on the comparison between the simulated EL and the phase-resolved measurements, it can also be concluded that the phase difference between the EL peaks and the applied voltage maxima observed experimentally is due to the saturation of field. EL peaks were found to be dependent on the rate of change of voltage applied as both magnitude and phase angles of these peaks are determined by the corresponding voltage symmetry.

Chapter Seven

CONCLUSIONS AND FUTURE WORK

7.1 Conclusions

In the past, the presence of impurities and defects has been widely considered as the main cause for electrical degradation of high voltage cable insulation. This is because they are able to act as points where field is intensified, leading to molecular deformation of the polymer and eventually catastrophic breakdown in the long run. With technological advancement in insulation manufacturing nowadays, degradation due to these factors has been minimized significantly and cable lifetime prolonged. Nevertheless, continuous application of electric field across the insulating material of high voltage cable over a long period of time allows electrical charge accumulation inside the dielectric medium. The existence of this so-called space charge may be used to analyze degradation and ageing of polymeric material, and the interaction between them will produce the emission of very faint light known as electroluminescence (EL).

A lot of research work has been undertaken to monitor the phenomenon in various polymeric materials, and it can be detected by using photomultiplier tube (PMT) or charge coupled device (CCD) camera. EL was examined in divergent and uniform electric field configurations under both dc and ac voltages. By applying dc stresses, researchers have observed that the increase of EL emission occurs after the polymer was subjected to electric field for a long period of time. This indicates that the occurrence of EL is predominantly caused by the recombination of charge carriers with opposite polarities that travel within the bulk of the material due to the application of field. In ac condition however, EL was observed to occur relatively quicker than in dc field; suggesting that the phenomenon is more of a surface rather than a bulk process. Charges are injected into and extracted from the polymer in every cycle of the ac voltage so recombination can occur almost instantaneously after the field is applied.

This thesis is concerned with developing an understanding of the processes that give rise to EL in polymeric insulation materials under uniform electric field arrangement. This is necessary before EL could be used as a probe for understanding of dielectric ageing as a prelude to electrical breakdown in these materials. In this work, the production of EL measured experimentally in different materials was undertaken using a range of applied voltage wave-shapes and the results compared with a bipolar charge injection model for EL based on a uniform field arrangement for the first time. In addition, the effect of chemical structure and the role of absorbed gases were also examined. The experimental detection system that has been developed enables a wide range of EL characteristics to be detected using a common CCD sensor and it includes the measurement of the total EL intensity, spectral analysis of the EL, phase-resolved EL for sinusoidal, triangular and rectangular wave-shapes as well as their asymmetrical counterparts. The use of the CCD sensor also has the advantage of enabling imaging of the EL to be performed in order to confirm that the light is being produced by the sample as well as enabling the spatial characteristics of the EL from the sample surface to be characterized.

Measurements of the EL intensity as a function of applied voltage have shown that the EL intensity is consistent with an exponential increase with applied voltage. This supports a key assumption in the bipolar charge recombination model where the charge injection is modelled as a simple exponential function of the electric field at the

injecting electrode. In addition, it was shown that the total EL intensity at a constant applied ac voltage is steady and consistent with measurement noise and photon counting statistics and therefore steady over time. However, no evidence was found for an initial exponential increase in the EL intensity due to the accumulation of trapped charge in the material adjacent to the electrode. An initial increase in the EL intensity is a key result in the bipolar charge recombination model for EL and hence either the initial increase was very rapid and could not be captured experimentally using the current system, or that the excitation process was due to hot electron impact excitation of the polymer. Further experiments would be required to identify which of the excitation schemes leads to the formation of EL in these materials.

The total EL intensity for different polymeric materials, namely low density polyethylene (LDPE), polyethylene terephthalate (PET) and polyethylene naphthalate (PEN) were examined. EL intensity was found to be greater in PET and PEN than LDPE confirming the conjecture that the aromatic backbone of the polymer chains of PET and PEN act as additional chromophores for the production of EL. This conclusion was supported by spectral measurements of the EL which demonstrated slight differences in the EL spectrum from each material and hence different recombination pathways.

In general all materials exhibited a peak in the EL spectra in the visible range between 500 and 600nm, and which increased in intensity with increasing applied voltage and due to molecular excitations within the bulk of the polymer. The EL intensity was found to be effectively zero in the near ultraviolet range of the electromagnetic spectrum; demonstrating that the light emission was due to processes occurring within the sample and not from gas discharge in the surrounding environment. In addition to this, the experimental results show a component of EL in the near infrared region which could be due to surface plasmons from the gold electrode or recombination in the surface states at the metal polymer electrode. The fact that the EL in the visible range increases in intensity much more than the near infrared emission may support the assumption that the near infrared emission is due to surface plasmons as this emission is not subject to charge injection onto the bulk of the polymer. In addition, the near infrared emission was not affected by the electronegativity of the environmental gas, SF_6, and that the electronegativity of the gas plays very little, if not no role in quenching this emission. However it was found that a high electronegative gas like SF_6

was able to suppress the formation of EL in the visible range (500 to 600nm) and hence quenches the excitation and recombination processes occurring in the bulk of the polymer by capturing free electrons. The environmental gas used therefore plays a fundamental role on the formation of EL in these polymers.

In this work a simulation model for EL under uniform electric fields in thin film polymeric materials with a plane-plane electrode geometry and where EL can be produced from both electrodes was developed from an existing bipolar charge recombination model for injection at a pin electrode for the first time. This simulation enables the phase-resolved EL intensity to be calculated by assuming injected charge carriers can recombine in the bulk of the polymer giving rise to light emission. The simulation model was further developed to allow the application of non-sinusoidal and asymmetric applied voltage waveforms enabling comparison with experiment. This also required further development of the HV supply using a HV amplifier to enable corresponding wave-shapes to be applied experimentally to the samples. This novel arrangement allows the study of EL using experiments and simulation with arbitrary wave-shapes for the first time.

The experimental results of the phase resolved EL intensity demonstrate good correspondence to the simulations of EL confirming that the bipolar charge recombination model applied to the plane-plane electrode case is able to fully describe the phase-resolved features of the measured EL intensity, and that the basic assumptions used in the model are appropriate. In particular, the simulations and experiments agreed with respect to:

1. The phase of the EL with respect to the phase of the applied voltage for sinusoidal, triangular and rectangular wave-shapes.
2. The shape of the EL distribution each half cycle of the applied voltage for each wave-shape.
3. The relative intensities of the EL intensity when asymmetric wave-shapes are considered.

7.2 Future Work

Several recommendations are proposed for the future directions of this project:

1. The work so far has demonstrated good correspondence between the measured and simulated phase resolved EL intensity. However a key result of the bipolar charge recombination model is that it predicts an initial exponential increase in the EL intensity cycle-by-cycle of the applied voltage. This is due to trapped charge accumulating in the material and steady state is only achieved when the charge injected per half cycle is equal to that recombining each half cycle. However, if the EL is the result of hot electron excitation rather than the recombination of charge carriers, then the phase resolved EL would be proportional to the injected current density. Hence it is critical in identifying the correct excitation mechanism to determine whether or not evidence for trapped charge accumulation is preset in the measured data. Hence the following experiment is suggested on unstressed samples in which the EL intensity is recorded after a sudden application of an ac voltage. A steady light emission intensity would support hot electron excitation or an increasing exponential increase in the EL intensity would support bipolar charge recombination as the process leading to EL.

2. EL is believed to occur as a result of the interaction between charge carriers that accumulate within polymeric material. Nowadays, space charge measurement such as pulse electro-acoustic (PEA) method has adopted an approach to monitor the behaviour of the charges under ac condition. Thus comparing the phase-resolved EL measurement with respect to the space charge ac measurement can possibly give clearer insight on the mechanisms leading to the occurrence of the phenomenon.

3. The polymeric samples used in this research work were from commercially available materials. It will be interesting to investigate EL phenomenon from dielectrics with some known characteristics such as the relative level of trapping sites for electronic charges within the medium. Polymers with different concentrations of nanocomposite blend will result in different abilities to trap

the charge carriers so EL observations on such materials might give some intriguing outcome to the whole emission processes.

4. So far this work has been concerned with understanding the processes leading to EL such that EL observations may be used to as a probe in the understanding of the electrical ageing processes that occur. The work here has shown that simulations combined with experiments can be used to interpret the EL characteristics. The next step therefore is to continue this work on electrically and thermally aged materials and to characterize the changes that occur in the EL.

REFERENCES

[1] B. M. Weedy, *Underground Transmission of Electric Power*, John Wiley & Sons, New York, 1980.

[2] P. Graneau, *Underground Power Transmission*, John Wiley & Sons, New York, 1979.

[3] P. V. Hunter and J. Temple Hazell, *Development of Power Cables*, George Newnes, London, 1956.

[4] M. B. Robinson, "UG/underwater cables can handle up to 1100kV", *Electrical World*, pp. 130, 1974.

[5] C. C. Barnes, *Power Cables*, Chapman and Hall, New York, 1966.

[6] L. A. Dissado and J. C. Fothergill, *Electrical Degradation and Breakdown in Polymers,* Peter Peregnius, London, 1992.

[7] S. S. Bamji, "Electroluminescence - A Technique to Detect the Initiation of Degradation in Polymeric Insulation", *IEEE Electrical Insulation Magazine*, Vol. 15, No. 3, May 1999, pp. 9-14.

[8] N. D. Kenney and M. J. Koulopoulous, "115kV and 138kV Polyethylene Insulated Cable Installations and Cable Evaluation Data", *CIGRE*, No. 21-07, 1968.

[9] R. P. Mott, "Status of 138kV Solid Dielectrics Cables Being Evaluated at Waltz Mill", *IEEE*, No. C75007-0, 1975.

[10] M. A Charoy and R. F. Jocteur, "Very High Tension Cables with Extruded Polyethylene Insulation", *IEEE Transactions on Power Apparatus and Systems*, Vol. PAS-90, No. 2, Mar. 1971, pp. 777-84.

[11] P. Graneau, "Thermal Failure of High Voltage Solid Dielectric Cables", *IEEE Power Engineering Society Winter Meeting*, No. A76037-2, 1976.

[12] O. Mattison and S. Wretemark, "Synthetic Insulated Cables", *CIGRE*, No. 21-09, 1976.

[13] R. Arrighi, "From Impregnated Paper to Polymeric Insulating Materials in Power Cables", *IEEE Transactions on Electrical Insulation*, Vol. 21, No. 1, Feb. 1986, pp. 7-18.

[14] J. Densley, R. Bartnikas and S. B. Bernstein, "Multi-stress Ageing of Extruded Insulation Systems for Transmission Cables", *IEEE Electrical Insulation Magazine*, Vol. 9, No. 1, Jan. 1993, pp. 15-17.

[15] A. K. Jonscher and R. Lacoste, "On a Cumulative Model of Dielectric Breakdown in Solids", *IEEE Transactions on Electrical Insulation*, Vol. E19, No. 6, Dec. 1984, pp. 567-77.

[16] L. A. Dissado, G. Mazzanti and G. C. Montanari, " The Role of Trapped Space Charges in the Electrical Aging of Insulating Materials", *IEEE Transactions on Dielectrics and Electrical Insulation*, Vol. 4, No. 5, Oct. 1997, pp. 496-509.

[17] L. Sanche, "Electronic Aging and Related Electron Interactions in Thin-Film Dielectrics", *IEEE Transactions on Electrical Insulation*, Vol. 28, No. 5, Oct. 1993, pp. 789-819.

[18] L. A. Dissado, G. Mazzanti and G. C. Montanari, "Discussion of Space-Charge Life Model Features in DC and AC Electrical Aging of Polymeric Materials", *IEEE 1997 Annual Report Conference on Electrical Insulation and Dielectric Phenomena*, Vol. 1, 1997, pp. 36-40.

[19] L. A. Dissado, G. Mazzanti and G. C. Montanari, "The Incorporation of Space Charge Degradation in the Life Model for Electrical Insulating Materials", *IEEE Transactions on Dielectrics and Electrical Insulation*, Vol. 2, No. 6, Dec. 1995, pp. 1147-58.

[20] Y. Li, T. Takada, H. Miyata and T. Niwa, "Observation of Charge Behaviour in Multiply Low-Density Polyethylene", *Journal of Applied Physics*, Vol. 74, No. 4, 15 Aug. 1993, pp. 2725-30.

[21] Y. Li and T. Takada, "Space Charge Distribution in Multi-Ply LDPE", *IEEE 1992 Annual Report Conference on Electrical Insulation and Dielectric Phenomena*, 1992, pp. 397-402.

[22] J. A. Giacometti, G. Minami, A. S. De Reggi, B. Dickens and D. L. Chinaglia, "Thermal Pulse Measurements on Electron-Beam Irradiated Fluoroethylene-Propylene Copolymer", *8th International Symposium on Electrets Proceedings*, 1994, pp. 212-17.

[23] A. Cherifi, M. A. Dakka and A. Toureille, "The Validation of the Thermal Step Method", *IEEE Transactions on Electrical Insulation*, Vol. 27, 1992, pp. 1152-58.

[24] P. Notingher Jr., S. Agnel and A. Toureille, "Thermal Step Method for Space Charge Measurements under Applied DC Field", *IEEE Transactions on Dielectrics and Electrical Insulation*, Vol. 8, No. 6, Dec. 2001, pp. 985-94.

[25] S. B. Lang and D. K. Gupta, "Laser Intensity Modulation Method: A Technique for Determination of Spatial Distributions of Polarization and Space Charge in Polymer Electrets", *Journal of Applied Physics*, Vol. 59, 1986, pp. 2151-60.

[26] P. Laurenceau, G. Dreyfus and J. Lewiner, "New Principle for the Detection of Potential Distributions in Dielectrics", *Physical Review Letters*, Vol. 38, No. 1, Jan. 1977, pp. 46-9.

[27] J. E. West, H. Von Seggern, G. M. Sessler and R. Gerhard, "The Laser-Induced-Pressure-Pulse Method: A Direct Method of Measuring Spatial Charge Distributions in Thin Dielectric Films", *Conference Record of the Industry Applications Society IEEE-IAS-1982 Annual Meeting*, 1982, pp. 1159-61.

[28] F. Chapeau, C. Alquie and J. Lewiner , "Pressure Wave Propagation Method for the Analysis of Insulating Materials: Application to LDPE Used in HV Cables", *IEEE Transactions on Electrical Insulation*, Vol. 21, 1986, pp. 405-10.

[29] M. Haardt and W. Eisenmenger, "High Resolution Technique for the Measuring Charge and Polarization Distribution in Dielectrics by Piezoelectrically Induced Pressure Step Waves (PPS)", *Conference on Electrical Insulation and Dielectric Phenomena*, 1982, pp. 46-51.

[30] T. Takada and T. Sakai, "Measurement of Electric Fields at a Dielectric/Electrode Interface Using an Acoustic Transducer Technique", *IEEE Transactions on Electrical Insulation*, Vol. 18, No. 6, Dec. 1983, pp. 619-28.

[31] T. Takada, "Acoustic and Optical Methods for Measuring Electric Charge Distributions in Dielectrics", *IEEE Transactions on Dielectrics and Electrical Insulation*, Vol. 6, No. 5, Oct. 1999, pp. 519-47.

[32] M. Fu, Thesis: "Space Charge Measurement in Polymer Insulated Power Cables Using the PEA Method", University of Southampton, 2002.

[33] C. Laurent, C. Mayoux and F. Massines, "Optical Emission due to Space Charge Effects in Polymers: An Insight into Wear-out and Breakdown Mechanisms", *Le Vide les Couches Minces*, No. 275, Jan. 1995, pp. 268-73.

[34] Y. Cao and S. Boggs, "Mechanism of High Field Electroluminescence and Determination of the Space Charge Limited Field in Polymeric Dielectrics", *IEEE Transactions on Dielectrics and Electrical Insulation*, Vol. 12, No. 4, Aug. 2005, pp. 690-9.

[35] C. Laurent, G. Teyssedre and G. C. Montanari, "Time-Resolved Space Charge and Electroluminescence Measurements in Polyethylene Under AC Stress", *IEEE Transactions on Dielectrics and Electrical Insulation*, Vol. 11, No. 4, Aug. 2004, pp. 554-60.

[36] J. Lewiner, "Evolution of Experimental Techniques for the Study of the Electrical Properties of Insulating Materials", *IEEE Transactions On Electrical Insulation*, Vol. 21, 1986, pp. 351-60.

[37] N. H. Ahmed and N. N. Srinivas, "Review of Space Charge Measurements in Dielectrics", *IEEE Transactions on Dielectrics and Electrical Insulation*, Vol. 4, No. 5, Oct. 1997, pp. 644-56.

[38] C. Laurent, F. Massines and C. Mayoux, "Optical Emission due to Space Charge Effects in Electrically Stressed Polymers", *IEEE Trans. On Diel. Elec. Insul.*, Vol. 4, 1997, pp. 585-602.

[39] I. L. Hosier, Thesis: "Morphology and Electrical Properties of Polyethylene Blends", University of Reading, 1996.

[40] D. McAllister, *Electric Cables Handbook*, Granada, 1983.

[41] K. S. Suh, C. R. Lee, J. S. Noh, J. Tanaka and D. H. Damon, "Electrical Conduction in Polyethylene with Semi-Conductive Electrodes", *IEEE Transactions on Dielectrics and Electrical Insulation*, Vol. 1, 1994, pp. 224-30.

[42] K. S. Suh, S. J. Hwang, J. S. Noh and T. Takada, "Effect of Constituents of XLPE on the Formation of Space Charge", *IEEE Transactions on Dielectrics and Electrical Insulation*, Vol. 1, 1994, pp. 1077-83.

[43] M. A. Brown, Thesis: "Spacecharge, Breakdown and Lifetime Estimation of Polyethylene Insulation Systems", University of Southampton, 2002.

[44] M. Ieda, "In Pursuit of Better Electrical Insulating Solid Polymers: Present Status and Future Trends (1986 Whitehall Memorial Lecture)", *IEEE Transactions on Electrical Insulation*, Vol. EI-21, No. 5, Oct. 1986, pp. 793-802.

[45] D. A. Seanor, *Electrical Properties of Polymers*, Academic Press Inc., London, 1982.

[46] T. J. Lewis, "Polyethylene under Electrical Stress", *IEEE Transactions on Dielectrics and Electrical Insulation*, Vol. 9, No. 5, Oct 2002, pp. 717-29.

[47] T. J. Lewis, "The Physico-Chemical Origins and Nature of Space Charge in Insulating Solids under Electrical Stress", *IEEE 7th International Conference on Conduction and Breakdown in Solid Dielectrics*, 2001, pp. 223-7.

[48] S. Serra, E. Tosatti, S. Iarlori, S. Scandolo, G. Santoro and M. Albertini, "Interchain States and the Negative Electron Affinity of Polyethylene", *1998 Annual Report Conference on Electrical Insulation and Dielectric Phenomena*, 1998, pp. 19-22.

[49] M. Meunier, N. Quirke, and A. Aslanides, "Characterisation of Charge Carrier Traps in Polymeric Insulators", *2000 Annual Report Conference on Electrical Insulation and Dielectric Phenomena*, 2000, pp. 21-24.

[50] J. P. Jones, J. P. Llewellyn and T. J. Lewis, "The Contribution of Field-Induced Morphological Change to the Electrical Aging and Breakdown of Polyethylene", *IEEE Transactions on Dielectrics and Electrical Insulation*, Vol. 12, No. 5, Oct. 2005, pp. 951-66.

[51] Y. Murata, "Photoelectric Emission and Contact Charging of some Synthetic High Polymers", *Japanese Journal of Applied Physics*, Vol. 18, No. 1, Jan. 1979, pp. 1-8.

[52] K. Tahira and K. C. Kao, "Anomalous Photocurrent Transient in Polyethylene", *Journal of Physics D. (Applied Physics)*, Vol. 18, No. 11, Nov. 1985, pp. 2247-59.

[53] T. J. Fabish and C. B. Duke, "Molecular Charge States and Contact Charge Exchange in Polymers", *Journal of Applied Physics*, Vol. 48, No. 10, Oct. 1977, pp. 4256-66.

[54] R. Liboff, *Introductory Quantum Mechanics*, Addison-Wesley, London, 2003.

[55] C. Laurent, C. Mayoux and S. Noel, "Mechanisms of Electroluminescence during Aging of Polyethylene", *J. Appl. Phys.*, Vol. 58, No. 11, 1985, pp. 4346-52.

[56] S. S. Bamji, A. T. Bulinski and R. J. Densley, "Degradation of Polymeric Insulation due to Photoemission Caused by High Electric Fields", *IEEE Trans. On Elec. Insul.*, Vol. 24, 1989, pp. 91-98.

[57] G. J. Zhang, K. Yang, M. Dong, W. B. Zhao and Z. Yan, "Surface Electroluminescence Phenomena Correlated with Trapping Parameters of

Insulating Polymers", *Applied Surface Science*, Vol. 254, No. 5, Dec. 2007, pp. 1450-5.

[58] G. Teyssedre, J. L. Franceschi and C. Laurent, "Cathodo- and Electro-Luminescence Spectra in Insulating Polymers: A Parallel Approach for Inferring Electrical Ageing Mechanisms", *2007 Annual Report Conference on Electrical Insulation and Dielectric Phenomena*, 2007, pp. 824-7.

[59] J. P. Crine, "A Molecular Model for the Electrical Aging of XLPE", *2007 Annual Report Conference on Electrical Insulation and Dielectric Phenomena*, 2007, 608-10.

[60] M. Ieda, "Dielectric Breakdown Process of Polymers", *IEEE Transactions on Electrical Insulation*, Vol. EI-15, No. 3, June 1980, pp. 206-24.

[61] C. Laurent and C. Mayoux, "Light Detection during the Initiation of Electrical Treeing at Room Temperature", *Journal of Physics D: Applied Physics*, Vol. 14, No. 10, Oct. 1981, pp. 1903-10.

[62] I. Tomonori, N. Takuo, Z. H. Fan, T. Thoru, S. Jun and M. Hiroyuki, "Electroluminescence in Additive-contained Low Density Polyethylene", *Proc. Electr. Insul. And Diel. Phen. CEIDP*, 1999, pp. 589-92.

[63] Z. H. Fan, M. Hiroyuki, T. Thoru, I. Tomonori and N. Takuo, "Evaluation of Electroluminescence in Polyethylene", *Proc. IEEE Int. Symp. On Electr. Insul. Mat.*, 1998, pp. 211-4.

[64] A. R. Leighton, R. D. Naybour, L. Warren, "Light Emission and Electrical Tree Initiation in Highly Stressed XLPE and the Effect of DC Pre-stressing", *Proc. IEEE Int. Conf. On Cond. and Break. in Sol. Diel.*, 1998, pp. 273-8.

[65] F. Kabir, J. M. Braun, J. Densley and R. N. Hampton, "Light Emission from Highly Stressed Polymeric Cable Insulation", *Conf. Record of the IEEE Int. Symp. On Electr. Insul.*, 1994, pp. 37-39.

[66] A. Tanida, Y. Muramoto and N. Shimizu, "Influence of Degradation on Electroluminescence in Polyethylene", *2004 Annual Report conference on Electrical Insulation and Dielectric Phenomena*, 2004, pp. 298-301.

[67] S. S. Bamji and A. T. Bulinski, "Electroluminescence - An Optical Technique to Determine the Early Stages of Polymer Degradation under High Electric Stresses", *2002 Conference on Precision Electromagnetic Measurements*, 2002, pp. 106-7.

[68] N. Shimizu, N. Nagura, S. Iemura and T. Takahashi, "Electroluminescence and Polymer Degradation", *2001 Annual Report Conference on Electrical Insulation and Dielectric Phenomena*, 2001, pp. 257-60.

[69] A. Mohd Ariffin, P. L. Lewin and S. J. Dodd, "Comparison of Electroluminescence Phenomenon in LDPE, PET and PEN under the Application of High Electrical Stress", *2006 IEEE Conference on Electrical Insulation and Dielectric Phenomena*, 2006, pp. 260-3.

[70] T. Mizuno, Y. S. Liu, W. Shionoya, K. Yasuoka, S. Ishii, H. Miyata and A. Yokoyama, "Electroluminescence in Insulating Polymers in AC Electric Fields", *IEEE Transactions on Dielectrics and Electrical Insulation*, Vol. 4, No. 4, Aug. 1997, pp. 433-8.

[71] G. Teyssedre, G. Tardieu, D. Mary and C. Laurent, "AC and DC Electroluminescence in Insulating Polymers and its Implication for Electrical Ageing", *Journal of Physics D. (Applied Physics)*, Vol. 34, No. 14, 21 July 2001, pp. 2220-9.

[72] Y. Cao and S. Boggs, "Electroluminescence in Divergent Field", *2003 Annual Report Conference on Electrical Insulation and Dielectric Phenomena*, 2003, pp. 261-4.

[73] J. Jonsson, B. Ranby, D. Mary, C. Laurent and C. Mayoux, "Electroluminescence from Polyolefins Subjected to a Homogeneous AC Field", *IEEE Transactions on Dielectrics and Electrical Insulation*, Vol. 2, No. 1, Feb. 1995, pp. 107-13.

[74] V. Griseri, L. A. Dissado, J. C. Fothergill, G. Teyssedre and C. Laurent, "Electroluminescence Excitation Mechanisms in an Epoxy Resin under Divergent and Uniform Field", *IEEE Transactions on Dielectrics and Electrical Insulation*, Vol. 9, No. 1, Feb. 2002, pp. 150-60.

[75] I. Kitani, T. Hirano and K. Arii, "Very Faint Light Emission in Low-Density Polyethylene Films under dc Field", *Jpn. J. Appl. Phys.*, Vol. 26, 1987, pp. 639-40.

[76] T. Lebey and C. Laurent, "Charge injection and Electroluminescence as a Prelude to Dielectric Breakdown", *J. Appl. Phys.*, Vol. 68(1), 1990, pp. 275-82.

[77] W. A. Hartman and H .L. Armstrong, "Electroluminescence in Organic Polymers", *J. Phys.*, Vol. 38, 1967, pp. 2393-95.

[78] S. S. Bamji, A. T. Bulinski and N. Shimizu, "Electroluminescence and Space Charge in Polymeric Insulation", *Proc. IEEE Int. Conf. on Properties and Applications of Diel. Material, ICPADM*, 2000.

[79] N. Hozumi, G. Teyssedre, C. Laurent and K. Fukunaga, "Behaviour of Space Charge Correlated with Electroluminescence in Cross-Linked Polyethylene", *Journal of Physics D: Applied Physics*, Vo. 37, No. 9, 2004, pp. 1327-1333.

[80] D. Mary, G. Teyssedre and C. Laurent, "Electroluminescence in Saturated Polyesters: Temperature Dependence and Correlation with Space Charge Measurements", *2003 Annual Report Conference on Electrical Insulation and Dielectric Phenomena*, 2003, pp. 201-4.

[81] G. Krause, R. Neubert and R. Pietsch, "Investigations of Electrical Aging in Polymers under High AC Field Strength", *1990 Annual Report: Conference on Electrical Insulation and Dielectric Phenomena*, 1990, pp. 288-94.

[82] L. Cisse, G. Teyssedre, D. Mary and C. Laurent, "Influence of Frequency, Electrode Material and Superimposed DC on AC Electroluminescence in Polymer Films", *IEEE Transactions on Dielectrics and Electrical Insulation*, Vol. 9, No. 1, Feb. 2002, pp. 124-9.

[83] G. Zhang, Y. Sun, W. Zhao and Z. Yan, "Surface Electroluminescence Phenomena of Insulating Polymers", *2003 Annual Report Conference on Electrical Insulation and Dielectric Phenomena*, 2003, pp. 253-6.

[84] C. Laurent, C. Mayoux and S. Noel, "Dielectric Breakdown of Polyethylene in Divergent Field: Role of Dissolved Gases and Electroluminescence", *J. Appl. Phys.*, Vol. 54, 1983, pp. 1532-69.

[85] S. S. Bamji, A.T. Bulinski and R. J. Densley, "Evidence of Near-Ultraviolet Emission during Electrical Tree Initiation in Polyethylene", *J. Appl. Phys.*, Vol. 61, 1987, pp. 694-9.

[86] S. S. Bamji and A. T. Bulinski, "Luminescence in Cross-linked Polyethylene of High Voltage Cables", *Proc. IEEE Int. Conf. on Properties and Applications of Diel. Materials ICPADM*, 1997, pp. 11-15.

[87] T. Mizuno, Y. S. Liu, W. Shionoya, K. Yasuoka and S. Ishii, "Investigation of Charge Injection in Gas-Impregnated Polyethylene by Measurement of Electroluminescence under AC Voltage", *Jpn. J. Appl. Phys.*, Vol. 36, 1997, pp. 754-60.

[88] S. S. Bamji, A. T. Bulinski, R. J. Densley and M. Matsuki, "Degradation Mechanism at XLPE/Semicon Interface Subjected to High Electric Stress", *IEEE Trans. Elec. Insul.*, Vol. 26, 1991, pp. 278-84.

[89] N. Shimizu, N. Nagura, T. Suzuki, and A. Tanida, "Electroluminescence and Degradation in PE caused by Electron Impact", *2003 Annual Report Conference on Electrical Insulation and Dielectric Phenomena*, 2003, pp. 361-4.

[90] N. Shimizu, N. Nagura and T. Suzuki, "Electroluminescence in PE Impregnated with Various Gases or Liquids", *Proceedings of the IEEE International Conference on Properties and Applications of Dielectric Materials*, Vol. 3, 2003, pp. 883-886.

[91] J. M. Alison and R. M. Hill, "A Model for Bipolar Charge Transport, Trapping and Recombination in Degassed Crosslinked Polyethene", *Journal of Physics D. (Applied Physics)*, Vol. 27, No. 6, June 1994, pp. 1291-9.

[92] J. M. Alison, J. V. Champion, S. J. Dodd and G. C. Stevens, "Dynamic Bipolar Charge Recombination Model for Electroluminescence in Polymer Based Insulation during Electrical Tree Initiation", *Journal of Physics D. (Applied Physics)*, Vol. 28, No. 8, Aug. 1995, p 1693-701.

[93] S. Le Roy, G. Teyssedre, P. Segur and C. Laurent, "Modelling of Space Charge, Electroluminescence and Current in Low Density Polyethylene under DC and AC Field", *Conference on Electrical Insulation and Dielectric Phenomena (CEIDP)*, 2004, pp. 29-32.

[94] S. Le Roy, G. Teyssedre, C. Laurent and P. Segur, "Numerical Modeling of Space Charge and Electroluminescence in Polyethylene under DC Field", *Annual Report Conference on Electrical Insulation and Dielectric Phenomena (CEIDP)*, 2002, pp. 172-5.

[95] K. Wu and L. A. Dissado, "Model for Electroluminescence in Polymers during the Early Stage of Electrical Tree Initiation", *Proceedings of the 2004 IEEE International Conference on Solid Dielectrics*, Vol. 2, 2004, pp. 505-8.

[96] S. Le Roy, G. Teyssedre and C. Laurent, "Charge Transport and Dissipative Processes in Insulating Polymers: Experiments and Model", *IEEE Transactions on Dielectrics and Electrical Insulation*, Vol. 12, No. 4, Aug. 2005, pp. 644-54.

[97] F. Boufayed, G. Teyssedre, C. Laurent, S. Le Roy, L. A. Dissado, P. Segur and G. C. Montanari, "Models of Bipolar Charge Transport in Polyethylene", *Journal of Applied Physics*, Vo. 100, No. 10, Nov. 2006, pp. 104105-1-10.

[98] W. Choo and G. Chen, "Electric Field Determination in DC Polymeric Power Cable in the Presence of Space Charge", *Annual Report Conference on Electrical Insulation and Dielectric Phenomena (CEIDP)*, 2007, pp. 489-92.

[99] B. Sanden, E. Ildstad and R. Hegerberg, "Conduction Current and Space Charge Formation in XLPE Insulation", *Proceedings of the 1995 IEEE 5th International Conference on Conduction and Breakdown in Solid Dielectrics*, 1995, pp. 144-8.

[100] L. Boudou and J. Guastavino, "Influence of Temperature on Low-Density Polyethylene Films through Conduction Measurement", *Journal of Physics D. (Applied Physics)*, Vol. 35, No. 13, July 2002, pp. 1555-61.

[101] P. Pipinys, A. Rimeika and V. Lapeika, "DC Conduction in Polymers under High Electric Fields", *Journal of Physics D. (Applied Physics)*, Vol. 37, No. 6, Mar 2004, pp. 828-31.

[102] J. V. Champion, S. J. Dodd and G. C. Stevens, "Long Term Light Emission Measurement and Imaging during the Early Stages of Electrical Breakdown in Epoxy Resin", *Journal of Physics D. (Applied Physics)*, Vol. 27, 1994, pp. 604-610.

[103] P. L. Lewin, S. J. Dodd and A. Mohd Ariffin, "Simulation of Electroluminescence using a Bipolar Recombination Model", *in Proceedings of 9th IEEE International Conference on Solid Dielectrics*, 2007, pp. 15-18.

[104] R. W. Hare, R. M. Hill and C. J. Budd, "Modelling Charge Injection and Motion in Solid Dielectrics under High Electric Field", *Journal of Physics D: Applied Physics*, Vol. 26, No. 7, July 1993, pp. 1084-93.

[105] R. W. Hare, Thesis: "Modelling Space charge in Solid Dielectrics", University of Bristol, 1993.

[106] W. H. Press, S. A. Teukolsky, W. T. Vetterling and B. P. Flannery, "Numerical Recipes: The Art of Scientific Computing", Cambridge University Press, New York, 1998.

[107] G. Teyssedre, C. Laurent, G. C. Montanari, F. Palmieri, A. See, L. A. Dissado and J. C. Fothergill, "Charge Distribution and Electroluminescence in Cross-linked Polyethylene under DC Field", *Journal of Physics D. (Applied Physics)*, Vol. 34, No. 18, Sept. 2001, pp. 2830-44.

[108] N. Cariou-Saintemarie, A. E. Davies and J. G. Head, "Electroluminescence Measurements in Polyethylene Insulation", *Eighth International Conference on Dielectric Materials, Measurements and Applications*, 2000, pp. 430-3.

[109] K. I. Wong, P. L. Lewin and A. E. Davies, "Electroluminescence of Low Density Polyethylene under Uniform AC Electrical Field", *2002 Annual Report Conference on Electrical Insulation and Dielectric Phenomena*, Oct. 2002, pp. 664-7.

[110] K. I. Wong, P. L. Lewin and S. J. Dodd, "Electroluminescence Phenomena of Low Density Polyethylene Film under Applied AC Voltage", *2003 Annual Report Conference on Electrical Insulation and Dielectric Phenomena*, 2003, pp. 245-8.

[111] F. L. Pedrotti and L. S. Pedrotti, *Introduction to Optics*, Prentice Hall, Englewood Cliffs, 1996.

[112] J. V. Champion, S. J. Dodd and G. C. Stevens, "Quantitative Measurement of Light Emission during the Early Stages of Electrical Breakdown in Epoxy and Unsaturated Polyester Resins", *J. Phys. D: Appl. Phys.*, Vol. 26, No. 5, May 1993, pp. 819-28.

[113] N. Cariou-Saintemarie, Thesis: "Initiation of Electrical Degradation in High Voltage Polymeric Cable Insulation: Electroluminescence Detection", University of Southampton, 2001.

[114] K. I. Wong, Thesis: "Study of Early Electrical Aging of Polyethylene using Electroluminescence Technique", University of Southampton, 2003.

[115] S. J. Dodd, P. L. Lewin and K. I. Wong, "Phase Resolved Electroluminescence Measurements in Thin Films of Low Density Polyethylene using a Charge Coupled Device Camera", *IEEE Transactions on Dielectrics and Electrical Insulation*, Vol. 13, No. 1, Feb. 2006, pp. 168-180.

[116] A. Mohd Ariffin, P. L. Lewin and S. J. Dodd, "Comparison of Electroluminescence of Different High Voltage Cable Materials under Identical Experimental Conditions", *IEEE International Symposium on Electrical Insulation*, June 2006, pp. 166-9.

[117] K. Kojima, Y. Takai and M. Ieda, "Electroluminescence in Polyethylene Terephthalate (PET) I. Impulse Voltage", *Japanese Journal of Applied Physics*, Vol. 21, No. 6, June 1982, pp. 860-4.

[118] K. Kojima, Y. Takai and M. Ieda, "Electroluminescence in Polyethylene Terephthalate (PET) II. AC Voltage", *Japanese Journal of Applied Physics*, Vol. 22, No. 9, Sept. 1983, pp. 1436-8.

[119] K. Kojima, Y. Takai and M. Ieda, "Electronic Conduction in Polyethylene Naphthalate at High Electric Fields", *Journal of Applied Physics*, Vol. 59, No. 8, Apr. 1986, pp. 2655-9.

[120] A. S. Hockenberger, S. Koral and M. A. Wilding, "Recovery from Strain and Shrinkage Measurements of Poly(m-methylene terephthalate) and Poly(ethylene 2,6-naphthalate) Fibers", *Textile Research Journal*, Vol. 75, No. 2, Feb. 2005, pp. 111-16.

[121] M. G. Bulmer, *Principles of Statistics*, Dover, New York, 1979.

[122] R. Lupton, *Statistics in Theory and Practice*, Princeton University Press, New York, 1993.

[123] J. Jonsson, B. Ranby, P. Canet, D. Mary, C. Laurent and C. Mayoux, "Search for Electroluminescence from Polymer Films subjected to High Fields", *IEEE 1992 Annual Report Conference on Electrical Insulation and Dielectric Phenomena*, pp. 339-44.

[124] A. Petre, D. Mary and D. Marty-Dessus, "Electroluminescence and Space Charge Measurements for the Study of PEN Ageing under UV Irradiation", *Journal of Optoelectronics and Advanced Materials*, Vol. 6, No. 3, Sept. 2004, pp. 1049-54.

[125] G. Teyssedre, C. Laurent, G. C. Montanari, A. Campus and D. H. Nilsson, "From LDPE to XLPE: Investigating the Change of Electrical Properties. Part II: Luminescence", *IEEE Transactions on Dielectrics and Electrical Insulation*, Vol. 12, Nol. 3, June 2005, pp. 447-54.

[126] S. S. Bamji and A. T. Bulinski, "Spatial and Spectral Resolution of Electroluminescence in XLPE", *1999 Annual Report Conference on Electrical Insulation and Dielectric Phenomena*, Vol. 1, pp. 15-18.

[127] S. S. Bamji and A. T. Bulinski, "Luminescence in Polymeric Insulation and its Implication of Insulation Aging", *Proceedings of the International Symposium on Electrical Insulating Materials*, 2001, pp. 453-8.

[128] N. Nagura, S. Iemura, T. Takahashi and N. Shimizu, "Influence of Voltage Interruption on Electroluminescence Intensity in LDPE", *2002 Annual Report Conference on Electrical Insulation and Dielectric Phenomena*, pp. 930-3.

[129] R. Ishii, S. Iemura, M. Kubo, N. Nagura and N. Shimizu, "Electroluminescence for XLPE Cable Diagnosis", *Proceedings of the IEEE International Conference on Properties and Applications of Dielectric Materials*, Vol. 1, 2003, pp. 199-202.

[130] A. Mohd Ariffin, P. L. Lewin, S. J. and Dodd, "Investigation on Electroluminescence Phenomenon in Insulating Polymers under the Influence of Different Gas Environments", *15th International Symposium on High Voltage Engineering*, Aug. 2007.

[131] A. Mohd Ariffin, P. L. Lewin and S. J. Dodd, "The Influence of Absorbed Gases on Electroluminescence Phenomenon in Polymeric Materials Subjected to High Electrical Stress", *Conference on Electrical Insulation and Dielectric Phenomena*, Oct. 2007, pp. 33-36.

[132] Y. Tomkiewicz and E. L. Garwin, "Optical Absorption Spectra of Some Potentially Interesting Gases for Cherenkov Counters", *Nuclear Instruments and Methods*, Vol. 114, No. 3, Feb. 1974, pp. 413-6.

[133] D. Mary, G. Teyssedre and C. Laurent, "Electroluminescence in Saturated Polyesters: Temperature Dependence and Correlation with Space Charge Measurements", *2003 Annual Report Conference on Electrical Insulation and Dielectric Phenomena*, 2003, pp. 201-4.

[134] A. Mohd Ariffin, P. L. Lewin and S. J. Dodd, "Determining the Occurrence of Electroluminescence in Polymeric Materials with respect to the Applied Alternating Electrical Stress", *Proceedings of the 9th IEEE International Conference on Solid Dielectrics*, July 2007, pp. 703-6.

[135] D. Mary, M. Albertini and C. Laurent, "Understanding Optical Emissions from Electrically Stressed Insulating Polymers: Electroluminescence in Poly(ethylene Terephthalate) and Poly(ethylene 2,6-Naphthalate) Films", *Journal of Physics D: Applied Physics*, Vol. 30, No. 2, Jan. 1997, pp. 171-84.

[136] T. Mizuno, Y. S. Liu, W. Shionoya, M. Okada, K. Yasuoka, S. Ishii, A. Yokoyama, H. Miyata, "Electroluminescence from Surface Layer of Insulating Polymer under AC Voltage Application", *IEEE Transactions on Dielectrics and Electrical Insulation*, Vol. 5, No. 6, Dec. 1998, pp. 903-8.

[137] N. Shimizu, H. Katsukawa, M. Miyauchi, M. Kosaki, and K. Horii, "Space Charge Behaviour and Luminescence Phenomena in Polymers at 77K", *IEEE Transactions on Electrical Insulation*, Vol. 14, No. 5, Oct. 1979, pp. 256-63.

[138] R. Pietsch, "Influence of Space Charges and Content of Oxygen on the Luminescence Light and Dielectric Aging Effects", *IEEE International Symposium on Electrical Insulation*, 1992, pp. 57-61.

[139] G. Teyssedre, L. Cisse, D. Mary and C. Laurent, "Identification of the Components of the Electroluminescence Spectrum of PE Excited in Uniform

Fields", *IEEE Transactions on Electrical Insulation*, Vol. 6, No. 1, Feb. 1999, pp. 11-19.

[140] J. S. Q. Liu and M. L. Brongersma, "Omnidirectional Light Emission via Surface Plasmon Polaritons", *Applied Physics Letters*, Vol. 90, No. 9, Feb. 2007, pp. 91116-1-3.

[141] C. Laurent, C. Mayoux, S. Noel and N. I. Sinisuka, "A Study of Emission Lines from Electrical Trees", *IEEE Transactions on Electrical Insulation*, Vol. 18, No. 2, Apr. 1983, pp. 125-30.

APPENDICES

Appendix A: MATLAB® coding to simulate EL

A.1 Basic programming using 50Hz sinusoidal ac voltage

```
0001 clc
0002 clear
0003
0004 %-----CONSTANT PARAMETERS-----
0005 e0=8.8542e-12;  %permittivity of free space
0006 er=2.3;         %relative permittivity
0007 f=50;           %frequency of applied ac voltage
0008 r=8;            %number of ac cycles
0009 a=3e-3;         %value for alpha (a)
0010 b=7e-8;         %value for beta (b)
0011 Meh=1.25e12;    %e,m-h,t recombination coefficient
0012 Mhe=1.25e12;    %h,m-e,t recombination coefficient
0013 qe=-1.6e-19;    %charge for electron
0014 qh=1.6e-19;     %charge for hole
0015
0016 %-----VARIABLE PARAMETERS-----
0017 V=input('Applied Voltage (kV): ');
0018 L=input('Sample Thickness (um): ');
0019
0020 %-----BASIC CONVERSIONS-----
0021 V=1000*V;           %input voltage in kV
0022 L=1e-6*L;           %sample thickness in um
0023 e0er=e0*er;         %overall permittivity
0024 w=2*pi*f;           %value for omega (w)
0025 X=0.01*1e-6;        %space charge thickness extimation in um
0026
0027 %-----VAPPDOTPERL CALCULATION-----
0028 tmax=(2*r*pi)/w;    %maximum time for applied ac cycles
0029 dt=pi/(1000*w);     %time increment
0030 t=0:dt:tmax;         %time setting
0031 N=length(t);         %total number of elements per run
0032 for i=1:N            %total number of elements
0033 VappdotperL(i)=(V*w/L)*cos(w*t(i));
0034 end
0035
0036 %-----SOLVING FOR ELECTRIC FIELD USING RUNGE-KUTTA METHOD-----
0037 E(1)=0; T(1)=0; j=1;    %initial conditions
0038 h=2*dt;                 %value of h for iteration
0039 for i=1:(N-1)/2;        %number of elements for iteration
0040 K1(i)=h*(VappdotperL(j)-sign(E(i))*(a/e0er)*exp(sign(E(i))*b*E(i)));
0041 Einc1=E(i)+(K1(i)/2);
0042 K2(i)=h*(VappdotperL(j+1)-sign(E(i))*(a/e0er)*exp(sign(E(i))*b*Einc1));
0043 Einc2=E(i)+(K2(i)/2);
0044 K3(i)=h*(VappdotperL(j+1)-sign(E(i))*(a/e0er)*exp(sign(E(i))*b*Einc2));
0045 Einc3=E(i)+K3(i);
```

```
0046 K4(i)=h*(VappdotperL(j+2)-sign(E(i))*(a/e0er)*exp(sign(E(i))*b*Einc3));
0047 E(i+1)=E(i)+(1/6)*(K1(i)+2*K2(i)+2*K3(i)+K4(i));
0048 T(i+1)=T(i)+h;
0049 j=j+2;
0050 end
0051
0052 %-----PLOTTING ELECTRIC FIELD AGAINST TIME-----
0053 figure(1)
0054 plot(T,E), xlabel('Time (s)'), ylabel('Electric Field (V/m)')
0055 hold on
0056
0057 %-----DIVIDING PLOT INTO FOUR SECTIONS, AND-----
0058 %-----CONVERTING SECTIONS INTO MATRIX FORM------
0059 tt=0.04/dt;          %number of elements for VappdotperL
0060 for j=1:4            %number of sections
0061     for i=1:tt/2      %number of elements per section
0062         d=fix(i+((j-1)*tt/2));
0063         Ee(j,i)=E(d);
0064     end
0065 end
0066
0067 %-----PLOTTING ELECTRIC FIELD OF THE FOURTH SECTION-----
0068 E4=Ee(4,:);          %taking the fourth row values
0069 dnew=2*dt;           %increment time for fourth section
0070 tnew=0.04-dnew;      %maximum time for fourth section
0071 t2=0:dnew:tnew;      %defined time setting for fourth section
0072 figure(2)
0073 plot(t2,E4), xlabel('Time (s)'), ylabel('Electric Field (V/m)')
0074 hold on
0075
0076 %-----CURRENT DENSITY CALCULATION USING VALUES OF-----
0077 %-------ELECTRIC FIELD FROM THE FOURTH SECTION--------
0078 M=length(E4);
0079 for i=1:M
0080     J4(i)=sign(E4(i))*a*exp(sign(E4(i))*b*E4(i));
0081 end
0082
0083 %-----PLOTTING CURRENT DENSITY AGAINST TIME-----
0084 figure(3)
0085 plot(t2,J4), xlabel('Time (s)'), ylabel('Current Density (A/m^2)')
0086 hold on
0087
0088 %-----CREATING STEADY STATE CONDITIONS FOR-----
0089 %-----ELECTRICAL FIELD AND CURRENT DENSITY-----
0090 %-----FOR ELECTROLUMINESCENCE CALCULATIONS-----
0091 E1=[E4 E4 E4 E4 E4 E4 E4 E4 E4 E4];     %20 cycles of E
0092 E2=[E1 E1 E1 E1 E1 E1 E1 E1 E1 E1];     %200 cycles of E
0093 E3=-E2;                                %200 cycles of -E
0094 J1=[J4 J4 J4 J4 J4 J4 J4 J4 J4 J4];     %20 cycles of J
0095 J2=[J1 J1 J1 J1 J1 J1 J1 J1 J1 J1];     %200 cycles of J
0096 J3=-J2;                                %200 cycles of -J
0097
0098 %-----CALCULATING ELECTROLUMINESCENCE INTENSITY-----
0099 %------------WITHIN A PERIOD OF 4 SECONDS-----------
0100 tend=4-dnew;
0101 t3=0:dnew:tend;
0102 K=length(t3);
0103 for i=1:K                              %calculation for electrode 1
0104     pet(1)=0; pht(1)=0;
0105     if sign(E2(i))<=0
0106         pem(i)=J2(i)*(dnew/X);         %density of mobile electrons
0107         phm(i)=0;
0108     else
0109         phm(i)=J2(i)*(dnew/X);         %density of mobile holes
0110         pem(i)=0;
0111     end
0112     rem(i)=abs(Meh*pem(i)*pht(i));     %e,m-h,t recombination
0113     rhm(i)=abs(Mhe*phm(i)*pet(i));     %h,m-e,t recombination
0114     I1(i)=1e-25*(rem(i)+rhm(i))/dnew;       %intensity from electrode 1
0115     pet(i+1)=pet(i)+pem(i)-qe*rem(i)+qh*rhm(i); %e,t density
0116     pht(i+1)=pht(i)+phm(i)-qh*rhm(i)+qe*rem(i); %h,t density
0117     pem(i)=0; phm(i)=0;                %no mobile charges
0118 end
0119 for i=1:K                              %calculation for electrode 2
0120     pet(1)=0; pht(1)=0;
0121     if sign(E3(i))<=0
0122         pem(i)=J3(i)*(dnew/X);         %density of mobile electrons
0123         phm(i)=0;
0124     else
0125         phm(i)=J3(i)*(dnew/X);         %density of mobile holes
```

```
0126         pem(i)=0;
0127     end
0128     rem(i)=abs(Meh*pem(i)*pht(i));  %e,m-h,t recombination
0129     rhm(i)=abs(Mhe*phm(i)*pet(i));  %h,m-e,t recombination
0130     I2(i)=0.8*1e-25*(rem(i)+rhm(i))/dnew;   %intensity from electrode 2
0131     pet(i+1)=pet(i)+pem(i)-qe*rem(i)+qh*rhm(i); %e,t density
0132     pht(i+1)=pht(i)+phm(i)-qh*rhm(i)+qe*rem(i); %h,t density
0133     pem(i)=0; phm(i)=0;             %no mobile charges
0134 end
0135 for i=1:K
0136     I(i)=I1(i)+I2(i);               %total intensity from two electrodes
0137 end
0138
0139 %-----PLOTTING ELECTROLUMINESCENCE INTENSITY AGAINST TIME-----
0140 figure(4)
0141 plot(t3,I), xlabel('Time (s)'), ylabel('EL Intensity (a.u.)')
0142 hold on
0143
0144 %-----DIVIDING PLOT INTO 100 SECTIONS, AND-----
0145 %-----CONVERTING SECTIONS INTO MATRIX FORM------
0146 for j=1:100          %number of sections
0147     for i=1:tt/2     %number of elements per section
0148         d=fix(i+((j-1)*tt/2));
0149         Ii(j,i)=I(d);
0150     end
0151 end
0152
0153 %-----PLOTTING ELECTROLUMINESCENCE OF THE 100TH SECTION-----
0154 I100=Ii(100,:);          %taking the fourth row values
0155 figure(5)
0156 plot(t2,I100), xlabel('Time (s)'), ylabel('EL Intensity (a.u.)')
0157 hold on
```

A.2 Program modifications to incorporate 50Hz triangular applied voltage

In order to simulate EL using triangular waveform, only the formulations for the Laplacian field, $\dot{V}(t)/L$ was altered. The modifications are as follows:

```
0027 %-----VAPPDOTPERL CALCULATION-----
0028 tmax=(2*r*pi)/w;     %maximum time for applied ac cycles
0029 dt=pi/(1000*w);      %time increment
0030 t=0:dt:tmax;         %time setting
0031 N=length(t);         %total number of elements per run
0032 for i=1:(N-1)/32;               %quadrant 1 calculation
0033     Vv(i)=V/(L*0.005);
0034 end
0035 for i=((N-1)/32)+1:3*(N-1)/32;  %quadrant 2 & 3 calculations
0036     Vv(i)=-V/(L*0.005);
0037 end
0038 for i=(3*(N-1)/32)+1:(N-1)/8;   %quadrant 4 calculation
0039     Vv(i)=V/(L*0.005);
0040 end
0041 VappdotperL=[Vv Vv Vv Vv Vv Vv Vv Vv];  %applied field for 8 cycles
0042 VappdotperL(N)=V/(L*0.005);             %last value set to maximum
```

A.3 Program modifications to incorporate 50Hz square applied voltage

Similar to simulating EL using triangular waveform, only the formulations for the Laplacian field, $\dot{V}(t)/L$ was altered for square voltages. The waveform is based on Figure 6.10 and the modifications are as follows:

```
0027 %-----VAPPDOTPERL CALCULATION-----
0028 tmax=(2*r*pi)/w;     %maximum time for applied ac cycles
0029 dt=pi/(1000*w);      %time increment
0030 t=0:dt:tmax;         %time setting
0031 N=length(t);         %total number of elements per run
0032 for i=1:200;         %calculations for 0ms<t<2ms
0033     Vv(i)=V/(L*2000e-6);
0034 end
0035 for i=201:((N-1)/16)-200;       %calculations for 2ms<t<8ms
0036     Vv(i)=0;
0037 end
0038 for i=((N-1)/16)-199:((N-1)/16)+200;   %calculations for 8ms<t<12ms
0039     Vv(i)=-V/(L*2000e-6);
0040 end
0041 for i=((N-1)/16)+201:((N-1)/8)-200;   %calculations for 12ms<t<18ms
0042     Vv(i)=0;
0043 end
0044 for i=((N-1)/8)-199:(N-1)/8;     %calculations for 18ms<t<20ms
0045     Vv(i)=V/(L*2000e-6);
0046 end
0047 VappdotperL=[Vv Vv Vv Vv Vv Vv Vv Vv];  %applied field for 8 cycles
0048 VappdotperL(N)=V/(L*2000e-6);           %last value set to maximum
```

Appendix B: Supplementary data for experimental setup and procedures

B.1 Emitech K550X coater sputtering rate

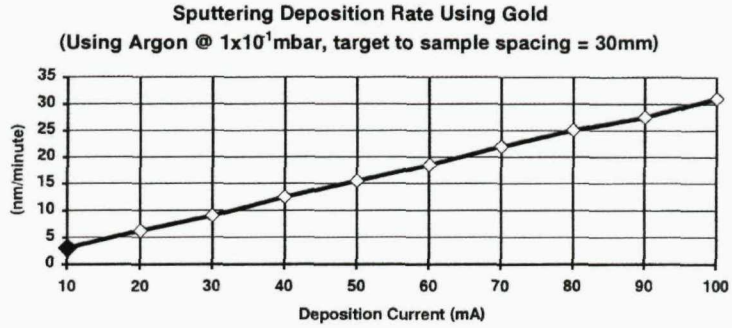

B.2 Optical calibration of the measured light intensity

Using UV/visible spectrophotometer, the transmission profile for light passing through LDPE, PET and PEN film is obtained and shown below. From this result, it has been shown that the transmittance spectra of the three materials without any gold layer sputtered on the surface are almost the same. In addition to this, the samples under test were sputtered with gold layer of the same thickness; therefore the transmission loss of light travelling from the bulk of the material, across the gold layer to the detection system should be relatively similar for each type of dielectric. With the exception for spectral analysis, all other EL measurements were undertaken without any filters present in front of the CCD camera. It can thus be said that optical calibration is not necessary for spatial, temporal and phase-resolved measurements and the difference in the total intensity of the measured EL corresponds to the processes that leads to the emission.

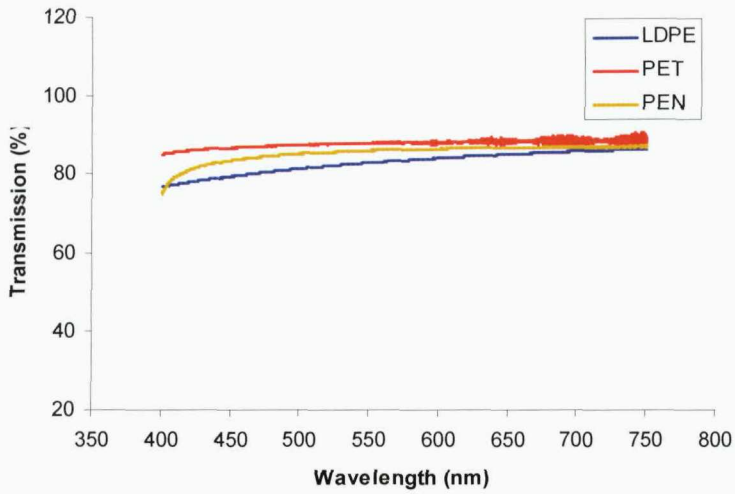

B.3 Peltier cooled CCD camera quantum efficiency

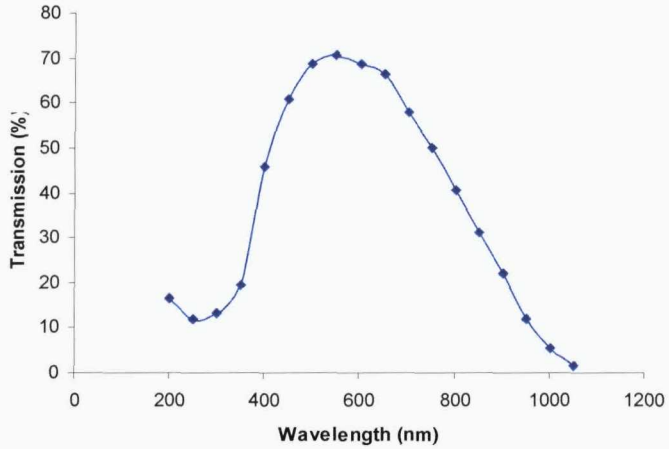

B.4 Measurement results to correct readout delay

Two phase-resolved measurements were made [114] using different numbers of pixel rows exposed for EL emission. It was found that by adjusting the plots by 18.2μs per pixel row, the peaks of EL occur at the same point of time.

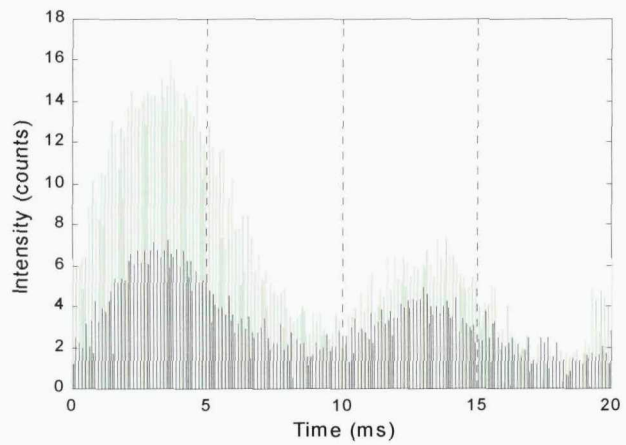

Appendix C: Summary of operating instructions to perform EL experiments

The AT1 system for EL imaging, spatial, temporal and spectral measurement operates in MS-DOS mode. The point-on-wave measurement is taken using the Bilbao system that works on Windows.

C.1 Image acquisition

- Go to **Screen 21**
- Set Exposure Time: [**600**]s
- To save image, store data on disk: [**filename.dat**]
- Set Format Number: [**choose the format with no filters, typically 1**]
- Press F3 to capture the image
- To view the file, go to **Screen 31**

C.2 Spatial measurement

- Go to **Screen 60**
- Press Alt F5 to extract 2D-file
- Choose Column/Row to extract data along x-/y-axis
- Go to **Screen 61** to save file
- Press F5 to save it as ASCII file
- File can now be opened using Notepad

C.3 Temporal measurement

- The specific area (box) for measurement is defined (150x150 pixel^2)
- Go to **Screen 25**
- Set Exposure Time Per Point: [**0.5**]s
- Set Number Of Points To Scan: [**2000**]
- Set Format Number: [**choose the format with no filters, typically 1**]
- Press F2 to initiate measurement from the defined area
- Go to **Screen 61** to save file
- Press F5 to save it as ASCII file
- File can now be opened using Notepad

C.4 Spectral measurement

- The specific area (box) for measurement is defined (50x50 pixel²)
- Go to **Screen 25**
- Set Exposure Time Per Point: [**15.0**]s
- Set Number Of Points To Scan: [**8-12**]
- Set Format Number: [**choose format according to desired wavelength**]
- Go to **Screen 61** to save file
- Press F5 to save it as ASCII file
- File can now be opened using Notepad

C.5 Point-on-wave measurement

- First EL image is taken using AT1 system and adjusted so that only a number of pixel rows is exposed to the CCD camera
- Then measurements are taken using Bilbao system
- Number Of Pixel Rows Exposed: [**100**]
- Number Of Points Per Trigger: [**450**]
- Number Of Measurements Taken: [**1000**]
- Measurements are plotted for 1 cycle and corrected according to the readout time delay

Appendix D: Raw experimental data and additional results

D.1 Temporal behaviour and voltage dependence of EL for different LDPE, PET and PEN samples

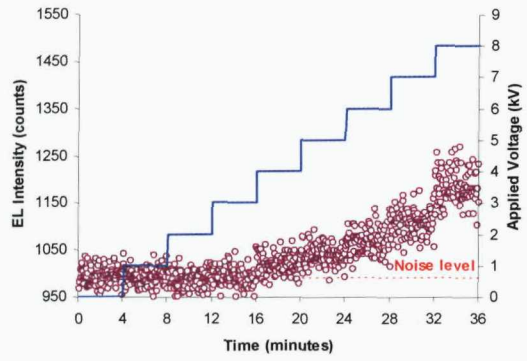

LDPE (Sample I)

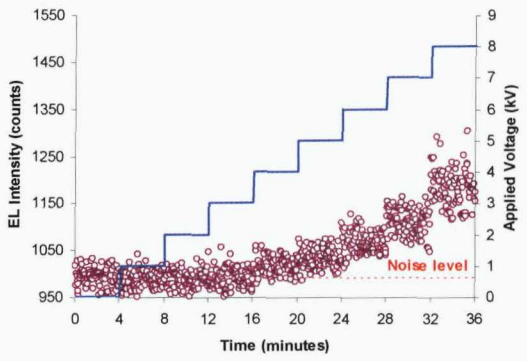

LDPE (Sample II)

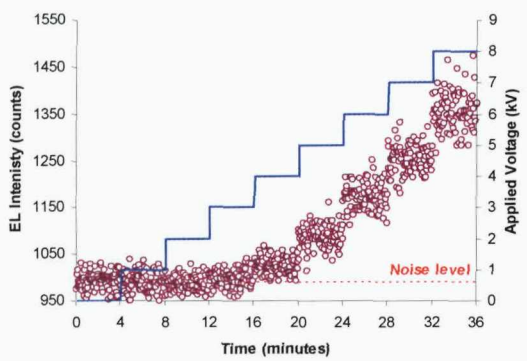

PET (Sample I)

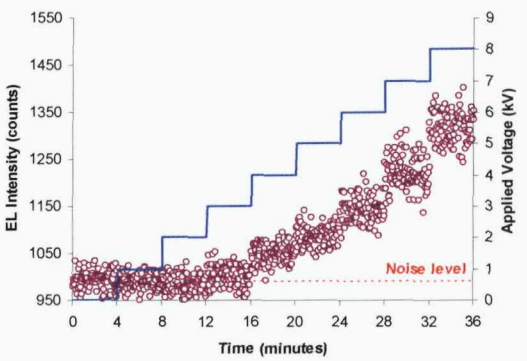

PET (Sample II)

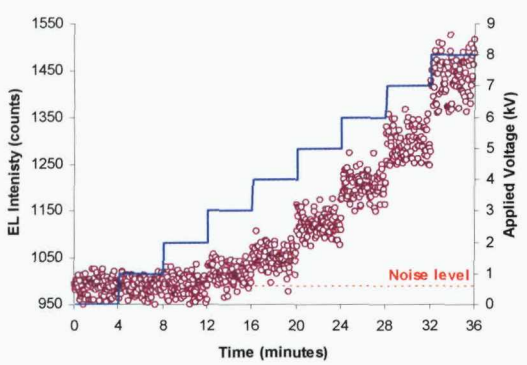

PEN (Sample I)

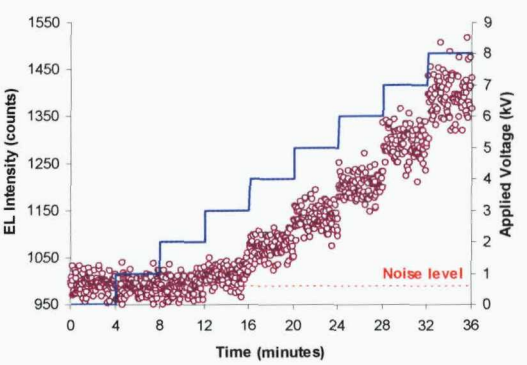

PEN (Sample II)

D.2 Spatial distribution of EL under different gas environments

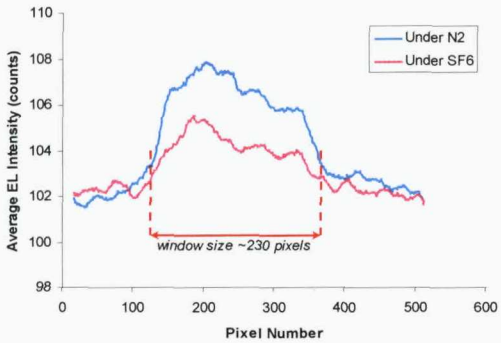

LDPE subjected to 3.5kV rms

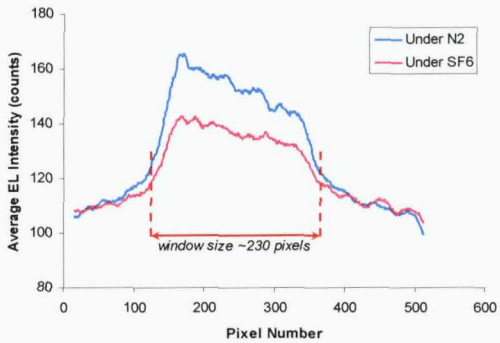

LDPE subjected to 4.0kV rms

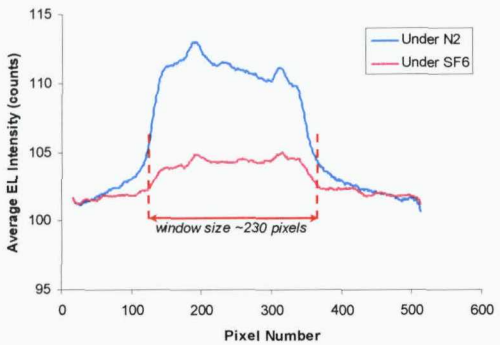

LDPE subjected to 5.0kV rms

D.3 Spectral analysis of EL under different gas environments

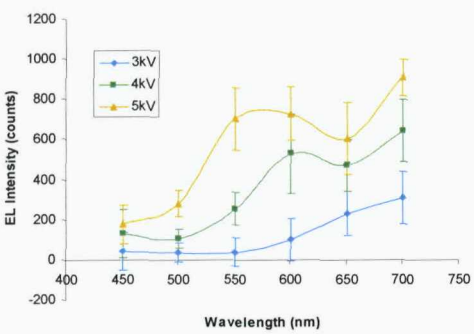

Under nitrogen (N_2)

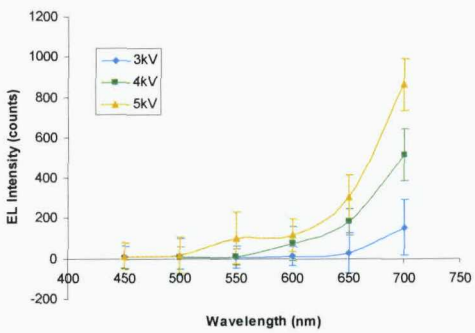

Under sulphur hexafluoride (SF_6)

D.4 Comparison of phase-resolved EL measurements under (a) N_2 and (b) SF_6

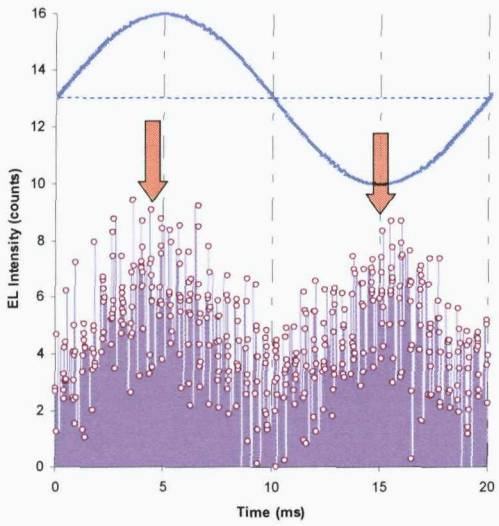

(a) LDPE subjected to 3.0kV rms

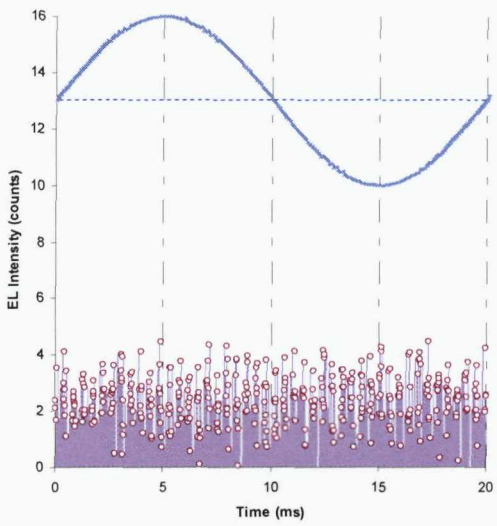

(b) LDPE subjected to 3.0kV rms

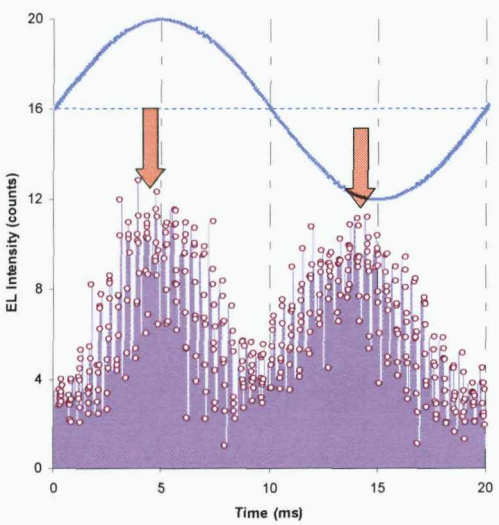

(a) LDPE subjected to 5.0kV rms

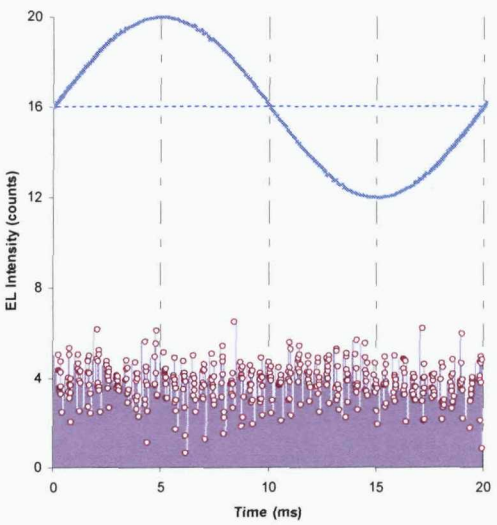

(b) LDPE subjected to 5.0kV rms

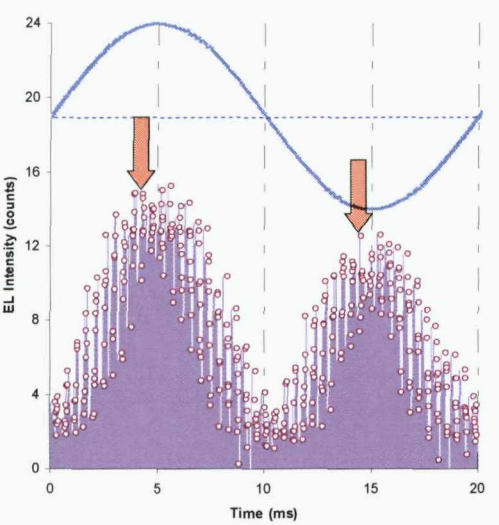

(a) PEN subjected to 3.0kV rms

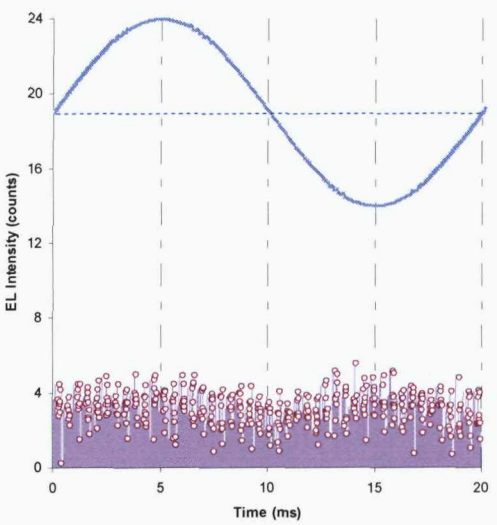

(b) PEN subjected to 3.0kV rms

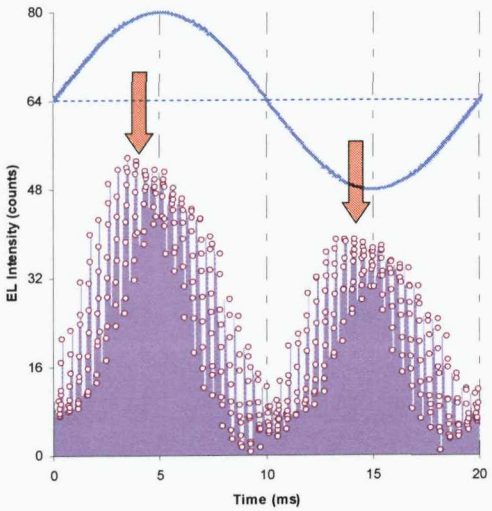

(a) PEN subjected to 5.0kV rms

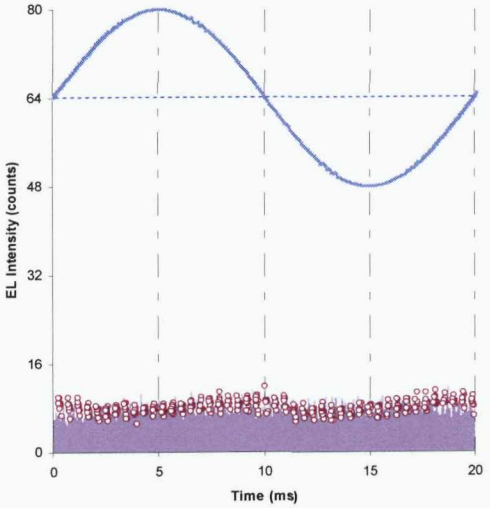

(b) PEN subjected to 5.0kV rms

D.5 Raw data for Figure 5.16 (a)

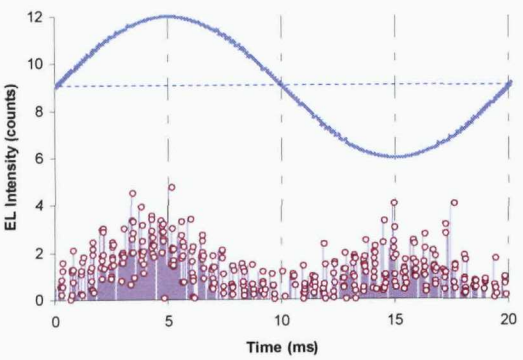

LDPE subjected to 3.0kV rms

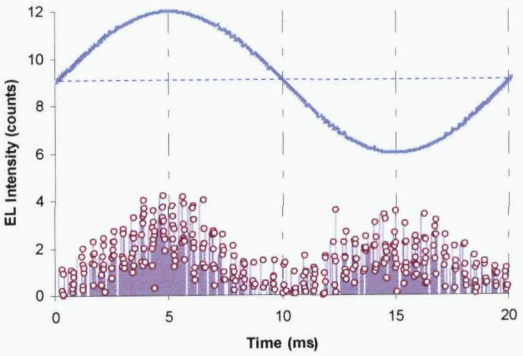

LDPE subjected to 3.5kV rms

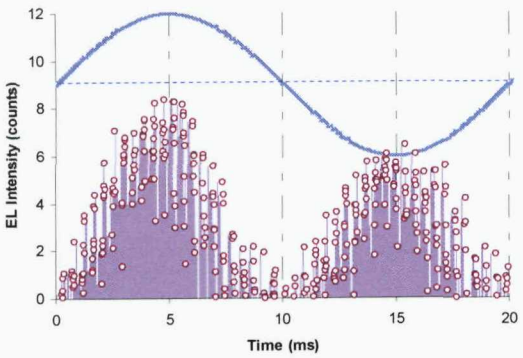

LDPE subjected to 4.0kV rms

D.6 Raw data for Figure 5.16 (b)

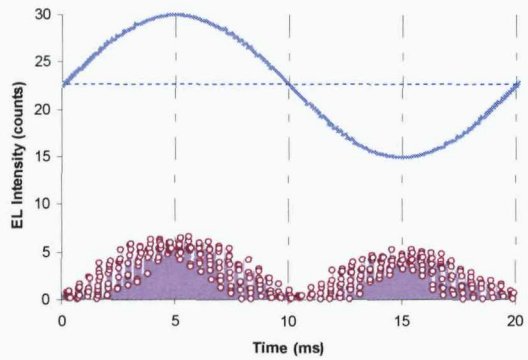

PEN subjected to 3.5kV rms

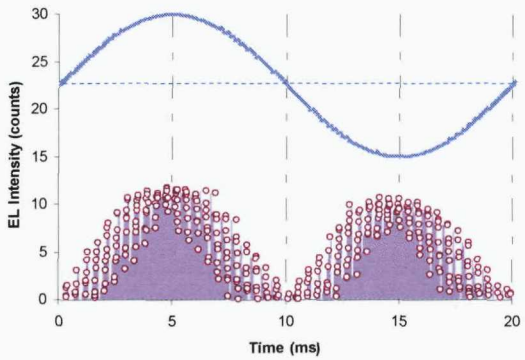

PEN subjected to 4.0kV rms

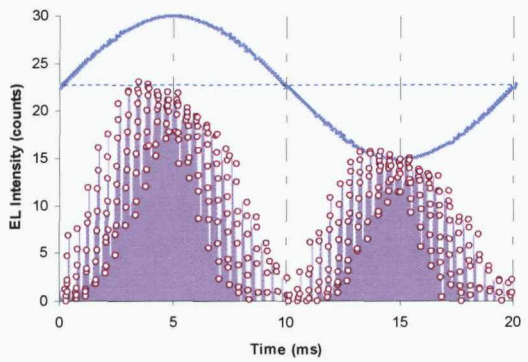

PEN subjected to 4.5kV rms

D.7 Supplementary results for phase-resolved EL measurement using LDPE

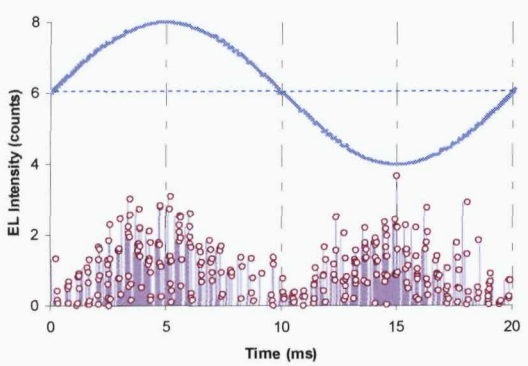

LDPE subjected to 3.0kV rms

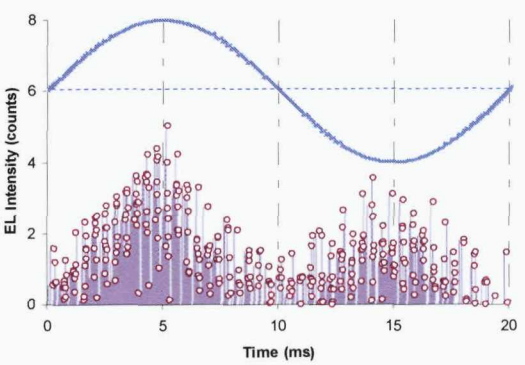

LDPE subjected to 3.5kV rms

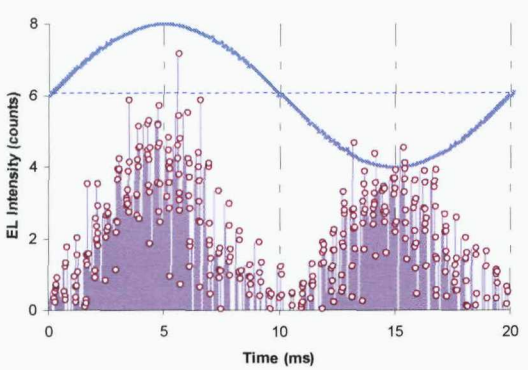

LDPE subjected to 4.0kV rms

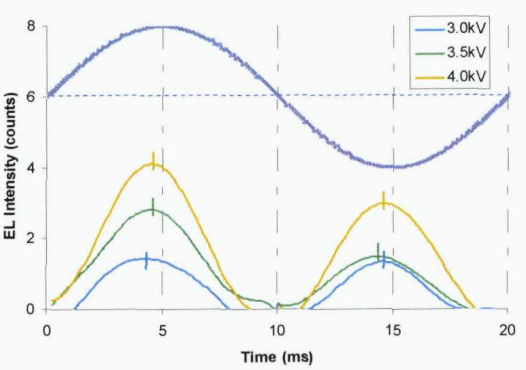

Simplified result

D.8 Raw data for Figure 5.17 (a)

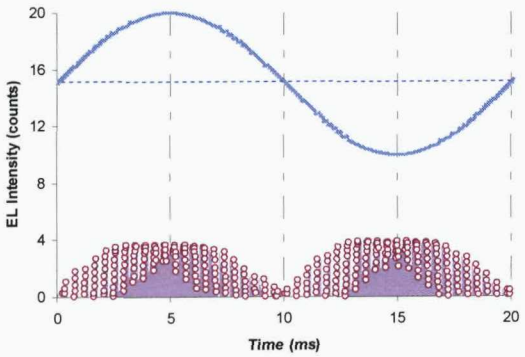

LDPE subjected to 4.0kV rms

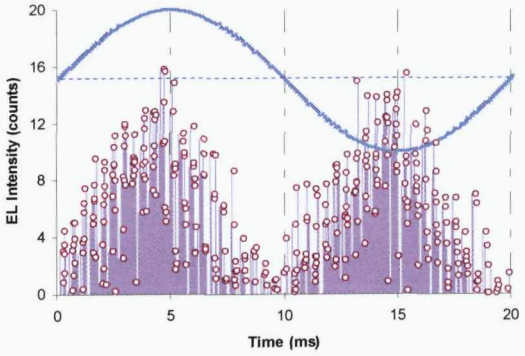

LDPE subjected to 5.5kV rms

D.9 Raw data for Figure 5.17 (b)

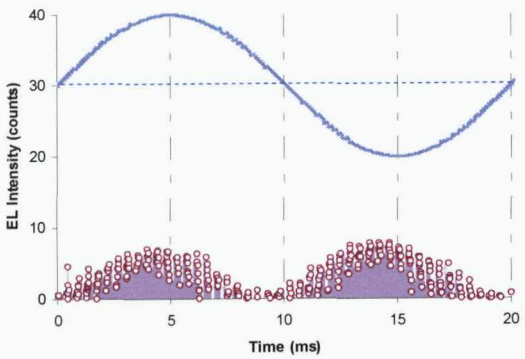

PEN subjected to 5.0kV rms

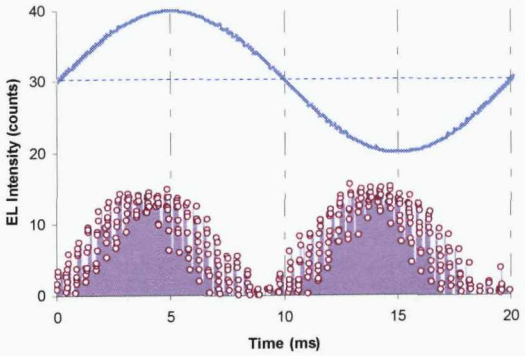

PEN subjected to 5.5kV rms

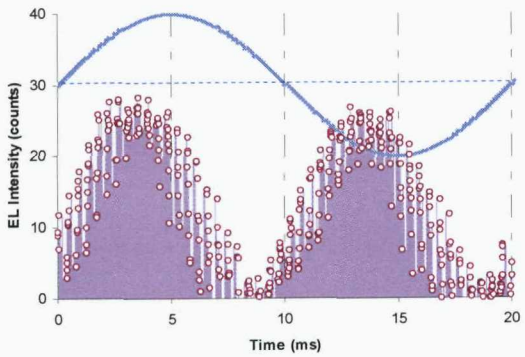

PEN subjected to 6.0kV rms

D.10 Raw data for Figure 5.20 using (a) triangular and (b) square waveforms

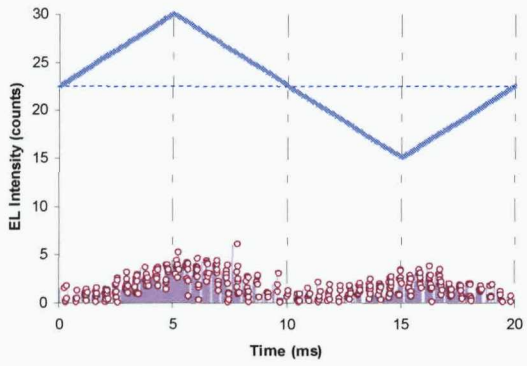

(a) LDPE subjected to 4.24kV peak

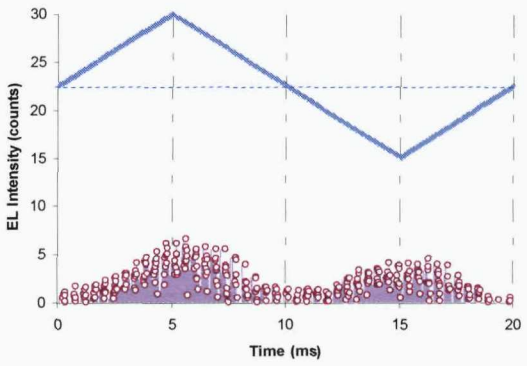

(a) LDPE subjected to 4.95kV peak

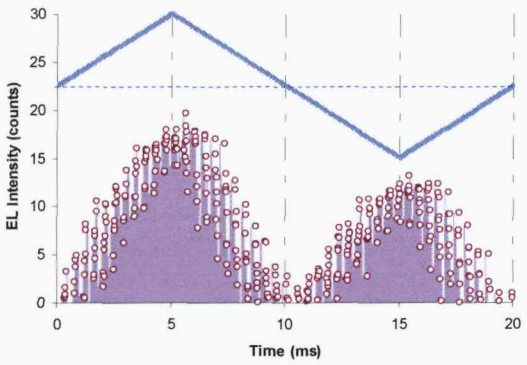

(a) LDPE subjected to 5.66kV peak

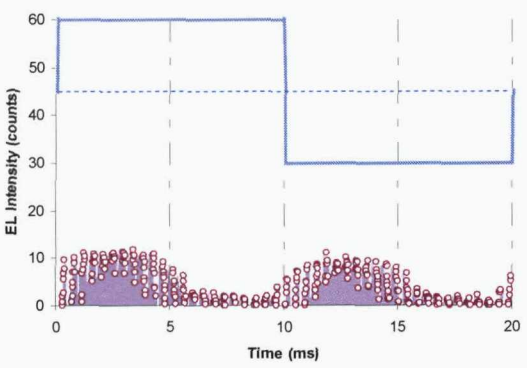

(b) LDPE subjected to 4.24kV peak

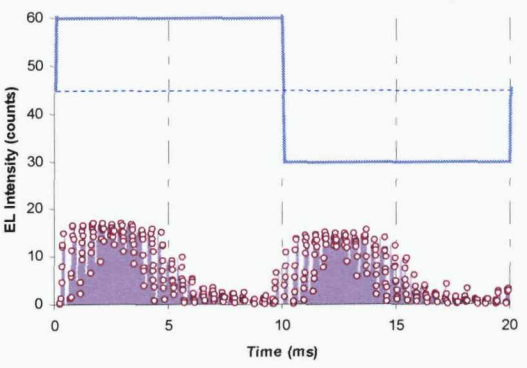

(b) LDPE subjected to 4.95kV peak

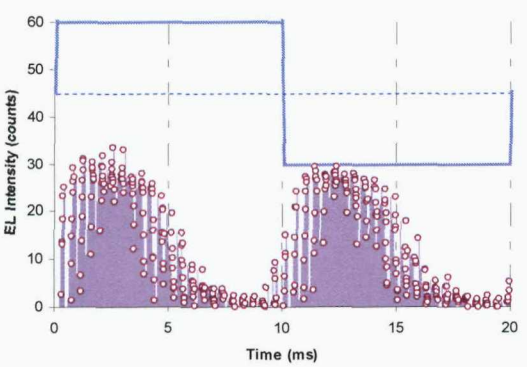

(b) LDPE subjected to 5.66kV peak

D.11 Raw data for Figure 5.21 (a)

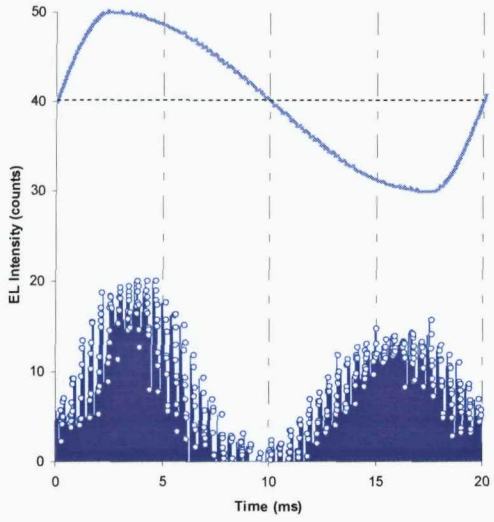

25% symmetry

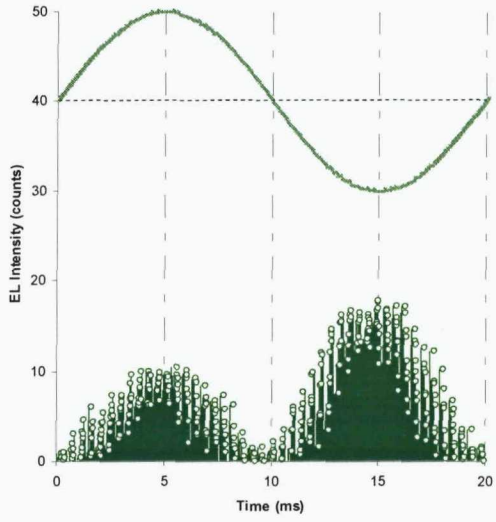

50% symmetry

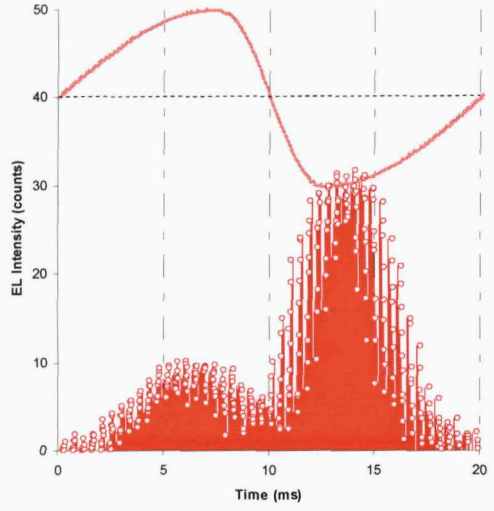

75% symmetry

D.12 Supplementary results for the effect of voltage symmetry (sinusoidal waveform)

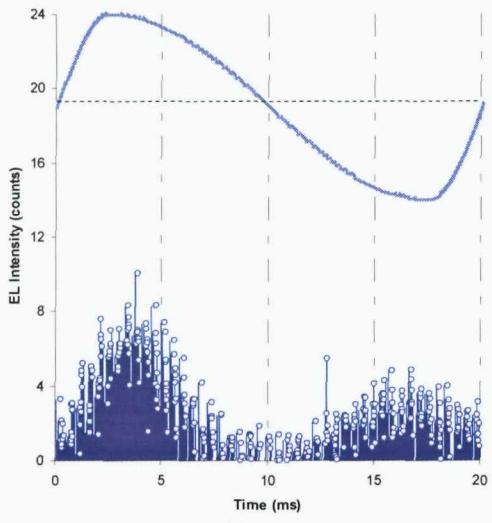

25% symmetry

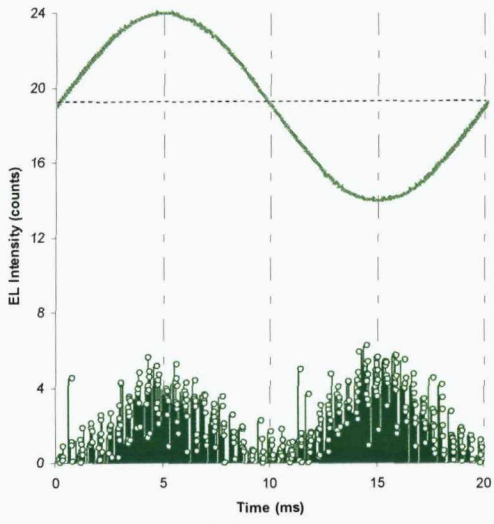

50% symmetry

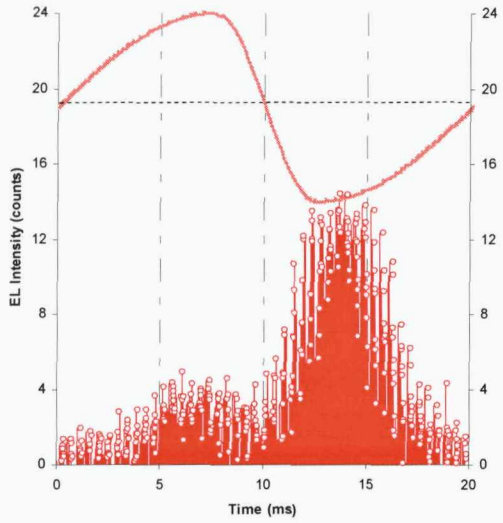

75% symmetry

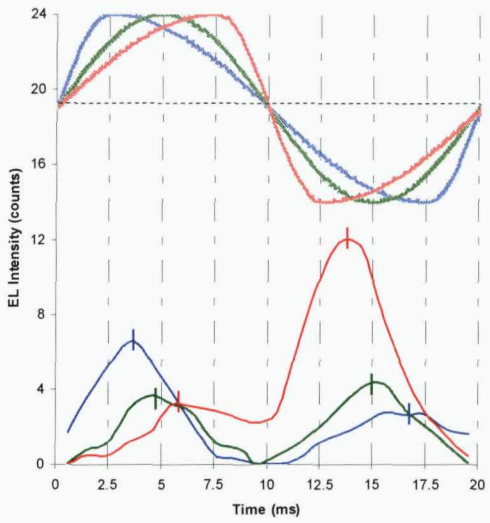

Simplified result

D.13 Raw data for Figure 5.21 (b)

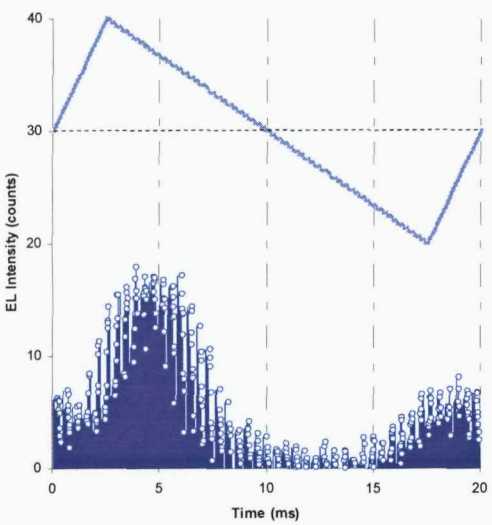

25% symmetry

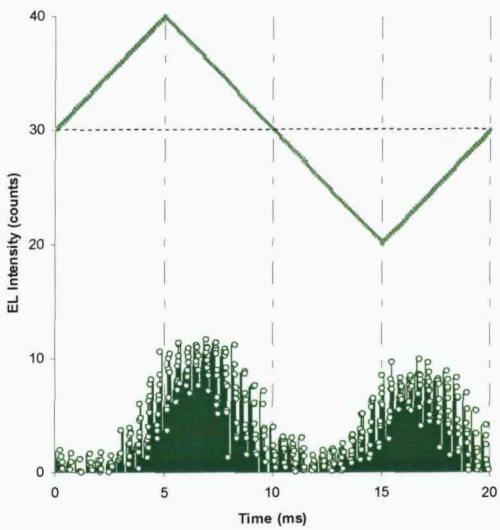

50% symmetry

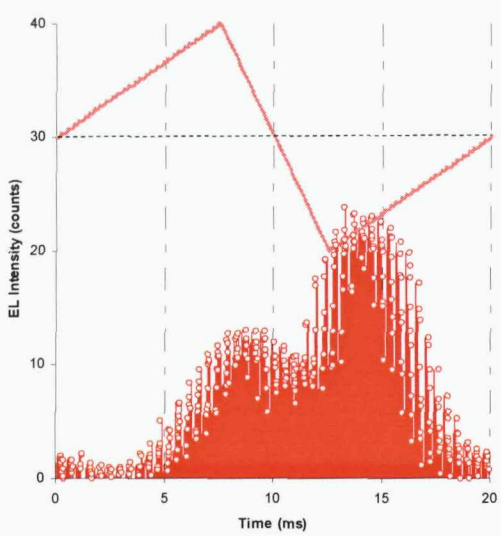

75% symmetry

D.14 Supplementary results for the effect of voltage symmetry (triangular waveform)

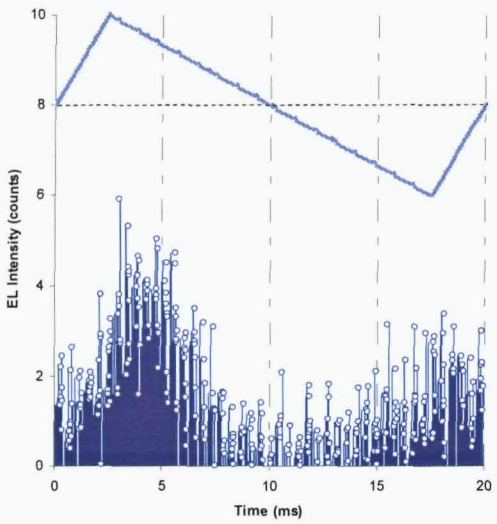

25% symmetry

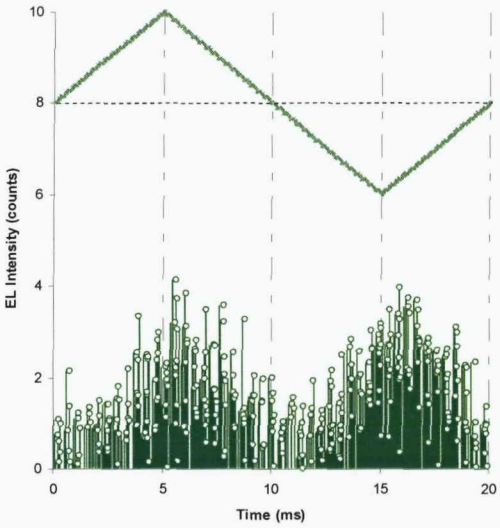

50% symmetry

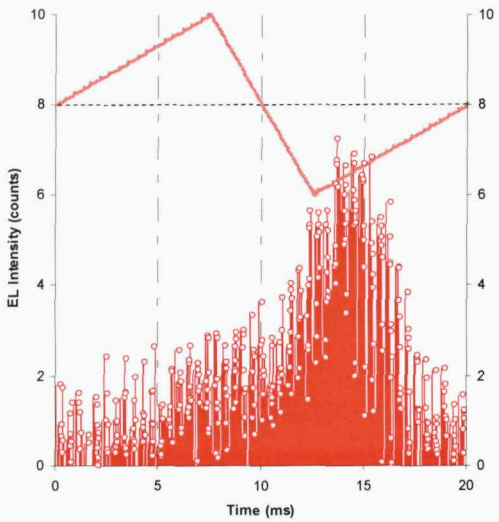

75% symmetry

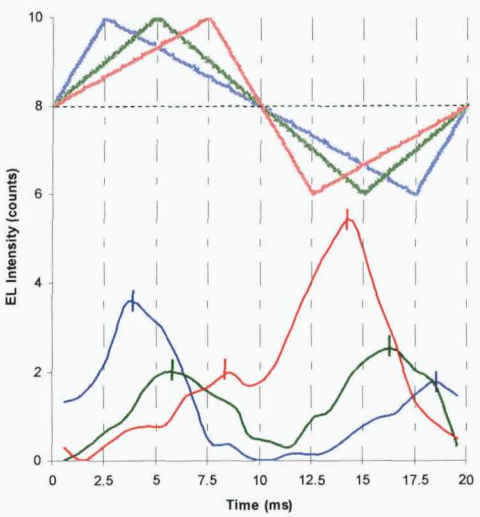

Simplified result

D.15 Raw data for Figure 5.22 (a)

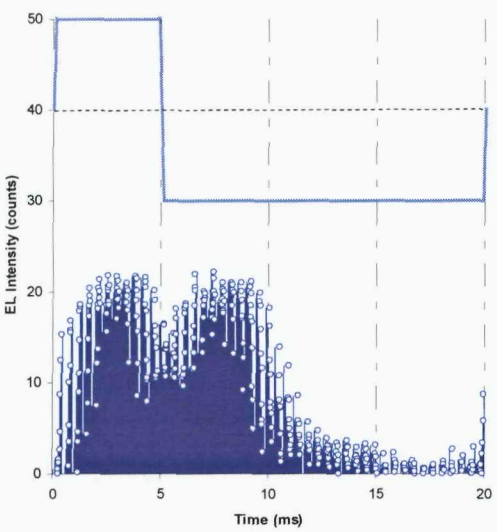

25% symmetry

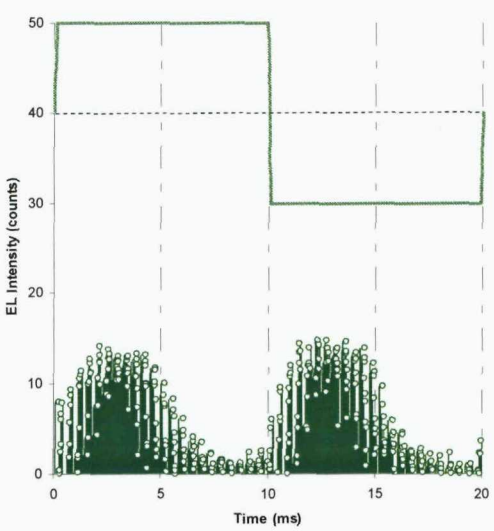

50% symmetry

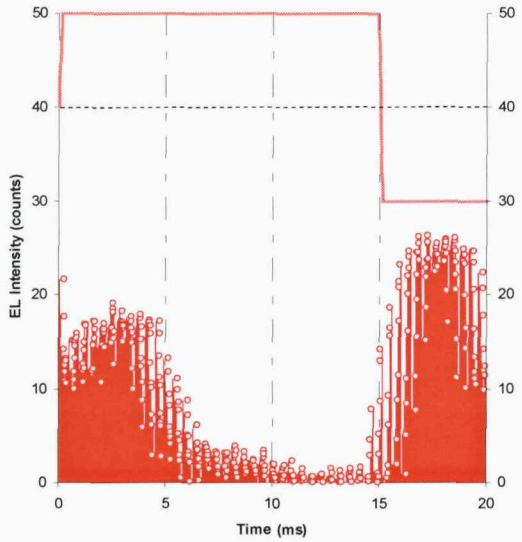

75% symmetry

D.16 Raw data for Figure 5.22 (b)

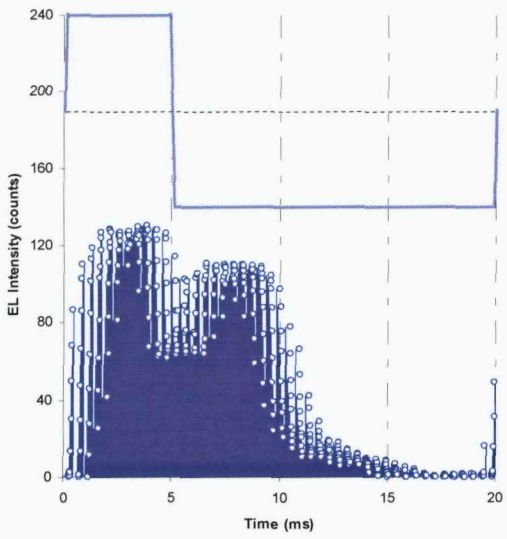

25% symmetry

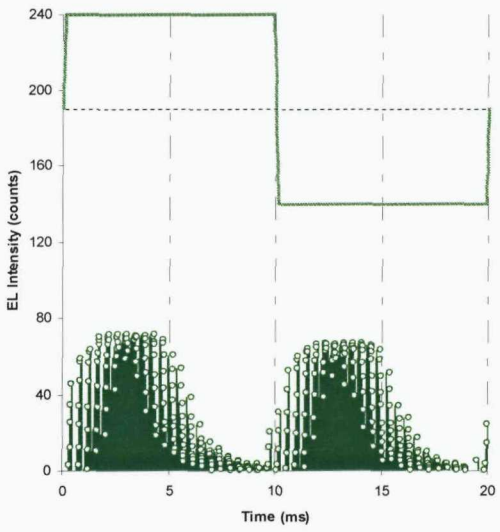

50% symmetry

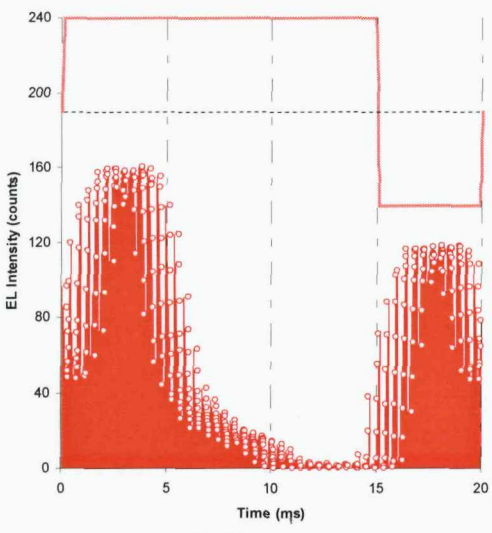

75% symmetry

D.17 Normalized spectral measurements for LDPE, PET and PEN samples

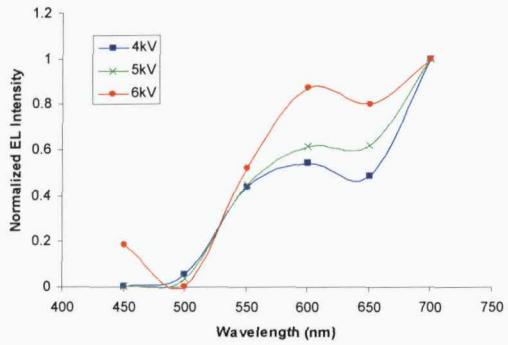

LDPE (Sample I)

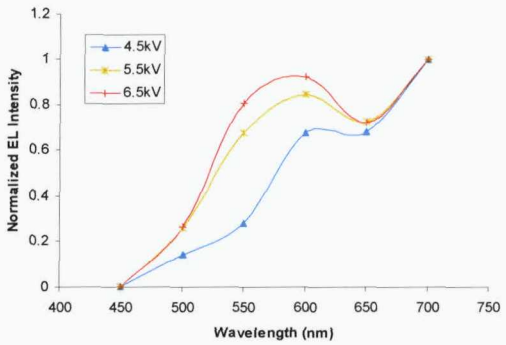

LDPE (Sample II)

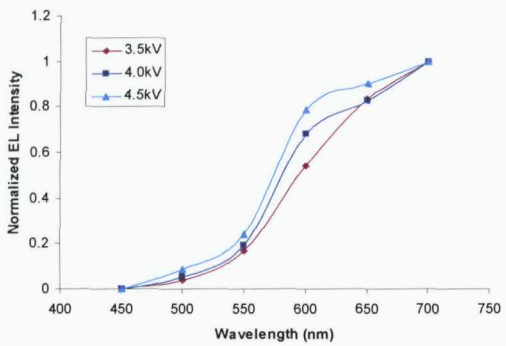

PET (Sample I)

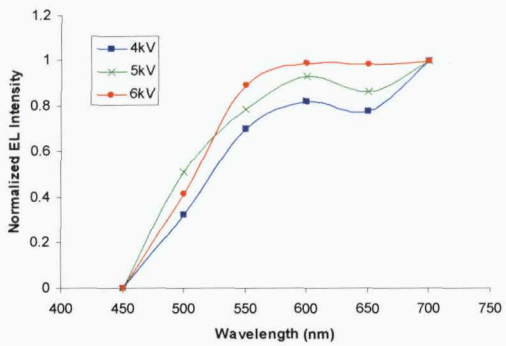

PET (Sample II)

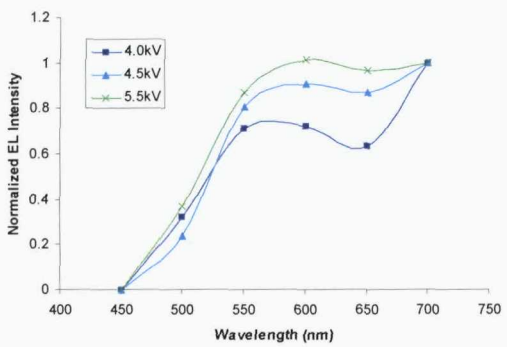

PEN (Sample I)

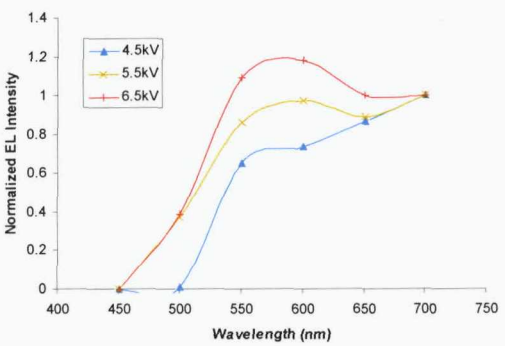

PEN (Sample II)

LIST OF PUBLICATIONS

A. Mohd Ariffin, P. L. Lewin and S. J. Dodd, "Comparison of Electroluminescence of Different High Voltage Cable Materials under Identical Experimental Conditions", *IEEE International Symposium on Electrical Insulation*, June 2006, pp. 166-9.

A. Mohd Ariffin, P. L. Lewin and S. J. Dodd, "Comparison of Electroluminescence Phenomenon in LDPE, PET and PEN under the Application of High Electrical Stress", *IEEE Conference on Electrical Insulation and Dielectric Phenomena*, Oct. 2006, pp. 260-3.

A. Mohd Ariffin, P. L. Lewin and S. J. Dodd, "Determining the Occurrence of Electroluminescence in Polymeric Materials with respect to the Applied Alternating Electrical Stress", *Proceedings of the 9th IEEE International Conference on Solid Dielectrics*, July 2007, pp. 703-6.

P. L. Lewin, S. J. Dodd and A. Mohd Ariffin, "Simulation of Electroluminescence using a Bipolar Recombination Model", *Proceedings of 9th IEEE International Conference on Solid Dielectrics*, July 2007, pp. 15-18.

A. Mohd Ariffin, P. L. Lewin, S. J. and Dodd, "Investigation on Electroluminescence Phenomenon in Insulating Polymers under the Influence of Different Gas Environments", *15th International Symposium on High Voltage Engineering*, Aug. 2007.

A. Mohd Ariffin, P. L. Lewin and S. J. Dodd, "The Influence of Absorbed Gases on Electroluminescence Phenomenon in Polymeric Materials Subjected to High Electrical Stress", *Conference on Electrical Insulation and Dielectric Phenomena*, Oct. 2007, pp. 33-36.

A. Mohd Ariffin and P. L. Lewin, "Phase-Resolved Measurement and Modelling of Electroluminescence Phenomenon in Polyethylene Subjected to High Electrical Stress", *International Conference on Condition Monitoring and Diagnosis*, Apr. 2008, pp. 264-7.

(In Press) A. Mohd Ariffin, P. L. Lewin, D. H. Mills and S. J. Dodd, "The Effect of Voltage Waveform on Phase-Resolved Electroluminescence Measurements", *Conference on Electrical Insulation and Dielectric Phenomena*, Oct. 2008.